



Universidad de Concepción
Dirección de Postgrado
Facultad de Ciencias Físicas y Matemáticas
Programa de Doctorado en Ciencias Aplicadas
con Mención en Ingeniería Matemática

**UNA CONTRIBUCIÓN A LAS SIMULACIONES NUMÉRICAS
DE TANQUES DE SEDIMENTACIÓN Y APLICACIONES
RELACIONADAS**

**(A CONTRIBUTION TO THE NUMERICAL SIMULATION
OF SETTLING TANKS AND RELATED APPLICATIONS)**

Tesis para optar al grado de Doctor en Ciencias
Aplicadas con mención en Ingeniería Matemática

CAMILO IGNACIO MEJÍAS NEIRA
CONCEPCIÓN-CHILE
2019

Profesor Guía: Raimund Bürger
CI²MA y Departamento de Ingeniería Matemática
Universidad de Concepción, Chile

Cotutor: Stefan Diehl
Centre for Mathematical Sciences
Lund University, Suecia

Abstract

This dissertation deals with diverse mathematical and numerical aspects with new models and methods that try explain industrial processes about wastewater treatment, with focus in activated sludge settling, this processes are commonly treat with physical models excluding reactive part of the problem.

At the first part, we introduce a new time-discretization method that enable a more efficient simulation and it is compared with other methods. Different methods of discretization are presented, and are applied to two batch sedimentation cases: Kynch test and Diehl test above clear liquid. Performance is measured regarding the numerical error and the computational time. The proposed method is found to be easier to implement but slightly less efficient in terms of computational time.

Next, we introduce a new model of batch sedimentation coupled with a simplified model of kinetic reaction concerning denitrification. This is an important practical problem due to the possibility of secondary denitrification causing flocs of activated sludge to rise to the top of the settler due to nitrogen gas bubbles forming in the flocs. We present a model that takes into consideration both hindered settling and compression behavior and also the reaction terms describing growth and decay of biomass, we aboard the governing equations, spatial and time discretization, numerical method and theoretical results and showed an examples using Kynch and Diehl test even at “overcompressed” case.

Additionally, we present a new model of secondary settling tank. The model incorporate both fluids flows and gravitational settling with compression behaviour and also enables the incorporation of kinetic of biological reactions to be included in the model. The model is based on conservation laws and the solid and fluids phase velocities are replaced by a mixture velocity expressed by the given volumetric flows and model variables, and a solid-fluid relative velocity, prescribed by a constitutive functions. Explicit expression for the total fluxes of solid and liquid phases are derived. Constitutive functions for hindered and compressive settling are presented and the choice of initial data

and feed input functions for a reactive denitrification model are discussed. Numerical scheme is derived and a number of simulation results are presented for a reaction model with nitrification. Moreover, corresponding error and convergence rates are presented.

For all the situations described above, several numerical experiments illustrating the correct performance of the methods, and confirming the theoretical results, are reported.

Finally, we propose different ways for make a future work in order to apply mathematical models and numerical schemes as a solution to the industrial processes, for example, build a package with this results and others, into a comercial software.



Preface

Meanwhile finishing my Mathematical Engineering at Universidad de Concepción I applied for a PhD position at the same University. I started the post-graduate program at Centro de Investigación en Ingeniería Matemática (CI²MA). My PhD has been funded by REDOC CTA, Universidad de Concepción, CRHIAM, Basal and CONICYT in different stages during my studies and internships for research in the field of mathematical modelling and numerical techniques.

This Thesis is based on the following publications:

- R. Bürger, S. Diehl, and C. Mejías. On time discretizations for the simulation of the batch settling-compression process in one dimension. *Water Science and Technology*, 73(5):1010 – 1017, 2016.
- R. Bürger, J. Careaga, S. Diehl, C. Mejías, I. Nopens, P.A. Vanrolleghem, and E. Torfs. Simulations of reactive settling of activated sludge with a reduced biokinetic model. *Computers and Chemical Engineering*, 92:216 – 229, 2016.
- R. Bürger, S. Diehl, and C. Mejías. A difference scheme for a degenerating convection-diffusion-reaction system modelling continuous sedimentation. *ESAIM: Mathematical Modelling and Numerical Analysis*, 52(2):365 – 392, 2018.

Are, major parts is based upon contributions presented and published at the following conferences or proceedings:

- R. Bürger, S. Diehl, and C. Mejías. R. Bürger, S. Diehl, and C. Mejías. A model for continuous sedimentation with reactions for wastewater treatment. In G. Mannia, editor, *Frontiers in Wastewater Treatment and Modelling (FICWTM 2017)*, *Lecture Notes in Civil Engineering*, volume 4, pages 596 – 601, Cham, Switzerland, 2017. Springer International Publishing.

- R. Bürger, J. Careaga, S. Diehl, C. Mejías, and R. Ruiz-Baier. Convection-diffusion-reaction and transport-flow problems motivated by models of sedimentation: some recent advances. In P.N. de Souza and M. Viana, editors, *Proceedings of the International Congress of Mathematicians, Rio de Janeiro 2018 Vol. IV: Invited Lectures*, Singapore. World Scientific, in press.

Finally, at the end of fourth year of PhD I started a new way from the initial research: together with Diego Maldonado, another colleague for the undergraduate studies, we co-founded a company, namely *Hibring Ingeniería*, and the objective includes mathematical modelling and numerical techniques in industrial solutions for companies. First we won a public funding for start the company in December of 2017 and we developed different software and made experimental researching for settling velocities of particulate systems.



In the memory of Dr. Luis Sanchez, who teach to me to think different.



Declaration

I declare that I wrote this thesis: introduction and conclusion. The other Chapters are part of our publish papers. I declare that I was participate in numerical schemes in those papers, compute the examples and generate error tables. I declared that I built examples figures for Chapter 1 and Chapter 3.



Acknowledgements

First of all, I wanna thank to my advisors Raimund and Stefan for the infinite patience (well, not all the time) meanwhile doing my studies, compute simulations and had some math or real-life issues. All the time, sooner or later they were with some an advise or idea for solve problems. I know that sometimes I was unpredictable, but they trusted in me all the time. Thanks! Special thanks for Stefan too, for hosted me in Lund, Sweden two times and shared a kebab-pizza sometimes or all the lunches at Ideon park. I had a excellent life-experience even in Malmö, as Lund too. Thanks. Writing this words, I remember the first time when I decided to work with Raimund, at the third year of my undergraduate studies and I came to his office and I asked if we can work together because I wanted to produce a paper before my thesis and use that for applying to an international PhD and Raimund agreed that and we start to work with different courses, sometimes I was the only student (not every time the best) until a breakfast in a Hotel in La Serena, where Raimund offered me the possibility to doing the PhD with him here in Concepción and not choose leave to the other country. At the first instance I was dubitative but now I think was the best decision. Thanks Raimund for that, I really appreciate it.

Along my studies I was hosted at CI²MA, an excellent place for doing my work at the top of a hill, with 122 stairs. Thanks to professor Gabriel Gatica for makes a lot of efforts in built and maintenance this center as we know todays, and also thanks to for all the advices and support along my studies even though hard discussions sometimes were necessary. In the same way, the advices of prof. Freddy Paiva was every time a good voice for support to me and helped me in solving problems even from start my undergraduate studies at this University! Thanks.

I wanna to thanks many people, friends that supported me and I know this sheet is short for this instance, but I can't forget all my office-mates at CI²MA, the *classic-group*, the philosophic talks, the high-level conversations in maths, politics, academy, etc. When I left the center I really missed this talks. Thanks for contribute to my formation as

a knowledge person. Special thanks to Felipe Lepe, Elvis G., Victor Osoreo, Joaquín, Rafa, Yolanda, and Felipe zizu, etc, etc. Special thanks to Pepe, that was really an important voice behind computers and offices for my personal development. Thanks of all.

I wanna to thank to Catalina, my girlfriend for supporting me all the time, for understanding the international internship for many months and waited me and supported me even at a distance, I believe that without your patiences and advices it would had been impossible to me keep maintenance and walk forward all the time. You were and you are very important to me. Thanks

When a was child, I received an advice 'If you're doing things every time in the right sense, you will get ever good results'. Thanks for my parents, my mom, for the spiritual and morality education that provided support every time.

"Hibring Ingeniería", wasn't only my idea. We talked many hours with many 'behind-camera' people at CI²MA and Mathematical Engineering Department. I'm only the visible face, but I need to thanks to Diego to taking seat aboard to this mission and support all decisions, strategical plans, using your free time in Chile for are working whole days and night continuously in order to get a product. Thanks my friend for believe in this idea and make it a reality. Thanks to Rafa, Emilio, Daniel, Edison, Felipe Benítez, Elias, Richard, Manuel, Greco, in the order they incorporated to this business. Thanks for believed and gave your best effort and make the reality that we are now. A high potencial business.

Elisa and Diana were two important girls at my PhD, meanwhile, Elisa teach me about chemistry, biofilms, and treat to keep me open mind for understand process, with Diana we had strong academic discussions, similar research area and interest too. They are completely opposite, but I appreciate very much her time and confidence.

Finally give thanks to my life-friends, Eric and Michael, for supporting all the time, my best funny group friends, Lenicakaá, (Ale, Karla, Nico, Leo) for providing enjoyable afternoons around a bonfire, in whatever place at the mountains.

Thanks to the institutions that funding my studies, research, internship, congress assistance, etc. In chronological order I acknowledge: Red Doctoral REDOC.CTA, MINEDUC project UCO1202, Universidad de Concepción scholarship, BASAL project CMM, Universidad de Chile and CI²MA, CRHIAM Proyecto Conicyt Fondap 15130015, CRHIAM scholarship and Conicyt scholarship 21160651.

Contents

Abstract	iii
Preface	v
Acknowledgements	ix
List of Figures	xvii
List of Tables	xix
Introduction	1
Introducción (in spanish)	14
1 On time discretizations for the simulation of the batch settling - compression process in one dimension	27
1.1 Introduction	28
1.2 Methods of discretization	30
1.2.1 The explicit Euler method	31
1.2.2 The semi-implicit (SI) method	32
1.2.3 The linearly implicit (LI) method	32
1.2.4 Other time-stepping methods	34
1.3 Results and discussion	34
1.3.1 Influence of compression in experiments	38
2 A model of batch settling withal reactions	41
2.1 Introduction	41
2.1.1 Related work	42
2.1.2 Novelty of this work	43
2.1.3 Outline of the chapter	44
2.2 Governing model	45

2.2.1	Governing partial differential equations, initial and boundary conditions	47
2.2.2	Model parameters and constitutive functions	47
2.3	Numerical method	48
2.3.1	Spatial discretization	50
2.3.2	Time discretization	51
2.3.3	Numerical method in final form	53
2.3.4	A theoretical result	54
2.4	Numerical results	56
2.4.1	Examples 1 to 3: Kynch test (batch settling of an initially homogeneous suspension)	56
2.4.2	Examples 4 and 5: Diehl test (batch settling of suspension initially located above clear liquid)	59
2.4.3	Examples 6 and 7: overcompressed test (expansion of compressed sludge)	62
2.4.4	Numerical solution versus discretization	64
3	A difference scheme for a degenerating convection-diffusion-reaction system modelling continuous sedimentation	69
3.1	Introduction	69
3.1.1	Related work	71
3.1.2	Outline of the remainder of this chapter	72
3.2	Model formulation	74
3.2.1	Specific assumptions for wastewater treatment	75
3.2.2	Balance equations	76
3.2.3	Phase, bulk and relative velocities	77
3.2.4	Solid and liquid total fluxes	79
3.2.5	Model equations in final form	80
3.2.6	Constitutive assumptions for hindered and compressive settling	83
3.2.7	Initial data and feed input functions	83
3.3	A numerical scheme	84
3.3.1	Spatial discretization	84
3.3.2	Explicit fully discrete scheme	86
3.3.3	CFL condition	88
3.3.4	Properties of the numerical scheme	88
3.4	Numerical Examples	96
3.4.1	Example 1: variations of feed flow and particle concentration	100
3.4.2	Example 2: variations of the feed percentages	101
3.4.3	Example 3: transitions between steady states	102
3.4.4	Approximate errors	103

Summary and concluding remarks	107
Bibliography	119



List of Figures

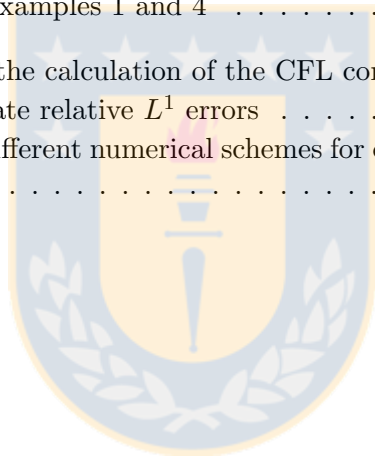
1	Dorr Thickener in 1905	2
2	Three thickeners in Pelambres mine, Chile	3
3	Salamanca thickeners	4
4	Short-circuit analysis	5
5	Overview of a biological wastewater treatment facility	8
6	Schematic view of the problem and his variables.	13
1.1	Numerical solution of the Kynch test (left) and Diehl test (right) using Euler method	34
1.2	Kynch test simulated by the LI method	35
1.3	Diehl test simulated by the LI method	35
1.4	Efficiency plots for the Kynch test (left) and the Diehl test (right) . . .	36
1.5	LI method applied to Kynch test	37
1.6	Influence of compression term at different functions	39
2.1	A schematic view of a settler vessel	46
2.2	Example 1 (Kynch test, $d_S = 10^{-6} \text{ m}^2 \text{ s}^{-1}$)	55
2.3	Example 1 (Kynch test, $d_S = 10^{-6} \text{ m}^2 \text{ s}^{-1}$): long-time simulation ($T = 100 \text{ h}$)	57
2.4	Example 2 (Kynch test, $d_S = 9 \times 10^{-6} \text{ m}^2 \text{ s}^{-1}$)	58
2.5	Example 3 (Kynch test, $d_S = 1.3 \times 10^{-5} \text{ m}^2 \text{ s}^{-1}$)	59
2.6	Example 4 (Diehl test, $X(z, 0) = 7 \text{ kg m}^{-3}$ above $z = 0.5 \text{ m}$).	60
2.7	Example 5 (Diehl test, $X(z, 0) = 14 \text{ kg m}^{-3}$ above $z = 0.25 \text{ m}$)	61
2.8	Comparison between different examples.	61
2.9	Example 6 (overcompressed test, $X(z, 0) = 20 \text{ kg m}^{-3}$ below $z = 0.5 \text{ m}$)	63
2.10	Example 6 (overcompressed test, $X(z, 0) = 25 \text{ kg m}^{-3}$ below $z = 0.9 \text{ m}$)	64
2.11	Example 1 (Kynch test): comparison between a reference solution	66
2.12	Example 4 (Diehl test): comparison between a reference solution	67
3.1	Schematic view of secondary settling tank (SST) with variables and numerical discretization	73
3.2	Graphs of the constitutive functions used in Examples	97

3.3	Graphs of control parametes for examples	98
3.4	Example 1: Simulation of reactive settling in an SST	100
3.5	Example 1: Numerical solutions for coarse discretizations	101
3.6	Example 2: Simulation of reactive settling in an SST	102
3.7	Example 2: Numerical solutions for coarse discretizations	103
3.8	Example 3: Simulation reactive settling in an SST	104
3.9	Example 3: Numerical solutions for coarse discretizations	105
3.10	Batch sedimentation scheme. Solids particles turn down to the bottom under a external force, the gravity	111
3.11	Schematic view of the light influence across a transparent vessel.	113
3.12	Diagram of a prototype that measure the light quantity and transform to a concentration value	114
3.13	Flow diagram of <i>RelaveSeco</i> plataform	115
3.14	Screenshot of RelaveSeco plataform	116
3.15	Schematic view of a granule	117



List of Tables

1	Levels of wastewater treatment	7
2	Niveles del tratamiento de aguas residuales	19
2.1	Parameter values employed for the simulation of reactive settling	49
2.2	Error table of Examples 1 and 4	68
3.1	Coefficients for the calculation of the CFL condition	99
3.2	Total approximate relative L^1 errors	106
3.3	Benchmark of different numerical schemes for compute a batch sedimentation	108



Introduction

“Ensure availability and sustainable management of water and sanitation for all”. Sustainable Development Goal No. 6 - United Nations General Assembly.

Water scarcity affects more than 40 percent of people around the world, an alarming figure that is projected to increase with the rise of global temperatures as a result of climate change. For this reason, in 2015, more than 190 world leaders committed to *17 Sustainable Development Goals* [115] to help us all end extreme poverty, fight inequality and injustice, and fix climate change. We each have a role to play if we are going to achieve these goals of a more prosperous, equitable, and sustainable world.

The Sustainable Development Goal No. 6 talks about water problem. More than half of the households worldwide have access to clean water in their homes; however, the number of people without adequate sanitation (a safe toilet) is increasing as people move into more crowded cities. Diseases caused by contaminated water kill more people every year than all forms of violence, including war. By prioritizing clean water, we can improve the health and livelihoods of millions of people [114].

Water problem is a global issue, taken for many nonprofit organisations (water.org [136], Global Citizen [63], World Health Organisation [138], etc.) and many efforts are made every day improve the water accessibility for everyone and for safe water bodies. This PhD thesis is based in one principle: Improve the understanding about solids particles inside a liquid as water for create better techniques in water recovery and reuse. This knowledge can be applied to industries 'or cities' developments.

Water reuse in industry

Water consumption is important for many industrial processes. The paper and chemical industry, medicine, vulcanology, bioreactors, wastewater treatment, among other

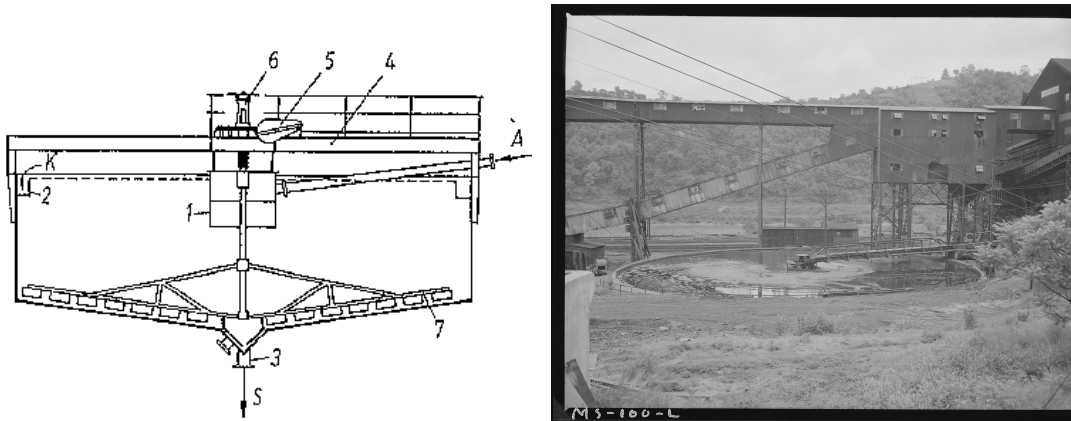


Figure 1: Dorr Thickener in 1905. (a) Original dorr thickener scheme. (1) Feed of mixture, (2) Clear water effluent, (3) thickened solid underflow. (b) Dorr thickener at mine. Buckeye Coal Company, Nemaocolin Mine, Nemaocolin, Greene County, Pennsylvania, 1946. Reprinted from National Archives at College Park, USA, by Department of the Interior. Solid Fuels Administration For War. (4/19/1943-6/30/1947), Retrieved October 20, 2018, from <https://catalog.archives.gov/id/540270>. Reprinted with permission.

areas require a large amount of water in their processes, which due to various factors cannot be eliminated directly to bodies of water. In general, they have a homogeneous initial suspension must be separated into a clarified liquid and a concentrated sediment inside a conditioned tank for the process. In all these cases, it is considered that the initial homogeneous suspension is composed of solid and fine particles, which are small compared to the tank that contains them.

In particular, in Chile, the copper mining industry is the largest industry owned by the country, contributing to a third of the world's production. It is an important part of the high and sustained growth that the Chilean economy has had in the last decades and its to importance for the development of our country is undeniable. Geographically, mining in Chile takes place mainly in desert and very remote areas, specifically in the Atacama Desert, the driest desert in the world, where water is a scarce resource, but at the same time vital for the separation of metals, like copper and dynamite rock. For this reason, the recovery of water and research into new technologies to obtain more efficient processes are of public interest and should be studied.

The continuous sedimentation of suspensions of fine solid particles dispersed in a viscous fluid is a process that recovers the water used in the processes of comminution (reduction of size) and flotation (separation of the desired mineral from the gangue) in sulphide copper mineral recovery plants. The first and most important stage of water



Figure 2: Thickeners in Pelambres mine, Chile. The rightmost thickener shows a short-circuit in gray color at center of the unit. Reprinted from CENTRA Ingeniería Adquisiciones Construcción, by CENTRA Ingeniería Adquisiciones Construcción, Retrieved October 20, 2018, from <http://www.centra.cl/construction-en/mining3-en/>. Shows with permission.

recovery is thickening, that is, continuous sedimentation, where large cylindrical ponds are used in which the separation of solids and liquids occurs due to gravity.

Here, together with the goal to recover as much of this resource as possible after the sedimentation process, we also seek to generate a tailing, that is, as dry as possible so that in its later deposit in collection sites the risks of producing pollution to the underground layers by means of percolated liquids it minimized.

Thickeners

The thickener is a device invented by John Van Nostrand Dorr (1872 –1962) in 1905 for gold concentrator plants in South Dakota and marks the beginning of the modern thickening era [37] (see Figure 1).



Figure 3: Salamanca thickeners. Both units presents a short-circuit in gray color at center Reprinted from CENTRA Ingeniería Adquisiciones Construcción, by CENTRA Ingeniería Adquisiciones Construcción, Retrieved October 20, 2018, from <http://www.centra.cl/construction-en/mining3-en/>. Reprinted with permission.

The concept of thickening is simple and lies in decanting; it consists in leaving a liquid and homogeneous mixture inside a tank and that the fine solid particles settle to in the bottom only by gravity, thus separating the solid material, from the clarified liquid in the upper part. There is evidence of this process in Egyptian culture, approximately 2,500 years BC. [59].

Previous to Dorr's innovation, the ponds only had a settling process, that is, a *batch* sedimentation system, which is a semi-continuous process, as documented by Agrícola as early as 1556 [2]. The contribution of Dorr lies in being the first to evolve this semi-continuous decantation process, to a continuous thickening process; which consists of a tank that is fed by a pipe inserted in it, called *feed*, which continuously adds material and this settles by gravity, thus obtaining in the bottom a thick mixture, which is removed by a pipe at the bottom of the tank, called *underflow*, while the clear water, at the top, is removed by a channel at the top, called *effluent* or *overflow* [52].

Many thickener designs exists in industry [36] (e.g. conventional, deep cone, high rate, in paste). In all of those cases the main part are the *feedwell*, that ensure the feed flow energy must be dissipated and directed vertical instead of horizontal and provide conditions to flocculate the solids so to first collect the solids and then settle them. Sometimes the feedwell mechanism produces *short circuiting*, which means that the flow short-circuits through the feedwell and can carry with it particles that have not been properly flocculated (Figure 3). The feed flow is more likely to escape the larger the feedwell diameter. The surface solids are fine particles that were not collected in

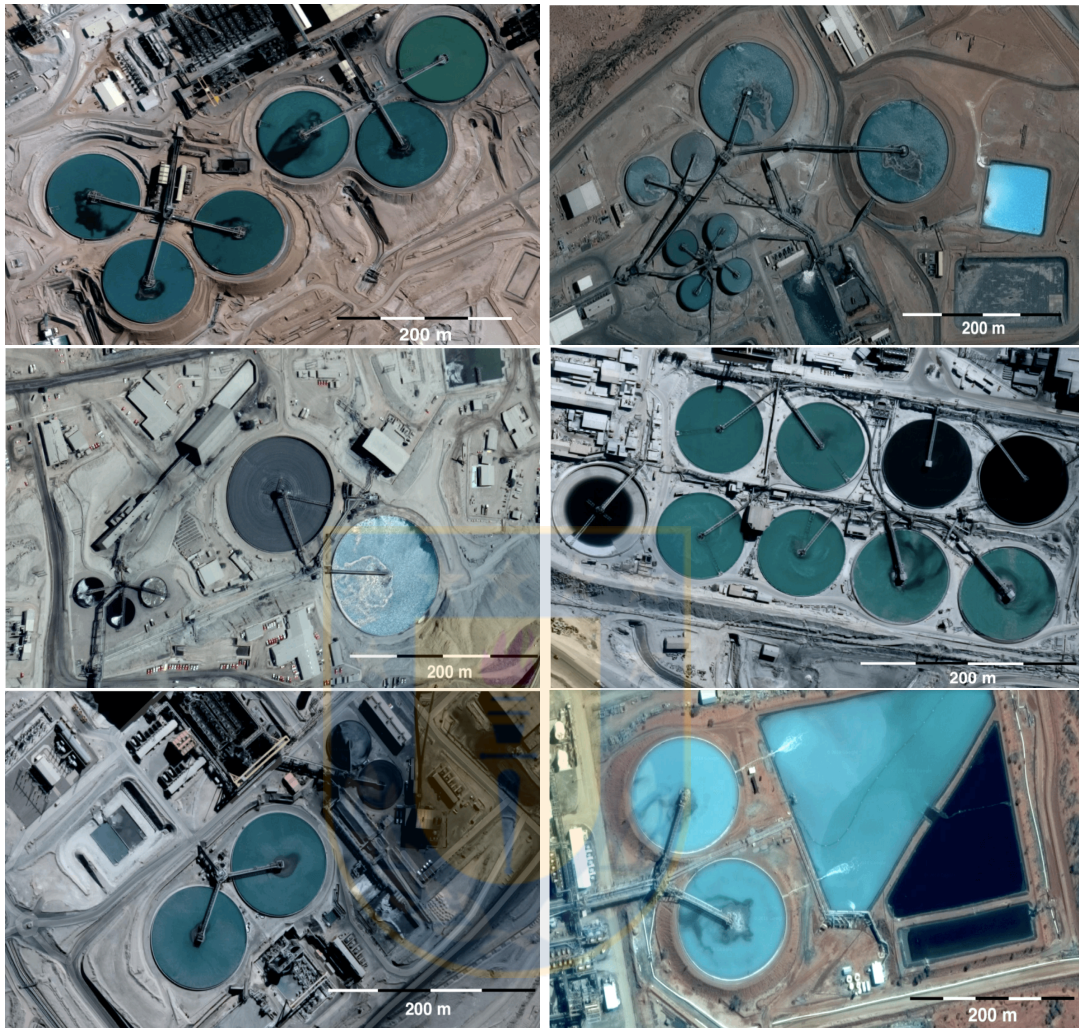


Figure 4: Short-circuit analysis. A couple of thickener in operation in Chile and Australia. In order from left to right and upper to down: (a) Escondida mine, Chile (b) Collahuasi mine, Chile (c) Candelaria mine, Chile (d) CODELCO Chuquicamata mine, Chile, (e) CODELCO DMH mine, Chile (f) APEX Wiluna Gold Mine, Australia. Adapted from Imagery ©2018 Google Maps, by Elias Godoy and Camilo Mejías, Retrieved October 01, 2018, from <http://www.maps.google.com/>. adapted with permission.

the feedwell and follow in the direction of this lost flow. The main issue is poor overflow clarity [78].

Short-circuiting is common in regular hydrometallurgical processes (Figures 2-3). An example of this is a quickly Satellite analysis using Imagery by Google Maps (Figure 4) and we can see at least 80% of different thickeners in Chile and Australia present

problems in initial mixing generating losses in water recovery. This is a huge motivation for improving mathematical models for understanding behaviours inside the thickener units to get a better operation control and save water cost and helping communities in their public health conditions related to clean drinking water and adequate treatment and disposal of industrial waters.

Another industry that concerns the sanitation objective (including the management of human waste and solid waste as well as stormwater-drainage-management) are Waste Water Treatment Plants (WWTPs). Wastewater treatment is a process used to convert dirty wastewater into an effluent that can be returned to the water cycle with minimum impact on the environment, or directly reused.

Wastewater treatment

Wastewater treatment consists of a series of physical, chemical and biological processes that aim to eliminate the contaminants present in effluent water for human use.

In Chile, the treatment of wastewater has increased substantially in recent years, reaching a level of coverage close to 99.8% with respect to the sewage collected from the national urban population, which has made it possible the gradual decontamination of the streams of maritime and continental waters.

Wastewater is liquid that normally comes from sinks, bathrooms, kitchens, industries, shops, etc; which are discarded to sewers. These culverts fluids flow into a sewage plant that has various levels of treatment (see Table 1), returning to the water sources a less polluted processed water than in the beginning.

The thickening process occurs in the secondary sedimentation tank (SST, *Secondary settling tank*), and it corresponds to the final step of the secondary stage of the treatment, where the biological flocs are removed. Filtrate, and treated water is produced with low levels of organic matter and suspended matter. Once the biological mass is removed, the resulting water is discharged (or reintroduced) back into the body of natural water (stream, river or bay) or other environment (surface or subsoil), etc. If necessary, an additional disinfection process can be applied before discharging. The process is carried out in a *Wastewater treatment plant*. In Figure 5 a schematic view of the process of the biological treatment of a plant [118] is shown.

The sedimentation and thickening models that will be treated are of a macroscopic nature and have the advantage that they can predict the behavior of a given thickener in relatively large time and space. On the contrary, microscopic information such as

Table 1: Levels of wastewater treatment. Reprinted from [98].

Level of treatment	Description
Preliminary	Remove large objects such as rags, sticks, floating elements, sand and grease that can cause maintenance or operational problems in the following processes.
Primary	Elimination of a portion of the solids and organic matter suspended from the wastewater.
Advanced Primary	Improved removal of suspended solids and organic matter. Typically accompanied by an addition of some chemical or a filtration process.
Secondary	Elimination of biodegradable organic material (in solution or suspension) and suspended solids. Disinfection is also typically included in the definition of a conventional secondary treatment.
Secondary with nutrient removal	Removal of organic material and suspended biodegradable solid and nutrients (nitrogen, phosphorus, or both).
Tertiary	Removal of residual suspended solids (after secondary treatment).
Advanced	Disposal of dissolved and suspended material after a normal biological treatment, when reuse of water is required for certain applications.

the position of a particle given at each instant, it is not possible to obtain and has little practical interest in a process of large scales. For these models, considerations are used that represent solid and liquid particles as continuous phases superimposed within the tank; specifically, we have a *liquid phase*, which is called the clarified water and one *solid phase* (or several *solid phases*), consisting of solids.

Contribution of the thesis

Numerous works including [12, 14, 15, 17–19, 24, 26, 27, 29, 31, 47, 120] have concentrated on the mathematical and numerical analysis of models of sedimentation-consolidation processes of flocculated suspensions given by strongly degenerate convection-diffusion equations of the type

$$\frac{\partial \phi}{\partial t} + \frac{\partial f(\phi)}{\partial x} = \frac{\partial^2 A(\phi)}{\partial x^2}. \quad (1)$$

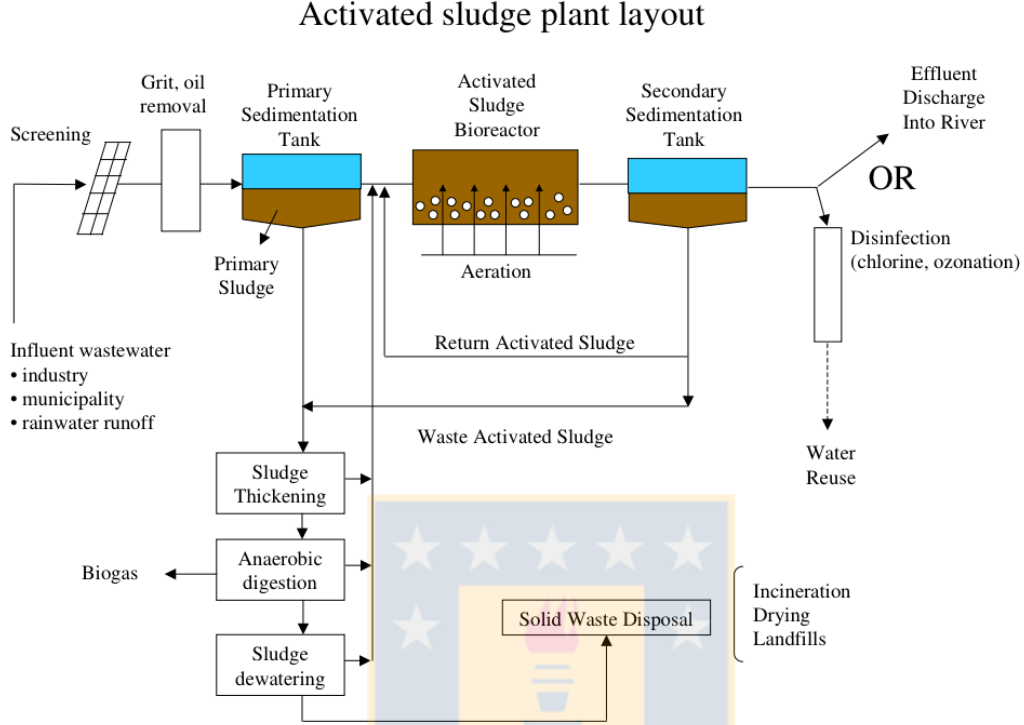


Figure 5: Overview of a biological wastewater treatment facility. Reprinted from [98].

Here the sought unknown is the local solids concentration ϕ as a function of height (or depth) x and time t . The material specific behaviour is described by two functions, namely $f = f(\phi)$ and $A = A(\phi)$. In the simplest setting, namely for batch settling in a column, the convective flux density function f is chosen as the Kynch batch flux density function $f(\phi) = f_b(\phi)$, and we have

$$A(\phi) = \int_0^\phi a(s) ds, \quad a(\phi) = \frac{|f_b(\phi)| \sigma'_e(\phi)}{\Delta \rho g \phi} \quad (2)$$

where g is the acceleration of gravity, $\Delta \rho$ is the solid-fluid density difference, and σ'_e is the derivative of the effective solid stress function that is usually assumed to satisfy

$$\sigma_e(\phi), \sigma'_e(\phi) \begin{cases} = 0 & \text{for } \phi \leq \phi_c, \\ > 0 & \text{for } \phi > \phi_c, \end{cases} \quad (3)$$

where ϕ_c is a critical concentration above which the particles touch each other. Note that (1) is strongly degenerate parabolic or hyperbolic-parabolic since $a(\phi) = 0$ for $u \in [0, \phi_c]$, where the location of the type-change interface $\phi = \phi_c$, i.e., the sediment level or sludge blanket height, is usually unknown beforehand. For batch settling in a column of height L , (1) is equipped with the zero-flux boundary conditions

The precise algebraic forms of the functions f and a , or of f and σ_e , depends on the material under consideration. The determination of $f = f_b$ from suitable settling tests was topic of the author's undergraduate thesis [94], see [8].

Continuously operated sedimentation tanks, which have one inlet and two outlets, are common in mineral processing and wastewater treatment plants. For such processes, additional difficulties arise in the governing partial differential equation (PDE) because of spatially discontinuous coefficients due to the in- and outflows of suspension [25–27, 40, 41, 43, 44].

In wastewater treatment plants, the situation is more complex, since the continuous sedimentation process is coupled to one or several biological reactors in the so-called activated sludge process (ASP). The processes in the biological reactors are often modelled by ordinary differential equations (ODEs). The entire model thus consists of a coupled system of nonlinear ODEs and PDEs.

The simulation model for secondary settling tanks in [18] was introduced mainly to resolve spatial discretization problems when both hindered settling and the phenomena of compression and dispersion are included. Straightforward time integration unfortunately means long computational times. In **Chapter 1** we introduce and investigate time-integration methods for more efficient simulations, but where other aspects such as implementation complexity and robustness are equally considered. The purpose of **Chapter 1** is to present a new linearly implicit (LI) time integration method, which falls within the class of semi-implicit methods for the discretization of (1) plus initial and boundary conditions. The new method is easier to implement than the nonlinearly implicit semi-implicit method described in [16]. That method has the favourable time step restriction common to all semi-implicit treatments of equation (1) but involves the necessity to solve nonlinear systems of algebraic equations. This is avoided by the approach to be pursued in this work.

This results are summarized in:

- R. Bürger, S. Diehl, and C. Mejías. On time discretizations for the simulation of the batch settling-compression process in one dimension. *Water Science and Technology*, 73(5):1010 – 1017, 2016.

Chapter 2 is focused on different kinds of models for secondary settling tanks (SSTs) in water resource recovery facilities. Such a model is extended herein to describe the sedimentation of multicomponent particles that react with several soluble constituents of the liquid phase. The governing model can be expressed as a system of nonlinear partial differential equations (PDEs) that can be solved consecutively in each time step by an explicit numerical scheme. Simulations of denitrification in SSTs illustrate the model and its discretization. Notation here is slightly different, but is according with terms in wastewater treatment community. The main variables are explained in Figure 6. The unknowns are X, L, \mathbf{p}_X and \mathbf{p}_L as functions of z and t .

We define the batch settling flux function $f_b(X) := Xv_{hs}(X)$, where X means concentration and is equivalent with ϕ explained previously. The hindered settling velocity $v_{hs}(X)$ (see [89]) and the function $d_{comp} = d_{comp}(X)$ accounts for the sediment compressibility [18]. The compression function d_{comp} are given by [27]

$$d_{comp}(X) := v_{hs}(X) \frac{\rho_s \sigma'_e(X)}{g \Delta \rho}, \quad (4)$$

where the solid and fluid densities, ρ_X and ρ_L are assumed constant and $\rho_L < \rho_X$, g is the acceleration of gravity, and $\sigma_e = \sigma_e(X)$ is the effective solid stress function, whose derivative satisfies

$$\sigma'_e(X) = \begin{cases} = 0 & \text{for } 0 \leq X < X_c, \\ > 0 & \text{for } X > X_c, \end{cases} \quad (5)$$

where X_c is the material-dependent critical concentration which solids particles start touch each other, and we define the primitive

$$D(X) := \int_{X_c}^X d_{comp}(s) ds. \quad (6)$$

So we can get the following equation

$$\frac{\partial X}{\partial t} = -\frac{\partial}{\partial z} \left(f_b(X) - \frac{\partial D(X)}{\partial z} \right) \quad 0 < z < B, \quad t > 0, \quad (7)$$

and can be solve as is known. In **Chapter 2** we add a source term from the chemical reactions that occurs inside of tank and we can get a equation as:

$$\frac{\partial X}{\partial t} = -\frac{\partial}{\partial z} \left(f_b(X) - \frac{\partial D(X)}{\partial z} \right) + R(X), \quad 0 < z < B, \quad t > 0, \quad (8)$$

where $R(X)$ is a source term that contains reaction and provides an accurate model for reactive settling. This is in fact the Bürger-Diehl model with a reaction term. As a consequence of (5)–(6), the PDE (8) is second-order parabolic wherever the solution X exceeds X_c and first-order hyperbolic for lower concentration values. Thus, the PDE (8) is called strongly degenerate parabolic or parabolic-hyperbolic, where the location of the type-change interface is not known beforehand. Moreover, due to the nonlinear and degenerate nature, discontinuities in the solution appear and special techniques for the numerical solution have to be used (which are incorporated in the numerical method outlined herein).

The total flux within the parenthesis on the right-hand side of (8) is

$$v(X, X_z)X = f_b(X) - \frac{\partial D(X)}{\partial z}. \quad (9)$$

This means that for (8) we can utilize ingredients of the numerical method by [18] with the addition of the reaction term. A way for $R(X)$ is consider that particulate microorganisms are divided into only two components: ordinary heterotrophic organisms (X_{OHO}) and undegradable organics (X_{U}) since we only need access to those state variables to describe the denitrification process. The total concentration of the flocculated particles is $X := X_{\text{OHO}} + X_{\text{U}}$. To find numerical updates for the two portions X_{OHO} and X_{U} of X , we use the idea by [41, 43]. To this end, we introduce the percentage $p := X_{\text{OHO}}/X$ when $X > 0$, so that $X_{\text{OHO}} = pX$ and $X_{\text{U}} = (1 - p)X$, and rewrite X_{OHO} Equation as

$$\frac{\partial(pX)}{\partial t} = -\frac{\partial}{\partial z}(v(X, X_z)pX) + R(X)pX, \quad 0 < z < B, \quad t > 0. \quad (10)$$

Slightly similar for X_{U} . The idea of the numerical method is the following. In each discrete time step, X is first updated via a discretized version of (8). This means that the flux (9) is known during this time step, which is essential for any finite volume numerical method. Since the flux of (10) is p times the known flux (9), it is only the variable p that needs to be updated, and this can be achieved by a discretized version of (10). Then the concentration of the second particulate component is simply $X_{\text{U}} = (1 - p)X$. Those results are summarized in:

- R. Bürger, J. Careaga, S. Diehl, C. Mejías, I. Nopens, P.A. Vanrolleghem, and E. Torfs. Simulations of reactive settling of activated sludge with a reduced biokinetic model. *Computers and Chemical Engineering*, 92:216 – 229, 2016.

Another extension of this new numerical method is explain in details in **Chapter 3** and is based on theory for the system of model PDEs and can be seen as an extension of the

Bürger-Diehl simulation model [18] that includes biological reactions of an activated sludge model no. 1 (ASM1) model by [69] or, in their widely form, different ASMx models. The approach is therefore different from previous investigations on reactive settling [57, 60, 65, 100]

The one-dimensional SST setup is outlined in Figure 6. The model describes the evolution of the concentrations of the solids and liquid phases, $X = X(z, t)$ and $L = L(z, t)$, as functions of depth z and time t . The solid and fluid densities, ρ_X and ρ_L , are assumed to be constant. Moreover, the model keeps track of k_X particulate and k_L liquid components ($k_L - 1$ substrates and water), whose concentrations are collected in vectors $\mathbf{C} = \mathbf{C}(z, t)$, $\mathbf{S} = \mathbf{S}(z, t)$ and $\mathbf{W} = \mathbf{W}(z, t)$ or equivalently, percentage vectors \mathbf{p}_X and \mathbf{p}_L :

$$\mathbf{C} = \mathbf{p}_X X = \begin{pmatrix} p_X^{(1)} \\ \vdots \\ p_X^{(k_X)} \end{pmatrix} X, \quad \sum_{i=1}^{k_X} p_X^{(i)} = 1,$$

$$\mathbf{p}_L L = \begin{pmatrix} p_L^{(1)} \\ \vdots \\ p_L^{(k_L)} \end{pmatrix} L = \begin{pmatrix} \mathbf{S} \\ W \end{pmatrix} = \begin{pmatrix} S^{(1)} \\ \vdots \\ S^{(k_L-1)} \\ W \end{pmatrix}, \quad \sum_{i=1}^{k_L} p_L^{(i)} = 1.$$

The governing model may include a full biokinetic ASMx at every depth z , and is based on the idea that hindered and compressive settling depend on the total particulate concentration (floculated biomass) X . The governing system of equations are given as follows:

$$\frac{\partial X}{\partial t} + \frac{\partial F_X}{\partial z} = \delta(z) \frac{X_f Q_f}{A} + \gamma(z) \tilde{R}_X, \quad \text{where } F_X = Xq + \gamma(z) \left(f_b(X) - \frac{\partial D(X)}{\partial z} \right),$$

$$\frac{\partial(\mathbf{p}_X X)}{\partial t} + \frac{\partial(\mathbf{p}_X F_X)}{\partial z} = \delta(z) \frac{\mathbf{p}_{X,f} X_f Q_f}{A} + \gamma(z) \mathbf{R}_X,$$

$$L = \rho_L \left(1 - \frac{X}{\rho_X} \right),$$

$$\frac{\partial(\bar{\mathbf{p}}_L L)}{\partial t} + \frac{\partial(\bar{\mathbf{p}}_L F_L)}{\partial z} = \delta(z) \frac{\bar{\mathbf{p}}_{L,f} L_f Q_f}{A} + \gamma(z) \bar{\mathbf{R}}_L, \quad \text{where } F_L = \rho_L \left(q - \frac{F_X}{\rho_X} \right),$$

$$p_L^{(k_L)} = 1 - \left(p_L^{(1)} + \dots + p_L^{(k_L-1)} \right),$$

where the variables are explained in Figure 6c. The unknowns are X, L, \mathbf{p}_X and $\bar{\mathbf{p}}_L$ as functions of z and t . Moreover $\bar{\mathbf{p}}_L$. Here we define $f_b(X)Xv_{hs}(X)$, where v_{hs} is the given hindered settling velocity function, and D is a function that describes the

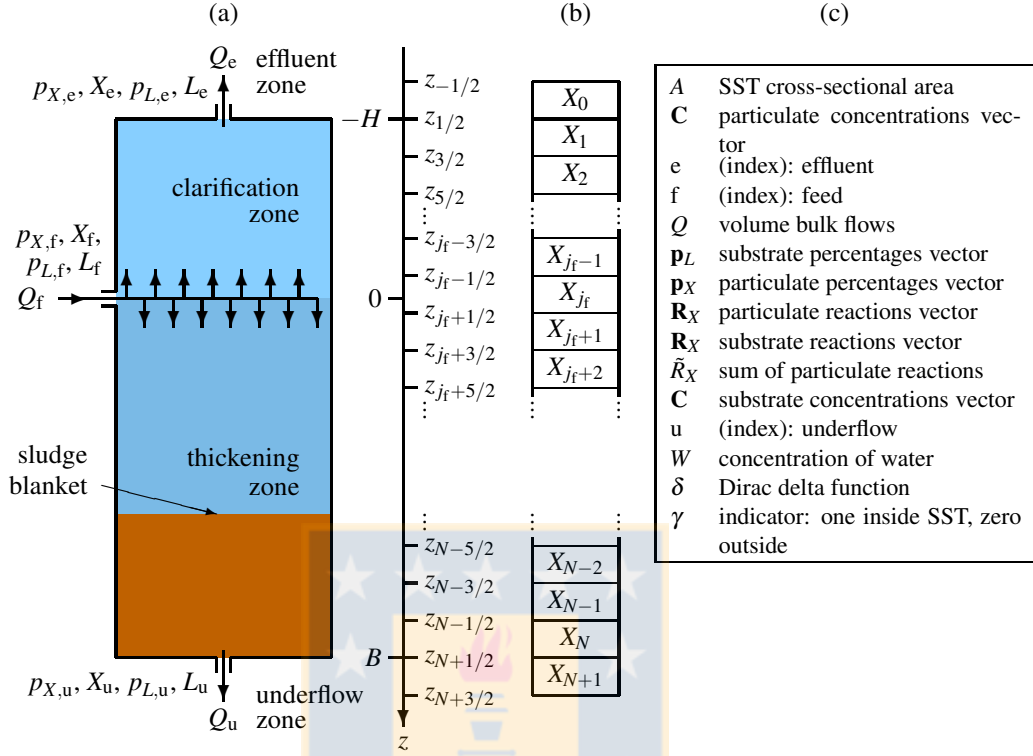


Figure 6: Schematic view of the problem and his variables. (a) An ideal secondary settling tank (SST) with variables of the feed inlet, effluent and underflow indexed with f , e and u , respectively. The effluent, clarification, thickening, and underflow zones correspond to the respective intervals $z < -H$, $-H < z < 0$, $0 < z < B$, and $z > B$. The sludge blanket (concentration discontinuity) separates the hindered settling zone and the compression zone. (b) Aligned illustration of the subdivision of the SST into layers. The SST is divided into N internal computational cells, or layer. (c) Nomenclature for PDE model. Reprinted from [22]

sediment compressibility and satisfies $D(X) = 0$ for velocity q is defined in terms of the given bulk flows as

$$q(z, t) = \begin{cases} \frac{Q_f(t) - Q_u(t)}{A} & \text{for } z < 0 \\ \frac{Q_e(t)}{A} & \text{for } z > 0. \end{cases}$$

Models of SSTs form a topic for well-posedness and numerical analysis even in one space dimension due to the spatially discontinuous coefficients of the underlying strongly degenerate parabolic, nonlinear model PDE. Here we concentrate on the development and analysis of a numerical scheme for the approximate solution of the model [23]. The main difficulties are its coupled nature, the discontinuous dependence of F_X on

spatial position z , and the strongly degenerate behaviour that comes from the fact that $D(X) = 0$ on an X -interval of positive length. This scheme combines a difference scheme for conservation laws with discontinuous flux [27] with an approach of numerical percentage propagation for multi-component flows [42]. The main result is an invariant-region property, which implies that physically relevant numerical solutions are produced.

Those results are summarized in:

- R. Bürger, S. Diehl, and C. Mejías. A difference scheme for a degenerating convection-diffusion-reaction system modelling continuous sedimentation. *ESAIM: Mathematical Modelling and Numerical Analysis*, 52(2): 365 – 392, 2018.
- R. Bürger, S. Diehl, and C. Mejías. A model for continuous sedimentation with reactions for wastewater treatment. In G. Mannia, editor, *Frontiers in Wastewater Treatment and Modelling (FICWTM 2017), Lecture Notes in Civil Engineering*, volume 4, pages 596 – 601, Cham, Switzerland, 2017. Springer International Publishing.
- R. Bürger, J. Careaga, S. Diehl, C. Mejías, and R. Ruiz-Baier. Convection-diffusion-reaction and transport-flow problems motivated by models of sedimentation: some recent advances. In P.N. de Souza and M. Viana, editors, *Proceedings of the International Congress of Mathematicians, Rio de Janeiro 2018 Vol. IV: Invited Lectures*, Singapore. World Scientific, in press.

Introducción

“Asegurar la disponibilidad y gestión sostenible del agua y saneamiento para todos.”. Objetivo de Desarrollo Sostenible Nro. 6 - Asociación General de Naciones Unidas.

La escasez de agua afecta a más del 40 por ciento de la población mundial, una cifra alarmante que probablemente crecerá con el aumento de las temperaturas globales producto del cambio climático. Por esta razón, es que en el año 2015, más de 190 líderes mundiales se comprometieron con *17 Objetivos de Desarrollo Sostenible* [115] para ayudarnos a todos a acabar con la pobreza extrema, combatir la desigualdad y la injusticia, y corregir el cambio climático. Cada uno de nosotros tiene un papel que desempeñar si vamos a lograr estos objetivos de un mundo más próspero, equitativo y sostenible.

El Objetivo de Desarrollo Sostenible No. 6 hace referencia al problema del agua. Si bien, más de la mitad de los hogares en todo el mundo tienen acceso a agua potable en sus hogares, hay un aumento del número de personas sin saneamiento adecuado (un baño seguro), el cual se agudiza a medida que las personas migran a las ciudades producto de la industrialización de países en vías del desarrollo. Como consecuencia de ello, las enfermedades causadas por el agua contaminada matan cada año a más personas que todas las formas de violencia juntas e incluida la guerra. Así, al priorizar el agua limpia, podemos mejorar la salud y los medios de vida de millones de personas [114].

El problema del agua, accesibilidad y saneamiento, es un problema global, y ha sido recogido por muchas organizaciones sin fines de lucro (water.org [136], Global Citizen [63], World Health Organization [138], etc.) quienes buscan concientizar a la población y proveer esfuerzos para mejorar el acceso a agua potable y limpia, así también a mantener o recuperar cuerpos de agua descontaminados (llámese cuerpos de agua, a todas las extensiones de agua que se encuentran por la superficie terrestre o en el subsuelo, tanto naturales como artificiales, es decir, lagos, ríos, lagunas, pozos,

etc.). Esta tesis doctoral se basa en un principio claro: Mejorar la comprensión de las partículas sólidas dentro de un líquido, como el agua, para crear mejores técnicas en la recuperación y reutilización del agua. Este conocimiento puede ser aplicado a industrias o desarrollo de ciudades.

Reutilización del agua en la industria

El consumo de agua es una parte importante en la mayoría de los procesos industriales, como por ejemplo, la industria papelera, química, medicina, vulcanología, bioreactores, tratamiento de aguas residuales, entre otras áreas requieren en sus procesos una gran cantidad de agua y, que por diversos factores, no pueden ser eliminadas directamente a cuerpos de agua sin provocar impactos negativos al entorno. A grandes rasgos, todos estos procesos son similares y poseen una suspensión inicial homogénea que debe ser separada en un líquido clarificado y un sedimento concentrado dentro de un tanque acondicionado para el proceso. En todos los casos, se considera que la suspensión inicial homogénea está compuesta por partículas sólidas y finas, las cuales son pequeñas comparadas con las escalas tanque que las contiene.

En particular, en Chile, la industria minera del cobre es la industria más grande que posee el país, en efecto, aporta un tercio de la producción mundial. Es parte importante del alto y constante crecimiento que ha tenido la economía chilena en las últimas décadas y es innegable su importancia para el desarrollo de nuestro país. Geográficamente hablando, la minería en Chile se desarrolla principalmente en zonas desérticas y muy remotas, específicamente en el Desierto de Atacama, el desierto más árido del mundo, en donde el agua es un recurso escaso, pero a la vez vital para la separación de los metales, como el cobre y la roca dinamitada. Por esta razón la recuperación del agua y la investigación sobre nuevas tecnologías que permitan obtener procesos más eficientes son de interés público y deben ser estudiados.

Después de los procesos de conminución (reducción de tamaño) y flotación (separación del mineral deseado de la ganga) en las plantas de recuperación de minerales de cobre sulfurados, se debe recuperar el agua utilizada en un proceso de sedimentación continua, en donde es necesario separar el agua de las suspensiones de partículas sólidas finas dispersas en un fluido viscoso. La primera y más importante etapa de recuperación de agua es el espesamiento, es decir, la sedimentación continua, donde se utilizan grandes estanques cilíndricos en los cuales se produce la separación de sólidos y líquidos por efecto de la gravedad.

Aquí, junto con desear recuperar la mayor cantidad posible de este recurso después del proceso de sedimentación, también se busca generar un relave lo más seco posible para que en su posterior depósito en lugares de acopio este minimice los riesgos de producir contaminación a las napas subterráneas por medio de líquidos percolados.

Espesadores

El espesador es un equipo inventado por John Van Nostrand Dorr (1872–1962) en 1905 para las plantas concentradoras de oro en Dakota del Sur y significa el comienzo de la era moderna de espesamiento [37] (ver Figura 1).

El concepto de espesamiento es simple y radica en la decantación; consiste en dejar una mezcla líquida y homogénea dentro de un tanque y que las partículas sólidas finas se acumulen en el fondo sólo por efecto de la gravedad, separando así el material sólido, del líquido clarificado en la parte superior. Existen evidencias de este proceso en la cultura egipcia, aproximadamente 2.500 años A.C. [59].

Antes de la innovación de Dorr, los estanques solo poseían un proceso de decantación, es decir un sistema *batch* de sedimentación, el cual es un proceso semi continuo, según documenta Agrícola ya en el año 1556 [2]. El aporte de Dorr radica en ser el primero en evolucionar este proceso semi continuo de decantación, a un proceso continuo de espesamiento; el cual consiste en un tanque que es alimentado por una tubería inserta en él, llamada *alimentación*, la cual agrega continuamente material y éste sedimenta por efecto de la gravedad, obteniendo así en el fondo una mezcla más espesa, la cual es retirada por una tubería en el fondo del tanque, llamada *descarga*, mientras que el agua clara, que se produce en la parte superior, se retira mediante una canaleta, llamada *efluente* [52].

Existen muchos diseños de espesantes en la industria [36] (por ejemplo, convencional, *deep cone*, *hight rate*, en pasta, entre otros). En todos esos casos, la parte principal es el *feedwell*, que garantiza que la energía del flujo de alimentación debe ser disipada y dirigida verticalmente, en lugar de horizontal, y proporciona las condiciones para flocular los sólidos para que primero recojan los sólidos y luego los sedimenten. A veces, el mecanismo del *feedwell* tiene problemas para mantener el correcto y produce un *cortocircuito*, esto significa que el flujo se cortocircuita a través del *feedwell* y puede transportar partículas que no han sido adecuadamente floculadas (Figura 3) Cuando esto sucede, el flujo de alimentación es más probable que escape a mayor diámetro del pozo de alimentación. Los sólidos de la superficie son partículas finas que no se recolectaron en el pozo de alimentación y siguen la dirección de este flujo perdido. El problema principal es la escasa claridad de desbordamiento [78].

Durante el proceso hidrometalúrgico en régimen, es común detectar un cortocircuito (Figura 2). Un ejemplo de esto es un rápido análisis satelital que usa imágenes de Google Maps (Figura 4) y podemos ver que al menos el 80% de espesantes diferentes en Chile y Australia presentan problemas en la mezcla inicial generando pérdidas en recuperación de agua. Esta es una gran motivación para mejorar los modelos matemáticos y así comprender los comportamientos dentro de las unidades de espesadores, obteniendo un mejor control de operación y ahorrar costos de agua y ayuda a las comunidades en sus condiciones de salud pública relacionadas con el agua potable limpia como también en el tratamiento y eliminación adecuada de aguas industriales para su captura. Mejorando así la calidad de vida de las personas.

Otra industria relacionada con el objetivo de saneamiento (que incluye la gestión de desechos humanos y sólidos, así como la gestión de aguas pluviales - drenaje) son las plantas de tratamiento de aguas residuales (PTAR). El tratamiento de aguas residuales es un proceso utilizado para convertir aguas residuales sucias en un efluente que puede devolverse al ciclo del agua con un impacto mínimo en el medio ambiente, o reutilizarse directamente.

Tratamiento de aguas servidas

El tratamiento de aguas residuales consiste en una serie de procesos físicos, químicos y biológicos que tienen como fin eliminar los contaminantes presentes en el agua efluente del uso humano.

En Chile, el tratamiento de las aguas servidas se ha incrementado sustancialmente en los últimos años, alcanzando un nivel de cobertura cercano al 99.8% respecto a las aguas servidas recolectadas de la población urbana nacional, lo cual ha posibilitado la descontaminación paulatina de los cursos de aguas marítimas y continentales.

Las aguas residuales son líquidos que normalmente provienen de lavamanos, baños, cocinas, industrias, comercios, etc; los cuales son desechados a las alcantarillas o cloacas. Estas alcantarillas desembocan en una planta de aguas servidas que tiene diversos niveles de tratamiento (ver Tabla 2), devolviendo a los cauces de agua un agua procesada menos contaminada que en un comienzo.

El proceso de espesamiento ocurre en los tanques de sedimentación secundaria (SST, *Secondary settling tank*, por sus siglas en inglés) y corresponde al paso final de la etapa secundaria del tratamiento, en donde se retiran los flóculos biológicos del material previamente filtrado, y se produce un agua tratada con bajos niveles de materia orgánica y materia suspendida. Una vez que la masa biológica es removida, el agua resultante,

Nivel de tratamiento	Descripción
Preliminar	Remover los objetos grandes tales como trapos, palos, elementos flotantes, arena y grasa que pueden causar problemas de mantenimiento u operacionales en los procesos siguientes.
Primaria	Eliminación de una porción de los sólidos y materia orgánica suspendidos del agua residual.
Primaria avanzada	Eliminación mejorada de sólidos y materia orgánica suspendidos. Típicamente acompañado por una adición de algún químico o un proceso de filtración.
Secundario	Eliminación de material orgánico biodegradable (en solución o suspensión) y sólidos suspendidos. Desinfección es también típicamente incluido en la definición de un tratamiento secundario convencional.
Secundario con eliminación de nutrientes	Eliminación de material orgánico y sólido suspendido biodegradable y nutrientes (nitrógeno, fósforo, o ambos).
Terciario	Eliminación de sólidos suspendidos residuales (después del tratamiento secundario).
Avanzado	Eliminación de material disuelto y suspendido después de un tratamiento biológico normal, cuando se requiere reutilizar el agua para ciertas aplicaciones.

Table 2: Niveles del tratamiento de aguas residuales [98].

es descargada (o reintroducida) de vuelta al cuerpo de agua natural (corriente, río o bahía) u otro ambiente (terreno superficial o subsuelo), etc. De ser necesario, antes de descargar se puede aplicar un proceso de desinfección adicional.

El proceso se lleva a cabo en una *Planta de tratamiento de aguas residuales*, en la 5 se muestra una vista esquemática del proceso del tratamiento biológico de una planta [118].

Los modelos de sedimentación y espesamiento que serán tratados son de carácter macroscópicos y poseen la ventaja que pueden ser capaces de predecir el comportamiento de un espesador dado en un tiempo y espacio relativamente grandes, por el contrario, la información microscópica tal como la posición de una partícula dada en cada instante, no es posible de obtener y tiene poco interés práctico en un proceso de grandes escalas. Para estos modelos, se utilizan consideraciones que representan las partículas sólidas y líquidas como fases continuas superpuestas dentro del tanque; en específico, se tiene una *fase líquida*, la cual se llama a la zona del agua clarificada y una (o varias) *fase sólida (fases sólidas)*, en donde se encuentra el sedimento que decanta.

Contribución de esta tesis

Numerosos trabajos incluidos [12, 14, 15, 17–19, 24, 26, 27, 29, 31, 47, 120] están enfocados en el modelo matemático y análisis numérico de procesos de sedimentación-consolidación de suspensiones floculadas dado por ecuaciones fuertemente degeneradas del tipo

$$\frac{\partial \phi}{\partial t} + \frac{\partial f(\phi)}{\partial x} = \frac{\partial^2 A(\phi)}{\partial x^2}. \quad (11)$$

Aquí lo desconocido es la concentración local de sólidos ϕ en función de la altura (o profundidad) x y el tiempo t . El comportamiento específico del material se describe mediante dos funciones, a saber: $f = f(\phi)$ y $A = A(\phi)$. En la configuración más simple, una sedimentación batch en una columna, la función de densidad de flujo convectivo f se elige como la función de densidad de flujo batch de Kynch $f(\phi) = f_b(\phi)$, y tenemos

$$A(\phi) = \int_0^\phi a(s) ds, \quad a(\phi) = \frac{|f_b(\phi)| \sigma'_e(\phi)}{\Delta \rho g \phi}, \quad (12)$$

donde g es la aceleración de gravedad, $\Delta \rho$ es la diferencia de densidades sólido-líquido, y σ'_e es la derivada de la función de estrés efectivo de sólido, donde el supuesto general es que satisface

$$\sigma_e(\phi), \sigma'_e(\phi) \begin{cases} = 0 & \text{for } \phi \leq \phi_c, \\ > 0 & \text{for } \phi > \phi_c, \end{cases}, \quad (13)$$

donde ϕ_c es una concentración crítica sobre la cual las partículas empiezan a interactuar unas a otras. Note que la ecuación 11 es parabólica fuertemente degenerada o bien, hiperbólica-parabólica ya que $a(\phi) = 0$ for $\phi \in [0, \phi_c]$, donde la ubicación de la interfaz de cambio de tipo $\phi = \phi_c$, es decir, el nivel de sedimento o la altura de la capa de lodo, generalmente se desconoce de antemano. Para la sedimentación batch en una columna de altura L , (11) está equipada con las condiciones de límite de flujo cero.

La forma algebraica precisa de las funciones f y a , o de f y σ_e , depende del material en consideración. La determinación de $f = f_b$ a partir de las pruebas de ajuste adecuadas fue tema de la tesis de ingeniería del autor [94], (ver [8]).

Los tanques de sedimentación de operación continua, que tienen una entrada y dos salidas, son comunes en las plantas de procesamiento de minerales y de tratamiento de aguas residuales. Para tales procesos, surgen dificultades adicionales en la ecuación

diferencial parcial (EDP) que rige debido a coeficientes espacialmente discontinuos debidos a las entradas y salidas de la suspensión [25–27, 40, 41, 43, 44].

En las plantas de tratamiento de aguas residuales, la situación es más compleja, ya que el proceso de sedimentación continua se acopla a uno o varios reactores biológicos en el llamado proceso de lodo activado (ASP, por sus siglas en inglés). Los procesos en los reactores biológicos a menudo se modelan mediante ecuaciones diferenciales ordinarias (EDO). El modelo completo consiste así en un sistema acoplado de EDOs no lineales y EDPs

El modelo de simulación para tanques de asentamiento secundarios en [18] se introdujo principalmente para resolver problemas de discretización espacial cuando se incluyen tanto el asentamiento obstaculizado como los fenómenos de compresión y dispersión. La integración de tiempo directa desafortunadamente significa tiempos computacionales largos. En **Capítulo 1** introducimos e investigamos métodos de integración de tiempo para simulaciones más eficientes, pero donde otros aspectos, como la complejidad de implementación y la robustez, se consideran igualmente. El propósito del **Capítulo 1** es implementar, aplicar y probar la convergencia de un nuevo método de integración de tiempo linealmente implícito (LI), que se encuentra dentro de la clase de métodos semi-implícitos para la discretización de (11) más las condiciones iniciales y de contorno. El nuevo método es más fácil de implementar que el método semi-implícito implícito no lineal descrito en [16]. Ese método disfruta de la restricción de paso de tiempo favorable común a todos los tratamientos semi-implícitos de (11) pero implica la necesidad de resolver sistemas no lineales de ecuaciones algebraicas. Esto se evita por el enfoque que se persigue en este trabajo.

Estos resultados están resumidos en:

- R. Bürger, S. Diehl, and C. Mejías. On time discretizations for the simulation of the batch settling-compression process in one dimension. *Water Science and Technology*, 73(5):1010 – 1017, 2016.

El **Chapter 2** esta centrado en diferentes tipos de modelos para tanques se asentamiento secundario (SST, por sus siglas en ingles) en instalaciones de recuperación de recursos hídricos. Dicho modelo se extiende aquí para describir la sedimentación de partículas multicomponentes que reaccionan con varios constituyentes solubles de la fase líquida. El modelo gobernante se puede expresar como un sistema de ecuaciones diferenciales parciales no lineales (EDPs) que se pueden resolver consecutivamente en cada paso de tiempo mediante un esquema numérico explícito. Las simulaciones de desnitrificación en SST ilustran el modelo y su discretización. La notación de este

capítulo es levemente diferente al anterior, pero es acorde al estándar de la comunidad de tratamiento de aguas servidas. Las principales variables están explicadas en la Figura 6. Las variables son X , L , \mathbf{p}_X and \mathbf{p}_L como función de z y t .

Definimos la función de flujo de sedimentación batch $f_b(X) := X v_{hs}(X)$, donde X es la concentración y es equivalente con la variable ϕ explicada previamente. La velocidad de sedimentación obstaculizada $v_{hs}(X)$ es tal como fue definida en [89] y la función $d_{comp} = d_{comp}(X)$ es la encargada de medir la compresibilidad del sedimento (ver [18]) y está dada por [27]:

$$d_{comp}(X) := v_{hs}(X) \frac{\rho_s \sigma'_e(X)}{g \Delta \rho}, \quad (14)$$

donde las densidades del sólido y del fluido, ρ_s y ρ_f se consideran constantes y tales que $\rho_f < \rho_s$; g es la aceleración de gravedad y $\sigma_e = \sigma_e(X)$ es la función de estrés efectivo de sólidos, cuya derivada satisface

$$\sigma'_e(X) = \begin{cases} = 0 & \text{para } 0 \leq X < X_c, \\ > 0 & \text{para } X > X_c, \end{cases} \quad (15)$$

donde X_c es la concentración crítica, que depende del material, y consiste en el punto en que las partículas sólidas empiezan a tocarse unas a otras. Definimos la primitiva

$$D(X) := \int_{X_c}^X d_{comp}(s) ds. \quad (16)$$

Así podemos obtener la siguiente ecuación:

$$\frac{\partial X}{\partial t} = -\frac{\partial}{\partial z} \left(f_b(X) - \frac{\partial D(X)}{\partial z} \right) \quad 0 < z < B, \quad t > 0, \quad (17)$$

y podemos resolver como es conocido. En **Capítulo 2** añadimos un término fuente proveniente de reacciones químicas que ocurren dentro del tanque y podemos obtener una ecuación como:

$$\frac{\partial X}{\partial t} = -\frac{\partial}{\partial z} \left(f_b(X) - \frac{\partial D(X)}{\partial z} \right) + R(X), \quad 0 < z < B, \quad t > 0, \quad (18)$$

donde $R(X)$ es un término fuente que contiene reacciones y provee un modelo más preciso para la sedimentación reactiva. Esto es, en efecto, el modelo de Bürger-Diehl con un término de reacción. Como consecuencia de (15)-(16), la EDP (18) es del tipo parabólica de segundo orden cuando X excede X_c y es hiperbólica de primer orden para concentraciones menores que X_c . Así, la EDP (18) es llamada parabólica fuertemente degenerada o ecuación parabólica-hiperbólica, donde la posición del tipo de cambio

de interface no es conocido a priori. Más aún, la naturaleza no lineal y degenerada, provoca que discontinuidades aparezcan en la solución aún si el dato inicial es suave, lo que provoca que técnicas numéricas especiales deben ser empleadas para su resolución.

El flujo total, dentro del paréntesis del lado derecho de (18) es

$$v(X, X_z)X = f_b(X) - \frac{\partial D(X)}{\partial z}. \quad (19)$$

Esto significa que para (18) podemos utilizar ingredientes del método numérico de [18] con la adición del término de reacción. Un camino para $R(X)$ es considerar que microorganismos particulados están clasificados sólo en dos grupos: organismos heterotróficos ordinarios (X_{OHO} , con OHO, por sus siglas en inglés) y orgánicos no degradables (X_{U} , con U, por su sigla en inglés de *undegradable*) y que se sustentan en los únicos estados posibles en el proceso que describe la denitrificación. De esta manera, la concentración total de partículas floculadas es $X := X_{\text{OHO}} + X_{\text{U}}$. Para actualizar numéricamente las variables X , X_{OHO} y X_{U} usamos las ideas propuestas en [41, 43], esto es, introducir la variable porcentaje o cociente $p := X_{\text{OHO}}/X$ cuando $X > 0$, así, $X_{\text{OHO}} = pX$ y $X_{\text{U}} = (1 - p)X$, y podemos reescribir (18) para X_{OHO} como

$$\frac{\partial(pX)}{\partial t} = -\frac{\partial}{\partial z}(v(X, X_z)pX) + R(X)pX, \quad 0 < z < B, \quad t > 0. \quad (20)$$

En el caso de X_{U} se procede similarmente. La idea del método numérico propuesto es el siguiente: En cada paso de tiempo discreto, X es la primera en ser actualizada a través de una discretización de (18). Esto significa que el flujo (19) es conocido durante este paso de tiempo, el cual es esencial para cualquier método numérico de volúmenes finitos. Debido a que el flujo de (20) es p veces el flujo conocido en (19), solo se necesita actualizar p , y se puede proceder con una versión discreta de (19). Luego la concentración del segundo componente particulado es simplemente $X_{\text{U}} = (1 - p)X$. Los resultados y detalles están explicados en:

- R. Bürger, J. Careaga, S. Diehl, C. Mejías, I. Nopens, P.A. Vanrolleghem, and E. Torfs. Simulations of reactive settling of activated sludge with a reduced biokinetic model. *Computers and Chemical Engineering*, 92:216 – 229, 2016.

Una extensión de este método numérico es explicado en detalles en **Capítulo 3** y está basado en la teoría para el modelo de sistema de ecuaciones diferenciales parciales y puede ser visto como una extensión del modelo de Bürger-Diehl [18] que incluye reacciones biológicas de un modelo de lodos activados número 1 (ASM1, por sus siglas en inglés) dado por [69] o, en su forma más amplia, diferentes modelos ASMx. La

aproximación es por lo tanto, diferente a las previas investigaciones en sedimentación reactiva [57, 60, 65, 100]).

En Figura 6 se muestra un tanque de sedimentación secundario en una dimensión junto con la distribución de sus principales variables de entrada y salida. El modelo describe la evolución de las concentraciones de las fases sólida y líquida, $X = X(z, t)$ y $L = L(z, t)$, como funciones de profundidad z y tiempo t . Las densidades de sólido y líquido, ρ_X y ρ_L , respectivamente, son consideradas constantes. Además, el modelo mantiene la cantidad de componentes particulados k_X y componentes líquidos k_L de manera constante en el tiempo. Note que la cantidad de sustratos es $k_L - 1$ si consideramos el agua como el k_L -ésimo componente líquido. Las respectivas concentraciones son almacenadas en los vectores $\mathbf{C} = \mathbf{C}(z, t)$, $\mathbf{S} = \mathbf{S}(z, t)$ y $W = W(z, t)$ o equivalentemente, en vectores de porcentajes \mathbf{p}_X y \mathbf{p}_L :

$$\mathbf{C} = \mathbf{p}_X X = \begin{pmatrix} p_X^{(1)} \\ \vdots \\ p_X^{(k_X)} \end{pmatrix} X, \quad \sum_{i=1}^{k_X} p_X^{(i)} = 1,$$

$$\mathbf{p}_L L = \begin{pmatrix} p_L^{(1)} \\ \vdots \\ p_L^{(k_L)} \end{pmatrix} L = \begin{pmatrix} \mathbf{S} \\ W \end{pmatrix} = \begin{pmatrix} S^{(1)} \\ \vdots \\ S^{(k_L-1)} \\ W \end{pmatrix}, \quad \sum_{i=1}^{k_L} p_L^{(i)} = 1.$$

El modelo gobernante puede incluir una biocinética completa ASMx en cada punto de profundidad z , y está basada en la idea del asentamiento compresivo y obstaculizado, que depende del total de la concentración particulada (biomasa floculada) X . El sistema gobernante de ecuaciones es:

$$\frac{\partial X}{\partial t} + \frac{\partial F_X}{\partial z} = \delta(z) \frac{X_f Q_f}{A} + \gamma(z) \tilde{\mathbf{R}}_X, \quad \text{where } F_X = Xq + \gamma(z) \left(f_b(X) - \frac{\partial D(X)}{\partial z} \right),$$

$$\frac{\partial(\mathbf{p}_X X)}{\partial t} + \frac{\partial(\mathbf{p}_X F_X)}{\partial z} = \delta(z) \frac{\mathbf{p}_{X,f} X_f Q_f}{A} + \gamma(z) \mathbf{R}_X,$$

$$L = \rho_L \left(1 - \frac{X}{\rho_X} \right),$$

$$\frac{\partial(\bar{\mathbf{p}}_L L)}{\partial t} + \frac{\partial(\bar{\mathbf{p}}_L F_L)}{\partial z} = \delta(z) \frac{\bar{\mathbf{p}}_{L,f} L_f Q_f}{A} + \gamma(z) \bar{\mathbf{R}}_L, \quad \text{donde } F_L = \rho_L \left(q - \frac{F_X}{\rho_X} \right),$$

$$p_L^{(k_L)} = 1 - \left(p_L^{(1)} + \dots + p_L^{(k_L-1)} \right),$$

donde las variables son explicadas en Figura 6c. Las variables a determinar son X, L, \mathbf{p}_X y \mathbf{p}_L como funciones de z y t , Además de \bar{p}_L . Definiendo $f_b(X)Xv_{hs}(X)$, donde v_{hs} es la velocidad de sedimentación obstaculizada dada, y D es una función que describe la compresibilidad del sedimento y satisface $D(X) = 0$ para una velocidad q es definida en términos del flujo *bulk* dado como

$$q(z, t) = \begin{cases} \frac{Q_f(t) - Q_u(t)}{A} & \text{for } z < 0 \\ \frac{Q_e(t)}{A} & \text{for } z > 0. \end{cases}$$

Los modelos de tanques de sedimentación secundarios forman un tópico por si mismo, ya sea para el buen planteamiento de las ecuaciones o bien para el análisis numérico de los métodos propuestos, incluso si se resuelve el problema en una dimensión espacial. Esto, al tratarse con coeficientes espacialmente discontinuos dentro de un modelo de EDPs no lineal y parabólico fuertemente degenerado. El desafío abordado en el presente capítulo fue desarrollar y analizar un esquema numérico coherente para aproximar la solución del modelo (ver [23]). Las principales dificultades identificadas fueron con la naturaleza acoplada del modelo, la dependencia discontinua de F_X en la posición espacial z y el comportamiento fuertemente degenerado proveniente del efecto de $D(X) = 0$ en un X -intervalo de largo positivo. Este esquema combina un esquema por diferencias finitas para las leyes de conservación con flujo discontinuo (ver [27]) con una aproximación de la propagación del porcentaje numérico para flujos multicomponente (ver [42]). El principal resultado es la propiedad de una región invariante, la cual implica que se producen soluciones físicamente relevantes.

Estos resultados están resumidos en:

- R. Bürger, S. Diehl, and C. Mejías. A difference scheme for a degenerating convection-diffusion-reaction system modelling continuous sedimentation. *ESAIM: Mathematical Modelling and Numerical Analysis*, 52(2):365 – 392, 2018.
- R. Bürger, S. Diehl, and C. Mejías. R. Bürger, S. Diehl, and C. Mejías. A model for continuous sedimentation with reactions for wastewater treatment. In G. Mannia, editor, *Frontiers in Wastewater Treatment and Modelling (FICWTM 2017)*, *Lecture Notes in Civil Engineering*, volume 4, pages 596 – 601, Cham, Switzerland, 2017. Springer International Publishing.
- R. Bürger, J. Careaga, S. Diehl, C. Mejías, and R. Ruiz-Baier. Convection-diffusion-reaction and transport-flow problems motivated by models of sedimentation: some recent advances. In P.N. de Souza and M. Viana, editors, *Proceedings of the International Congress of Mathematicians, Rio de Janeiro 2018 Vol. IV: Invited Lectures*, number 3489 – 3514, Singapore, 2018. World Scientific.

Chapter 1

On time discretizations for the simulation of the batch settling - compression process in one dimension

The main purpose of the Bürger-Diehl simulation model for secondary settling tanks was to resolve spatial discretization problems when both hindered settling and the phenomena of compression and dispersion are included. Straightforward time integration unfortunately means long computational times, so the next step in the development is to introduce and investigate time-integration methods for more efficient simulations, but where other aspects such as implementation complexity and robustness are equally considered. This is done for batch settling simulations. The key findings are partly a new time-discretization method and partly its comparison with other specially tailored and standard methods. Several advantages and disadvantages for each method are given. One conclusion is that the new linearly implicit method is easier to implement than another one (semi-implicit method), but less efficient based on two types of batch sedimentation test.

The results of this Chapter are published in:

- R. Bürger, S. Diehl, and C. Mejías. On time discretizations for the simulation of the batch settling-compression process in one dimension. *Water Science and Technology*, 73(5):1010 – 1017, 2016.

1.1 Introduction

Benchmark simulations of entire wastewater treatment plants (WWTPs) are today performed with one-dimensional simulation models of the secondary settling tank [61, 91]. In the model by [20, 24], sometimes referred to as “Bürger-Diehl model”, the physical phenomena of hindered settling, volumetric bulk flows, compression of the sludge at high concentrations and dispersion of the suspension near the feed inlet can be included in a flexible way. Each phenomenon is associated with a separate constitutive function with its model parameters, and can be activated or de-activated at the user’s discretion. The possibility to include sludge compression is particularly important, since this improves the predictive power considerably ([34, 66, 105, 120, 122]). However, the inclusion of physical phenomena that result in second-order derivative terms in the model partial differential equation (PDE), e.g. compression, means that straightforward time discretization by easy-to-implement, explicit methods such as the explicit Euler method leads to long simulation times.

In [18] the author provided implementation details of a numerical algorithm, which gives reliable simulations with respect to the underlying physical principles and can be obtained with a user-defined accuracy. For long-time simulations of entire WWTPs, it is important to keep discretization errors small. This calls for a fine resolution in both space (many layers in the settler) and time (short time steps), which implies long computational times. Conversely, fast computations obtained with a low resolution in space and time come at the cost of poor accuracy.

In scientific computing, the numerical error is a measure of how close a numerical solution is to the exact solution or reference solution (obtained by a very fine discretization) of the model, i.e., the governing differential equation. The efficiency of a numerical method is assessed by relating the numerical errors to the computational (central processing unit; CPU) times necessary to obtain the numerical solutions for different discretizations. It is then said that one numerical method is more efficient than another if it allows to obtain a numerical solution with a determined numerical error in less CPU time, or equivalently, a given budget of CPU time allows one to obtain a more accurate numerical solution by the first method than by the second.

The simulation model of [18] is based on a method-of-lines formulation of the underlying nonlinear PDE. This means a system of time-dependent ordinary differential equations (ODEs), one for each layer of the settler. Simulations of PDEs are stable and reliable if a so-called CFL (Courant-Friedrichs-Lewy) condition is satisfied. This gives a maximal time step Δt for each given layer thickness Δz . If only hindered settling and bulk flows

are included, then the CFL condition means that Δt can be chosen proportional to Δz , i.e., $\Delta t \sim \Delta z$, which results in fast simulations. When compression or dispersion is included and standard ODEs solvers used, the CFL condition states that $\Delta t \sim (\Delta z)^2$, which means very small Δt when the error should be reduced (small Δz is chosen).

The purpose of this contribution is to investigate different time-integration methods, of which one is new, with respect to efficiency and other aspects, such as implementation complexity. There is a qualitative difference in the numerical treatment depending on whether only hindered settling and bulk flows are considered or, if in addition, compression or dispersion are included. For clarity of presentation, we limit ourselves here to batch sedimentation in a vessel with a constant cross-sectional area, and for which the depth z is measured from the suspension surface downwards to the bottom at $z = B$. The model partial differential equation (PDE) is

$$\frac{\partial C}{\partial t} = -\frac{\partial f(C)}{\partial z} + \frac{\partial}{\partial z} \left(d(C) \frac{\partial C}{\partial z} \right), \quad 0 < z < B, \quad t > 0, \quad (1.1)$$

where the flux function $f(C) = C v_{\text{hs}}(C)$ contains the hindered settling velocity function $v_{\text{hs}}(C)$ and the compression function is $d(C) = K v_{\text{hs}}(C) \sigma'_e(C)$, where K is a constant containing the solid and fluid mass densities and the acceleration of gravity, and σ_e is the effective solid stress function, which is zero below a critical concentration and increasing above.

The investigated methods are used for the simulation of two different batch settling tests in a vessel with $B = 1$ m. While the present study is limited to batch settling in a column, the method proposed herein should be appropriate to handle SSTs as well (under suitable modifications that would mainly affect the convective flux, but not the compression term for whose discretization the present method has been tailored). It is therefore essential to demonstrate that the method can robustly handle several scenarios, in particular such that exhibit some spatial variation of the solution. For this reason we consider a conventional Kynch test [89], that is, the settling of an initially homogeneous suspension, and a Diehl test [45], where a body of concentrated suspension is initially located above clear liquid, separated by, e.g., a membrane. The Diehl test shows a stronger variation of the solution than the Kynch test. Both tests provide complementary information that can be used to identify large portions of the flux function f [8].

1.2 Methods of discretization

As hindered settling velocity function we choose for simplicity $v_{\text{hs}}(C) = v_0 e^{-rC}$ with $v_0 = 10$ m/h and $r = 0.45$ m³/kg, and the effective solids stress chosen is

$$\sigma_e(C) = \begin{cases} 0 & \text{for } 0 \leq C \leq C_c, \\ \alpha(C - C_c) & \text{for } C > C_c, \end{cases}$$

where $\alpha = 0.5$ m²/s² and $C_c = 6$ kg/m³. To obtain a working numerical method an important preparation is to compute the primitive

$$D(C) := \int_0^C d(s) ds$$

of the compression function $d(C)$. In the present case, with the functions $v_{\text{hs}}(C)$ and $\sigma_e(C)$ chosen herein, we can obtain $D(C)$ in closed algebraic form; if this is not possible (for other choices of these functions), the function $D(C)$ can be obtained numerically [18]. Now (1.1) can be written as

$$\frac{\partial C}{\partial t} = \frac{\partial}{\partial z} \left(-f(C) + \frac{\partial D(C)}{\partial z} \right).$$

For batch sedimentation, this PDE should be complemented with initial data $C(z, 0) = C_0(z)$ and zero-flux boundary conditions

$$-f(C) + \frac{\partial D(C)}{\partial z} \Big|_{z=0} = 0 = -f(C) + \frac{\partial D(C)}{\partial z} \Big|_{z=B}. \quad (1.2)$$

Suitable numerical schemes for the approximate solution of (1.1) are based on subdividing the depth interval $[0, B]$ into a number N of layers of equal thickness $\Delta z = B/N$. A discretization in space leads to the following method-of-lines formulation [18], which is a system of N ODEs

$$\frac{dC_1}{dt} = -\frac{G_{3/2}}{\Delta z} + \frac{J_{3/2}}{\Delta z}, \quad (1.3)$$

$$\frac{dC_j}{dt} = -\frac{G_{j+1/2} - G_{j-1/2}}{\Delta z} + \frac{J_{j+1/2} - J_{j-1/2}}{\Delta z}, \quad j = 2, \dots, N-1, \quad (1.4)$$

$$\frac{dC_N}{dt} = \frac{G_{N-1/2} - J_{N-1/2}}{\Delta z}, \quad (1.5)$$

where $C_j(t)$ is the concentration of layer j , $G_{j+1/2}$ denotes the numerical convective flux due to hindered settling between layer j and layer $j + 1$, which can be chosen, for instance, as the Godunov flux, and $J_{j+1/2}$ is the compressive numerical flux chosen as

$$J_{j+1/2} = \frac{D(C_{j+1}) - D(C_j)}{\Delta z}.$$

Note that (1.2) implies that the boundary fluxes $G_{1/2} = J_{1/2} = G_{N+1/2} = J_{N+1/2} = 0$. Implementation details on how to compute these fluxes are provided by [18]. The last term in (1.4) now becomes the usual second-order difference approximation of $\partial^2 D(C)/\partial z^2$, i.e.,

$$\frac{J_{j+1/2} - J_{j-1/2}}{\Delta z} = \frac{D(C_{j+1}) - 2D(C_j) + D(C_{j-1}))}{\Delta z^2}. \quad (1.6)$$

The method-of-lines formulation (1.3)–(1.5) is converted into a fully discrete scheme by time discretization. Although a variety of methods could be used for (1.3)–(1.5), there is nothing to gain by applying a standard ODE solver of accuracy higher than first order, e.g. a Runge-Kutta method. On the contrary, this will only cause longer computational times producing the same error as explicit Euler time stepping [49].

For the discussion of the various time-stepping methods, which will take the numerical solution from $t = t_n$ to $t_{n+1} = t_n + \Delta t$, it will be important to carefully distinguish between numerical fluxes and concentrations that are evaluated at the old time step t_n and those evaluated at t_{n+1} , which we mark by the respective upper index n and $n + 1$. The time-integration methods compared herein are the following, where k_1, k_2 are constants that depend on the choice of the functions f and d .

1.2.1 The explicit Euler method

The explicit Euler method is used for all simulations in [20, 24]. The CFL condition of the fully discrete scheme can be captured by $\Delta t \leq k_2 \Delta z^2$ when Δz is small. The method is easy to implement since all terms in the right-hand side of (1.3)–(1.5) are evaluated at $t = t_n$ and therefore each concentration C_j^{n+1} is an explicit function of the known ones at the previous time t_n . Thus, the fully discrete version of (1.4) is

$$\frac{C_j^{n+1} - C_j^n}{\Delta t} = -\frac{G_{j+1/2}^n - G_{j-1/2}^n}{\Delta z} + \frac{D(C_{j+1}^n) - 2D(C_j^n) + D(C_{j-1}^n)}{\Delta z^2}, \quad j = 2, \dots, N - 1,$$

with analogous formulas replacing the boundary updates (1.3) and (1.5).

1.2.2 The semi-implicit (SI) method

The SI method [16] is described in detail in [47]. The CFL condition is $\Delta t \leq k_1 \Delta z$. To advance the solution from t_n to t_{n+1} we must solve the following nonlinear system of algebraic equations, where C_j^{m+1} , $j = 1, \dots, N$, are the unknowns:

$$\frac{C_j^{m+1} - C_j^m}{\Delta t} = -\frac{G_{j+1/2}^m - G_{j-1/2}^m}{\Delta z} + \frac{D(C_{j+1}^{m+1}) - 2D(C_j^{m+1}) + D(C_{j-1}^{m+1})}{\Delta z^2}, \quad (1.7)$$

$j = 2, \dots, N - 1$, supplemented with analogous formulas replacing the boundary updates (1.3) and (1.5). These equations are solved iteratively, for example, by the Newton-Raphson method.

1.2.3 The linearly implicit (LI) method

The idea of the LI method goes back to [6] and is based on first considering the contribution from the compressive flux term (1.6) from time t_n to t_{n+1} . The purpose of the LI method is to avoid the numerical solution of the nonlinear system of equations (1.7). The nonlinearities in (1.7) are found in the evaluations of the function D . The idea is to replace $D(C_j^n)$ in (1.7) by ξq_j^n (where ξ is a parameter connected to the convergence of the method) so that

$$\frac{C_j^{n+1} - C_j^n}{\Delta t} = -\frac{G_{j+1/2}^n - G_{j-1/2}^n}{\Delta z} + \xi \frac{q_{j-1}^{n+1} - 2q_j^{n+1} + q_{j+1}^{n+1}}{\Delta z^2}, \quad (1.8)$$

and to find a simple update formula for q_j^n , $j = 1, \dots, N$, to be executed first in each time step. A stable implicit Euler time step implies the formula

$$\frac{q_j^{n+1} - q_j^n}{\Delta t} = \xi \frac{q_{j-1}^{n+1} - 2q_j^{n+1} + q_{j+1}^{n+1}}{\Delta z^2}.$$

This means that a linear system of equations should be solved for q_j^{n+1} at the next time step. Then (1.8) can be updated explicitly to obtain C_j^{m+1} .

To completely describe the LI method, we define

$$\xi := \gamma \max_{0 \leq C \leq C_{\max}} d(C),$$

where C_{\max} is a (nominal) maximum concentration and $\gamma > 1$ a parameter. This parameter can be chosen at the user's discretion. To provide some guidance we mention that based on theoretical considerations (not detailed here) and numerical evidence

(presented below), the closer $\gamma > 1$ is chosen to the value one, the more accurate is the scheme. However, the admissible time step Δt behaves as $\Delta t \rightarrow 0$ when $\gamma \rightarrow 1$. Consequently, the choice of γ is subject to the competing goals of accuracy (small errors) and speed (short CPU times) of the simulation. A detailed discussion of the optimal choice of γ under these restrictions is provided below.

To advance the solution from t_n to t_{n+1} , one proceeds as follows:

1. For $j = 1, \dots, N$, set $q_j^n = D(C_j^n)/\xi$.
2. Solve the following linear system for $q_1^{n+1}, \dots, q_N^{n+1}$:

$$\begin{aligned} \frac{q_1^{n+1} - q_1^n}{\Delta t} &= -\xi \frac{q_1^{n+1} - q_2^{n+1}}{\Delta z^2}, \\ \frac{q_j^{n+1} - q_j^n}{\Delta t} &= \xi \frac{q_{j-1}^{n+1} - 2q_j^{n+1} + q_{j+1}^{n+1}}{\Delta z^2}, \quad j = 2, \dots, N-1, \\ \frac{q_N^{n+1} - q_N^n}{\Delta t} &= \xi \frac{q_{N-1}^{n+1} - q_N^{n+1}}{\Delta z^2}. \end{aligned} \quad (1.9)$$

3. Calculate $C_1^{n+1}, \dots, C_N^{n+1}$ from

$$\begin{aligned} \frac{C_1^{n+1} - C_1^n}{\Delta t} &= -\frac{G_{3/2}^n}{\Delta z^2} + \frac{q_1^{n+1} - q_1^n}{\Delta t}, \\ \frac{C_j^{n+1} - C_j^n}{\Delta t} &= -\frac{G_{j+1/2}^n - G_{j-1/2}^n}{\Delta z} + \frac{q_j^{n+1} - q_j^n}{\Delta t}, \quad j = 2, \dots, N-1, \\ \frac{C_N^{n+1} - C_N^n}{\Delta t} &= \frac{G_{N-1/2}^n}{\Delta z} + \frac{q_N^{n+1} - q_N^n}{\Delta t}. \end{aligned}$$

Note that the linear system (1.9) can be written as follows, where $\mu := \Delta t/\Delta z^2$:

$$\begin{bmatrix} 1 + \xi\mu & -\xi\mu & 0 & \dots & 0 \\ -\xi\mu & 1 + 2\xi\mu & -\xi\mu & \ddots & \vdots \\ 0 & \ddots & \ddots & \ddots & 0 \\ \vdots & \ddots & -\xi\mu & 1 + 2\xi\mu & -\xi\mu \\ 0 & \dots & 0 & -\xi\mu & 1 + \xi\mu \end{bmatrix} \begin{pmatrix} q_1^{n+1} \\ \vdots \\ q_N^{n+1} \end{pmatrix} = \begin{pmatrix} q_1^n \\ \vdots \\ q_N^n \end{pmatrix},$$

This tridiagonal linear system of equations can easily be solved, for example by the Thomas algorithm [49]. A preliminary analysis on the stability of the scheme (not

presented here) implies that the CFL condition of the LI scheme is

$$\Delta t \leq \frac{\Delta z}{2 \max_{0 \leq C \leq C_{\max}} f'(C)} \left(1 - \frac{1}{\gamma}\right). \quad (1.10)$$

1.2.4 Other time-stepping methods

Any ODE solver could be used for the method-of-lines system (1.3)–(1.5). Possibly competitive methods are adaptive step-size methods and we choose here the ODE solver `ode15s` in Matlab (2014), which is an implicit multi-step method of variable order with step-size control. Of several standard ODE solvers investigated by [49] this was the second most efficient one (after the SI method) in the investigations with both stand-alone settler simulations and benchmark simulations for the entire activated sludge process.

1.3 Results and discussion

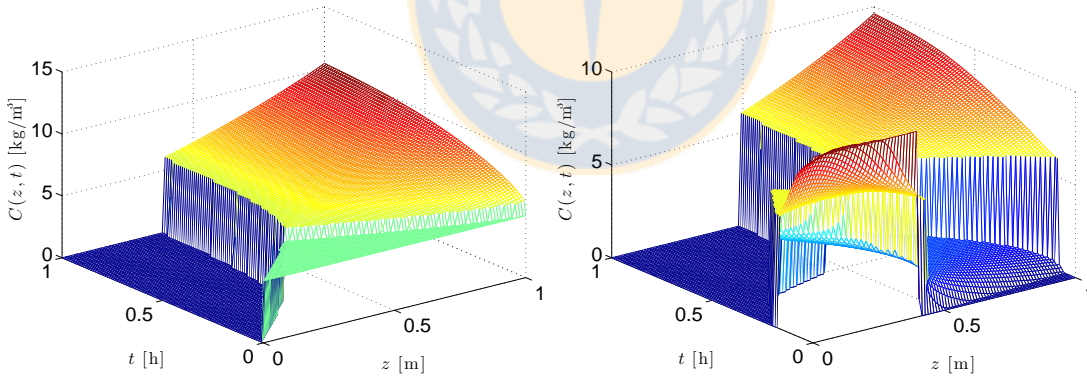


Figure 1.1: Numerical solution of the Kynch test (left) and Diehl test (right) using Euler method. Both figures are a projection from referential solution ($N = 2430$ layers) to a coarse mesh of 90 layers. Properly elaboration, published in [21].

For both the Kynch test and the Diehl test we measure the performance of the numerical methods in terms of numerical error and CPU time. The error of a total simulated solution $C_{\text{tot},N}$ with N layers up to a time T is calculated by comparing with a reference solution C_{ref} obtained by Euler's method and $N = 2430$ layers

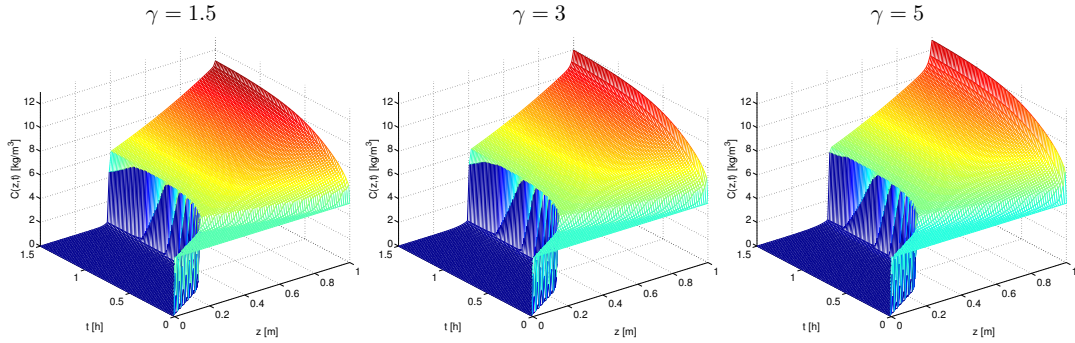


Figure 1.2: Kynch test simulated by the LI method with $N = 90$ layers for the values of $\gamma = 1.5$ (left), $\gamma = 3.0$ (center) and $\gamma = 5.0$ (right). Properly elaboration, published in [21].

($\Delta z = B/N = 1 \text{ m}/2430 \approx 0.41 \text{ mm}$) see Figure 1.1. The relative L^1 error is calculated as

$$E_N = \int_0^T \int_0^B |C_{\text{tot},N}(z,t) - C_{\text{ref}}(z,t)| dz dt \Big/ \int_0^T \int_0^B C_{\text{ref}}(z,t) dz dt .$$

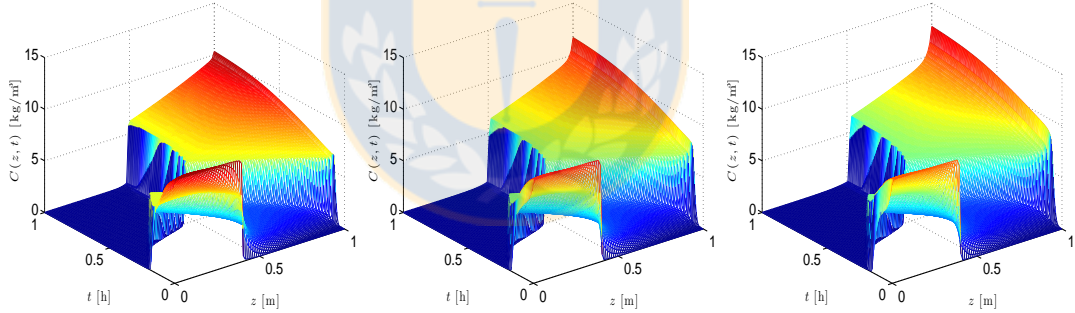


Figure 1.3: Diehl test simulated by the LI method with $N = 90$ layers for the values of $\gamma = 1.5$ (left), $\gamma = 3.0$ (center) and $\gamma = 5.0$ (right). Properly elaboration, published in [21].

For the Kynch test we choose an initial concentration of $C_0 = 5 \text{ kg/m}^3$ and $T = 1.5 \text{ h}$, which means that almost steady state has been reached. This test is also used to study the dependence of the numerical solutions produced by the LI method on the choice of the parameter γ . For each run, the time step Δt is chosen according to the CFL condition (1.10) (with equality). Note that the right-hand side of (1.10) is a decreasing function of γ and it tends to infinity as γ approaches one from above. Figure 1.3 shows numerical solutions obtained for three different values of γ . This figure and Figure 1.5 indicate that for a given number of layers $N > 30$, the values of γ closest to one produce

the solutions with the smallest errors, but the highest CPU times. We note that, for instance, for a given value of N the time step for $\gamma = 3$ can be chosen twice larger than that for $\gamma = 1.5$, so the total CPU time for $\gamma = 3$ should be about half of that for $\gamma = 1.5$. To assess which value of γ is optimal, an efficiency plot (of relative L^1 error versus CPU time) is helpful, see Figure 1.5. The curves are roughly L-shaped, indicating that γ should be chosen close to the point corresponding to the point of “bend”, since smaller or larger values would lead to larger numerical errors (at only slightly smaller CPU times) or to smaller numerical errors at much increased CPU times. Based on these considerations, the choice $\gamma = 3$ seems a good compromise for further comparison with other methods.

For the Diehl test (Diehl test) we choose the initial data

$$C(z, 0) = \begin{cases} 10 \text{ kg/m}^3 & \text{for } 0 < z < 0.4 \text{ m,} \\ 0 & \text{for } 0.4 \text{ m} < z < B = 1 \text{ m.} \end{cases}$$

Figure 1.2 and Figure 1.3 shows the numerical solution by the LI method with $\gamma = 1.5, \gamma = 3.0$ and $\gamma = 5.0$, and a contour plot of the reference solution. The right plot illustrates that in those regions where $C < C_c$, therefore $d = 0$, and (1.1) reduces to a first-order hyperbolic PDE, iso-concentration curves are straight lines, in complete agreement with the corresponding theory.

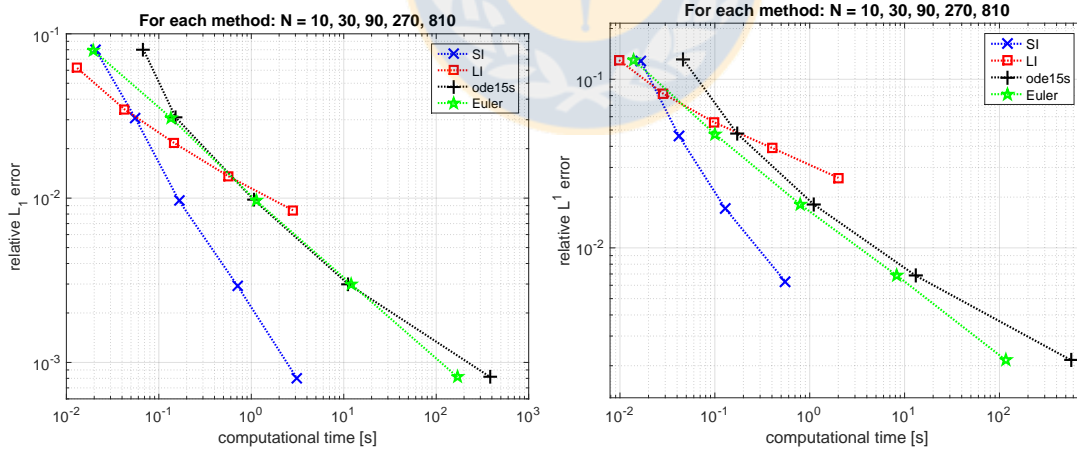


Figure 1.4: Efficiency plots for the Kynch test (left) and the Diehl test (right) and the Euler, SI and LI methods ($\gamma = 3$) and Matlab’s `ode15s` solver. In the right plot the cross corresponding to $N = 810$ for the SI method is not shown since the Newton-Raphson iterations did not converge, i.e., the method failed. Reprinted from [21].

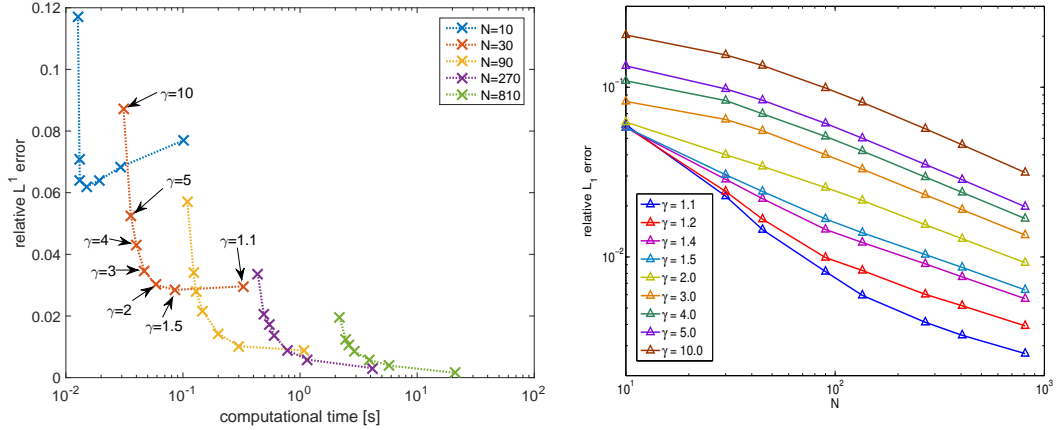


Figure 1.5: LI method applied to Kynch test: (left) efficiency plots (relative L^1 error versus CPU time) for the indicated values of N , determined for $\gamma = 10, 5, 4, 3, 2, 1.5, 1.1$ (from top to bottom, the curve for $N = 30$ is labeled for illustration). (Right) efficiency plots (relative L^1 error versus number of layers) in logarithmic scale. Properly elaboration, published in [21].

Figure 1.4 and Figure 1.2 shows the efficiency curves for all methods investigated plus those produced by employing Matlab’s `ode15s` solver. It turns out that the latter method is the least efficient, and that for both tests the implicit methods are most efficient, as expected from the corresponding CFL conditions. Moreover, for a given number of layers N , the LI method is the fastest, although not necessarily the one with the smallest error. Note that the efficiency curve for the SI method for the Diehl test (the right plot of Figure 1.3) is composed of four symbols only. In fact, no information is available for the run with $N = 810$ since the Newton-Raphson iterations did not converge for that case. While this situation could be easily overcome by the ad-hoc remedy of further reducing Δt (say, to 80% of its maximal value determined by the CFL condition), it alerts to a more fundamental problem observed with the SI method; namely that the convergence of (iterative) solvers for the nonlinear equations is not ensured a priori.

For accurate simulation results, Δz should be chosen small, wherefore the CFL condition implies that the explicit Euler method requires much smaller time steps than the other methods. On the other hand, the SI method needs more computations at every time step and requires the evaluation of the Jacobian matrix of the nonlinear algebraic system of equations. However, even when this system is solved by the Newton-Raphson method, the SI method has turned out to be far more efficient than explicit Euler [49]. To reduce the implementation complexity and to remove the necessity to solve numerically a system of nonlinear algebraic equations at every iteration in the SI method,

whose convergence depends on the Newton-Raphson iterations, the LI method can be used instead. The advantage of solving a linear system only in each iteration, which also means an easier implementation, is paid by the price of a larger numerical error.

1.3.1 Influence of compression in experiments

We use the same idea for visualize the influence of compression term in Kynch and Diehl test. In this case the iso-concentration lines lines, that are straight lines from a hyperbolic problem has been *curved* given by compression for a parabolic problem, see Figure 1.6



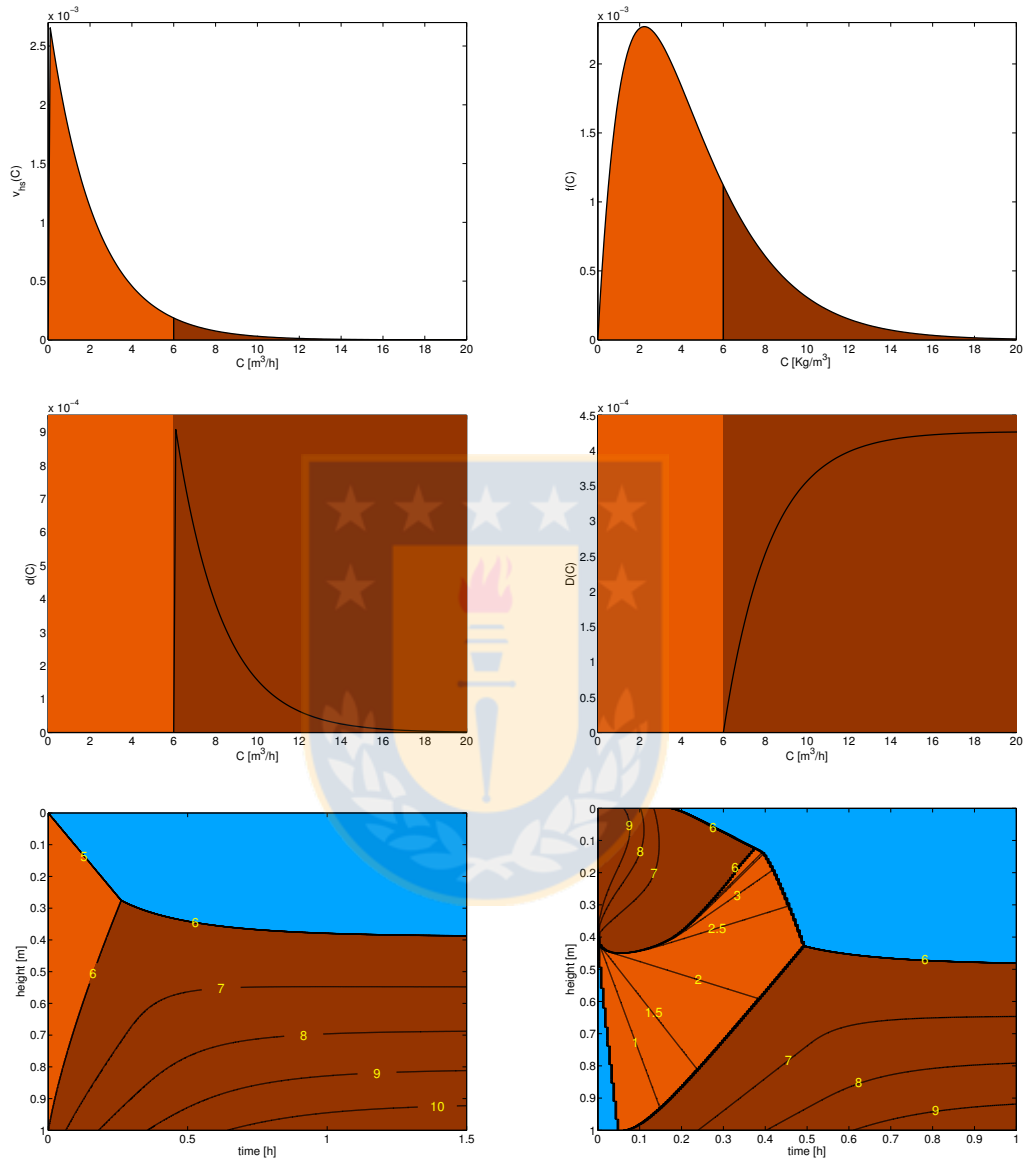


Figure 1.6: Influence of compression term at different functions. First row: Schematic view of V_{hs} and $f(C)$ showing the influence of compression term as $0 < C < C_c$ (light brown) and $C > C_c$ (dark brown). Second row: Compression terms are nonzero when $C > C_c$ (dark brown). Third row: contour plot of the reference solution, for Kynch test (left) and Diehl test (right) showing areas of $C = 0$ (blue), $0 < C < C_c$ (light brown) and $C > C_c$ (dark brown) and iso-concentration lines corresponding to the annotated values of C [kg/m^3]. Properly elaboration.

Chapter 2

A model of batch settling withal reactions

2.1 Introduction

Most models of the activated sludge process in wastewater treatment plants (WWTPs) are based on the assumption that all reactions occur in the biological reactor and that there are no reactions in the secondary settling tank (SST) [61]. It is, however, well known that certain biological reactions can occur in the settler. In particular, at long residence times and incomplete denitrification in the upstream bioreactor, denitrification can take place at the bottom of the tank, where the concentration of sludge is high, nitrate levels are substantial, biomass decay operates, and no oxygen is present. [112] and [88] reported measurements from three plants showing that of the total denitrification in each plant, 15%, 30% and 37% occurred in the settler, respectively. This is problematic since the produced N_2 can lead to bubbles that can attach to the sludge flocs, reduce their density, and lead to floating sludge which is disastrous for a settler. Thus, mathematical models that are able to capture the mechanical sedimentation-compression process in a SST in combination with biological reactions, in particular denitrification, are urgently needed to allow for the simulation of operational scenarios.

We are interested in modelling reactive settling, which is a process where biological conversions and physical sedimentation occur simultaneously. To describe the settling process, a consistent methodology was presented by [24] which considers both hindered and compression settling. Biological conversion processes in WWTPs are well known and dedicated models are available [69]. However, combining biological and settling

processes is not straightforward as it requires the extension of existing model equations as well as the development of a numerical method to deal with this extended set of equations.

It is the purpose of this chapter to advance a spatially one-dimensional, dynamical (time-dependent) deterministic model for this process of “reactive settling”, formulated as five scalar coupled partial differential equations (PDEs) that represent the mass balances for two particulate and three soluble components. The presentation includes a detailed description of a method for numerical solution of the PDE model, and therefore for numerical simulation of reactive settling.

The results of this Chapter are published in:

- R. Bürger, J. Careaga, S. Diehl, C. Mejías, I. Nopens, P.A. Vanrolleghem, and E. Torfs. Simulations of reactive settling of activated sludge with a reduced biokinetic model. *Computers and Chemical Engineering*, 92:216 – 229, 2016.

2.1.1 Related work

A couple of modelling approaches of reactive settling can be found in the literature. [60] presented a simulation study of two different models to account for the reactions taking place in the settler. Both models use the simulation model by [117] for the sedimentation process. The first model includes an extra model block in the return sludge line consisting of an empirical, algebraic elimination of oxygen and nitrate to account for the reactions in the settler. It is obvious that this first approach does not model the combination of sedimentation and reactions. The second model consists in placing the entire activated sludge model no. 1 (ASM1) model by [69], modelling the bioreactions, in each of the 10 layers in the Takács settler model. Improvements in nitrogen removal predictions were obtained and the first model was recommended mainly because of the much larger computational cost for the second one, but also because the second model overestimates the reactive capacity of the settler.

Further studies with the second model type and different ASMx models were reported by [57, 65, 100]. To compensate for the overestimation of the 10-layer reactive settler model, [65] introduced a reduction factor to the kinetics. Such factors are not present in the original mass balances and it is therefore not in agreement with a consistent modelling methodology [24] to introduce any such as a compensation for some other phenomenon — in this case the coarse spatial discretization (10 layers) of the settler for the numerical simulation.

Already without reactions, the Takács simulation model is not recommended because of failure of agreement with the solutions of the conservation of mass partial differential equation (PDE) in certain situations [19, 24, 41, 76], but also for other shortcomings during normal operating conditions specifically during wet weather [120].

A related application is reactive settling occurring in sequencing batch reactors (SBRs), for which modelling approaches without PDEs can be found [3, 83–86] modelled SBRs without reactive settling. SBRs are processes in which the bioreaction and settling processes occur in the same reactor, but sequenced in time, with reactor filling, reaction, settling and draw phases occurring sequentially in time rather than in space.

Convection-diffusion-reaction PDEs arise in many models of physical, chemical and biological processes. For the present nonlinear process of simultaneous sedimentation and reactions, PDE models and appropriate numerical methods are scarce in literature. A related application is a rotating wall vessel bioreactor developed by the National Aeronautics and Space Administration (NASA), USA, and used during the launch and landing of space shuttles to protect cultured cells from high shear forces. For this bioreactor, [33] presented a two-dimensional convection-diffusion-reaction model, simulated it with available finite-element-method software and validated against experimental data.

2.1.2 Novelty of this work

When only the settling process is considered, the settling tanks can be modelled by a single PDE describing the change of particulate concentration in depth. However, when biological reactions are added, the sludge can no longer be considered as a single particulate phase as different activated sludge components will be involved in different biological reactions. Moreover, additional equations to describe the concentration of soluble components over the depth of the settling tank need to be added. Hence, moving from a non-reactive settler to a reactive settler model does not only include additional rate expressions to account for biological reactions but also increases the number of state variables from a single particulate concentration to several particulate components in combination with soluble components. In this contribution, the settling model presented by [18, 24], called the Bürger-Diehl model, is extended with a reduced biological model where only denitrification reactions are considered.

The Bürger-Diehl model originates from the conservation of mass and can be stated as a scalar, nonlinear PDE for the sludge concentration as function of depth and time. Moreover, the Bürger-Diehl model has shown to provide a more realistic representation

of the sludge blanket height and thus the sludge accumulation in a secondary clarifier [120] which is an important driving factor for the denitrification process. It is the purpose of this contribution to make a first step towards extending these advances for the numerical treatment of non-reactive settling to the reactive case. To this end, we focus on a reduced-order problem for the biological reactions and confine to batch sedimentation in a closed vessel as a first approach.

We are interested in modelling reactive settling with a consistent modelling methodology [24] by starting with the mass balances and using appropriate numerical methods for the discretization of the model PDEs. Despite the simplicity of our reduced model, it accounts for three constitutive assumptions that determine its mathematical nature:

- (i) the hindered settling of the flocculated particles;
- (ii) compression of the flocculated particles at high concentrations when a network is formed;
- (iii) reaction terms containing nonlinear growth rate kinetics and a constant decay rate of biomass.

Properties (i) and (ii) are already realized in the Bürger-Diehl model described in a number of previous papers [18, 24, 120]. The combination of all three properties (i)–(iii) in the present PDE-based model, and the numerical method presented for its solution constitute, however, a new (original) contribution.

2.1.3 Outline of the chapter

The remainder of this Chapter is organized as follows. In Section 2.2 we introduce the governing model, which is defined by a system of convection-diffusion-reaction PDEs supplemented by suitable initial and boundary conditions. (The word “diffusion” is a common mathematical terminology for terms in the PDE with second-order spatial derivative; in our case such terms model either some diffusion or dispersion phenomena or, in the case of the particulate material, the compression of the network of flocculated particles at high concentrations.) Specifically, we first identify the unknown variables, then state the governing PDEs along with their initial and boundary conditions (Section 2.2.1), and finally introduce material specific constitutive model functions (Section 2.2.2), namely the specific growth rate related to biokinetics as well as the hindered settling and effective solid stress functions. In Section 2.3.2, the numerical method is introduced. After stating some preliminaries, we start from discretization in

space only, which is closely related to a system of method-of-lines ordinary differential equations (ODEs). We then outline a fully discrete, explicit scheme in Section 2.3.2. In Section 2.3.3 the final method is explained in almost algorithmic form so that it can easily be programmed. A theoretical result stating the method produces non-negative values only is stated in Section 2.3.4. Next, in Section 2.4, we present examples of numerical solutions of the governing model, where we are interested in three types of initial conditions: the traditional Kynch test (KT) [89], which describes the settling of an initially homogeneous suspension in a column; the Diehl test [45], in which the suspension is initially located above clear liquid; and the “overcompressed” test (OT), which corresponds to an initial configuration with a highly concentrated layer at the bottom. The initial condition for the Diehl test can be obtained either by a membrane, which is removed at $t = 0$, or by rising the sludge to the top by aeration, e.g., in an SBR. The OT corresponds to a hypothetical initial configuration of a layer of strongly concentrated sediment (e.g., after centrifugation) with clear liquid above where the “pressure” is released at $t = 0$, allowing the bed to expand. The OT was employed by [14, 32] as an example to illustrate the consequences of modelling sediment compressibility by a nonlinear, possibly degenerate diffusion term under extreme conditions. Since the particle velocities in OT are negative in some regions, contrary to the KT and DT, this experiment is important for testing a numerical scheme. Sections 2.4.1, 2.4.2 and 2.4.3 present the numerical results for KT, DT, and OT scenarios, respectively, and are followed by a brief discussion of numerical error and convergence properties of the scheme (Section 2.4.4).

2.2 Governing model

We study one-dimensional batch sedimentation of suspended particles in water with soluble substrates in a closed vessel with a constant cross-sectional area. The depth z is measured from the suspension surface $z = 0$ downwards to the bottom at $z = B$. For simplicity, we study the last settling phase of a SBR process where aeration is switched off and the sludge is allowed to settle. We assume that, in addition to particulate biomass, there is still a certain amount of dissolved nitrate (NO_3) in the water. As the biomass decays, readily biodegradable Chemical Oxygen Demand (COD) is produced, which can be converted to cell biomass using nitrate as electron acceptor and nitrogen gas (N_2) is produced.

The particulate microorganisms are divided into only two components: ordinary heterotrophic organisms (X_{OHO}) and undegradable organics (X_{U}) since we only need

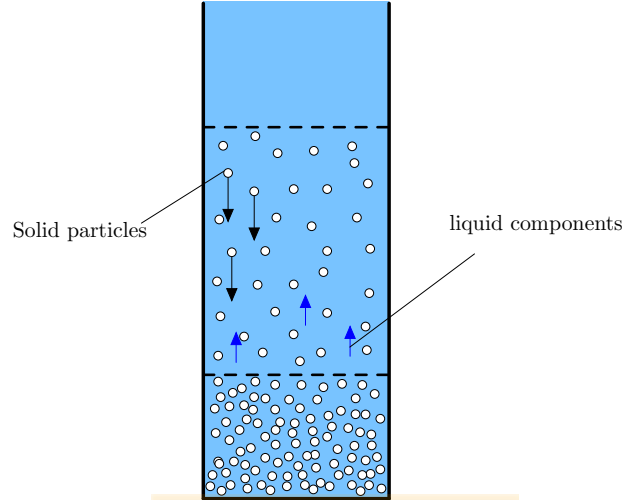


Figure 2.1: A schematic view of a settler vessel. Our focus is in the different components, solids particles and liquids components inside the settler and how they reacted between them. Properly elaboration.

access to those state variables to describe the denitrification process. The total concentration of the flocculated particles is $X := X_{\text{OHO}} + X_{\text{U}}$. Each particle is assumed to settle with a velocity $v = v(X, X_z)$ given by constitutive assumptions for hindered and compressive settling involving the local concentration X and its spatial derivative $X_z := \partial X / \partial z$. The notation for the soluble concentrations is S_{NO_3} for the nitrate, S_{S} for the readily biodegradable substrate and S_{N_2} for nitrogen gas. The small spatial movement of the substrate caused by the settling particles is captured by a single diffusion coefficient d_{S} in the model equations. Hence, particulate components undergo settling and biological reactions whereas soluble components are subject to diffusion and biological reactions. The resulting set of equations is able to describe the evolution of particulate concentrations (X_{OHO} and X_{U}) as well as concentrations of soluble components (S_{NO_3} , S_{S} , S_{N_2}) during the settling process.

Summarizing, the unknown variables are the five functions

$$X_{\text{OHO}}(z, t), \quad X_{\text{U}}(z, t), \quad S_{\text{NO}_3}(z, t), \quad S_{\text{S}}(z, t), \quad S_{\text{N}_2}(z, t)$$

sought for $0 \leq z \leq B$ and $t \geq 0$, and which are determined as solutions of five PDEs, supplied with initial and boundary conditions, stated in the next section.

2.2.1 Governing partial differential equations, initial and boundary conditions

At the start of settling, the initial concentration distribution of particles may be piecewise constant described by the function $X^0(z)$, whereas we assume that the substrate concentrations are constant: the nitrate concentration $S_{\text{NO}_3}^0$, readily biodegradable substrate S_{S}^0 and zero concentration of nitrogen gas. Each particle consists initially of a certain percentage p_0 of heterotrophs and the remainder is undegradable organics. The balance of mass yields the following partial differential equations for $0 < z < B$ and $t > 0$:

$$\frac{\partial X_{\text{OHO}}}{\partial t} = -\frac{\partial}{\partial z}(v(X, X_z)X_{\text{OHO}}) + (\mu(S_{\text{NO}_3}, S_{\text{S}}) - b)X_{\text{OHO}}, \quad (2.1)$$

$$\frac{\partial X_{\text{U}}}{\partial t} = -\frac{\partial}{\partial z}(v(X, X_z)X_{\text{U}}) + f_{\text{P}}bX_{\text{OHO}}, \quad (2.2)$$

$$\frac{\partial S_{\text{NO}_3}}{\partial t} = d_{\text{S}}\frac{\partial^2 S_{\text{NO}_3}}{\partial z^2} - \frac{1-Y}{2.86Y}\mu(S_{\text{NO}_3}, S_{\text{S}})X_{\text{OHO}}, \quad (2.3)$$

$$\frac{\partial S_{\text{S}}}{\partial t} = d_{\text{S}}\frac{\partial^2 S_{\text{S}}}{\partial z^2} - \left(\frac{\mu(S_{\text{NO}_3}, S_{\text{S}})}{Y} - (1-f_{\text{P}})b\right)X_{\text{OHO}}, \quad (2.4)$$

$$\frac{\partial S_{\text{N}_2}}{\partial t} = d_{\text{S}}\frac{\partial^2 S_{\text{N}_2}}{\partial z^2} + \frac{1-Y}{2.86Y}\mu(S_{\text{NO}_3}, S_{\text{S}})X_{\text{OHO}}, \quad (2.5)$$

which are posed along with the initial conditions

$$\begin{aligned} X_{\text{OHO}}(z, 0) &= p_0X^0(z), & X_{\text{U}}(z, 0) &= (1-p_0)X^0(z), \\ S_{\text{NO}_3}(z, 0) &= S_{\text{NO}_3}^0, & S_{\text{S}}(z, 0) &= S_{\text{S}}^0, & S_{\text{N}_2}(z, 0) &= 0, \end{aligned} \quad (2.6)$$

where $X^0(z)$ is a given function, p_0 , $S_{\text{NO}_3}^0$ and S_{S}^0 are given numbers, and the zero-flux boundary conditions are

$$\begin{aligned} v(X, X_z)X|_{z=0} &= v(X, X_z)X|_{z=B} = 0, \\ (S_{\text{NO}_3})_z(0, t) &= (S_{\text{NO}_3})_z(B, t) = 0, \\ (S_{\text{S}})_z(0, t) &= (S_{\text{S}})_z(B, t) = 0, \\ (S_{\text{N}_2})_z(0, t) &= (S_{\text{N}_2})_z(B, t) = 0. \end{aligned} \quad (2.7)$$

2.2.2 Model parameters and constitutive functions

The parameter Y is a dimensionless yield factor and b is the constant decay rate of heterotrophs. The specific growth rate function is the following product of two Monod

expressions:

$$\mu(S_{\text{NO}_3}, S_{\text{S}}) := \mu_{\text{max}} \frac{S_{\text{NO}_3}}{K_{\text{NO}_3} + S_{\text{NO}_3}} \frac{S_{\text{S}}}{K_{\text{S}} + S_{\text{S}}}, \quad (2.8)$$

where $\mu_{\text{max}} > b$ is the maximum growth rate and $K_{\text{NO}_3}, K_{\text{S}} > 0$ are half-saturation constants (see Table 3.1). This expresses that denitrification only takes place when favourable conditions for S_{NO_3} and S_{S} prevail. The constitutive function for the particle velocity $v(X, X_z)$ takes into account both hindered settling and compression and is of the form [24]

$$v(X, X_z) = \begin{cases} v_{\text{hs}}(X) & \text{for } X < X_c, \\ v_{\text{hs}}(X) \left(1 - \frac{\rho_s \sigma'_e(X)}{X g \Delta \rho} \frac{\partial X}{\partial z}\right) & \text{for } X > X_c. \end{cases} \quad (2.9)$$

Here, $v_{\text{hs}}(X)$ is the hindered settling velocity function, $\sigma'_e(X) := d\sigma_e(X)/dX$ is the derivative of the effective solids stress function $\sigma_e(X)$, ρ_s the density of the solids, $\Delta\rho$ the density difference between solids and liquid, and X_c is a critical concentration above which the particles touch each other and form a network which can bear a certain stress.

For the simulations, we choose [47, 119]

$$v_{\text{hs}}(X) = \frac{v_0}{1 + (X/\bar{X})^q}, \quad (2.10)$$

where the parameters v_0 , \bar{X} and q have the values given in Table 3.1 (Torfs et al., 2016), and

$$\sigma_e(X) = \begin{cases} 0 & \text{for } X < X_c, \\ \alpha(X - X_c) & \text{for } X > X_c, \end{cases} \quad (2.11)$$

where the values of α and the critical concentration X_c are indicated in Table 3.1.

2.3 Numerical method

We define the batch settling flux function $f_b(X) := X v_{\text{hs}}(X)$, set

$$d_{\text{comp}}(X) := v_{\text{hs}}(X) \frac{\rho_s \sigma'_e(X)}{g \Delta \rho}, \quad (2.12)$$

Table 2.1: Parameter values employed for the simulation of reactive settling. Reprinted from [13].

Model parameter	symbol	value and unit
parameter in hindered sett. function v_{hs} , cf. (2.10)	v_0	$1.76 \times 10^{-3} \text{ m s}^{-1}$
parameter in hindered sett. function v_{hs} , cf. (2.10)	\bar{X}	3.87 kg m^{-3}
parameter in hindered sett. function v_{hs} , cf. (2.10)	q	$3.58 [-]$
unbiodegradable fraction	f_P	$0.2 [-]$
critical concentration	X_c	5 kg m^{-3}
parameter in effective stress function σ_e , cf. (2.11)	α	$0.2 \text{ m}^2 \text{ s}^{-2}$
solid density	ρ_s	1050 kg m^{-3}
solid-fluid density difference	$\Delta\rho$	52 kg m^{-3}
acceleration of gravity	g	9.81 m s^{-2}
diffusion coefficient	d_S	$1.00 \times 10^{-6} \text{ m}^2 \text{ s}^{-1}$
heterotrophic yield	Y	$0.67 [-]$
heterotrophic maximal specific growth rate	μ_{max}	$4.8 \text{ d}^{-1} = 5.56 \times 10^{-5} \text{ s}^{-1}$
heterotropic decay rate	b	$0.6 \text{ d}^{-1} = 6.94 \times 10^{-6} \text{ s}^{-1}$
half-saturation coefficient (hsc) for heterotrophs	K_S	$20 \text{ g m}^{-3} = 0.02 \text{ kg m}^{-3}$
hsc for denitrifying heterotrophs	K_{NO_3}	$5.00 \times 10^{-4} \text{ kg m}^{-3}$

and define the primitive

$$D(X) := \int_{X_c}^X d_{\text{comp}}(s) \, ds. \quad (2.13)$$

The sum of (2.1) and (2.2) gives the following equation, which apart from the reaction term only contains derivatives of the total concentration X :

$$\begin{aligned} \frac{\partial X}{\partial t} = -\frac{\partial}{\partial z} \left(f_b(X) - \frac{\partial D(X)}{\partial z} \right) \\ + (\mu(S_{\text{NO}_3}, S_S) - (1 - f_P)b)X_{\text{OHO}}, \quad 0 < z < B, \quad t > 0. \end{aligned} \quad (2.14)$$

This is in fact the Bürger-Diehl model with a reaction term. As a consequence of (2.11)–(2.13), the PDE (2.14) is second-order parabolic wherever the solution X exceeds X_c and first-order hyperbolic for lower concentration values. Thus, the PDE (2.14) is called strongly degenerate parabolic or parabolic-hyperbolic, where the location of the type-change interface is not known beforehand. Moreover, due to the nonlinear and degenerate nature, discontinuities in the solution appear and special techniques for the numerical solution have to be used (which are incorporated in the numerical method outlined herein).

The total flux within the parenthesis on the right-hand side of (2.14) is

$$v(X, X_z)X = f_b(X) - \frac{\partial D(X)}{\partial z}. \quad (2.15)$$

This means that for (2.14) we can utilize ingredients of the numerical method by [18] with the addition of the reaction term. To find numerical updates for the two portions X_{OHO} and X_{U} of X , we use the idea by [41, 43]. To this end, we introduce the percentage $p := X_{\text{OHO}}/X$ when $X > 0$, so that $X_{\text{OHO}} = pX$ and $X_{\text{U}} = (1 - p)X$, and rewrite Equation (2.1) as

$$\frac{\partial(pX)}{\partial t} = -\frac{\partial}{\partial z}(v(X, X_z)pX) + (\mu(S_{\text{NO}_3}, S_{\text{S}}) - b)pX, \quad 0 < z < B, \quad t > 0. \quad (2.16)$$

The idea of the numerical method is the following. In each discrete time step, X is first updated via a discretized version of (2.14). This means that the flux (2.15) is known during this time step, which is essential for any finite volume numerical method. Since the flux of (2.16) is p times the known flux (2.15), it is only the variable p that needs to be updated, and this can be achieved by a discretized version of (2.16). Then the concentration of the second particulate component is simply $X_{\text{U}} = (1 - p)X$. The numerical updates of S_{NO_3} , S_{S} and S_{N_2} are then straightforward for the corresponding equations (2.3)–(2.5).

2.3.1 Spatial discretization

We introduce the spatial discretization by dividing the interval $(0, B)$ into N layers and set $\Delta z := B/N$. Let $X_j = X_j(t)$ and denote the approximate concentrations in layer j and likewise $P_j = P_j(t)$ the approximation of p . The numerical fluxes between layer j and $j + 1$ (therefore indexed by $j + 1/2$) are defined as follows. The convective flux f_{b} is discretized by the standard Godunov numerical flux, i.e.,

$$G_{j+1/2} := \begin{cases} \min_{X_j \leq X \leq X_{j+1}} f_{\text{b}}(X) & \text{if } X_j \leq X_{j+1}, \\ \max_{X_j \geq X \geq X_{j+1}} f_{\text{b}}(X) & \text{if } X_j > X_{j+1}. \end{cases} \quad (2.17)$$

If the numerical compressive flux is defined as

$$J_{j+1/2} := \frac{D(X_{j+1}) - D(X_j)}{\Delta z}, \quad (2.18)$$

then the total flux (2.15) between layers j and $j + 1$ is approximated by $F_{j+1/2} := G_{j+1/2} - J_{j+1/2}$. The corresponding flux of (2.16) is $P_{j+1/2}(G_{j+1/2} - J_{j+1/2})$, where $P_{j+1/2}$ needs to be defined. We use the idea of [43], which is the following. If the total flux $F_{j+1/2}$ is positive, this means that particles move in the direction of the z -axis

over the boundary between layer j to $j + 1$. Consequently, the value of $P_{j+1/2}$ at the boundary between the layers is the one in the layer above, i.e. P_j . If $F_{j+1/2} \leq 0$, then the value is P_{j+1} , i.e.

$$P_{j+1/2} = \begin{cases} P_{j+1} & \text{if } F_{j+1/2} \leq 0, \\ P_j & \text{if } F_{j+1/2} > 0. \end{cases} \quad (2.19)$$

Moreover, we define the soluble component diffusive fluxes

$$\mathcal{D}_{\Upsilon,j+1/2} := d_S \frac{S_{\Upsilon,j+1} - S_{\Upsilon,j}}{\Delta z}, \quad j = 1, \dots, N-1, \quad \Upsilon \in \{\text{NO}_3, \text{S}, \text{N}_2\} \quad (2.20)$$

and finally introduce the zero boundary fluxes and percentages

$$\begin{aligned} G_{1/2} = G_{N+1/2} = J_{1/2} = J_{N+1/2} = P_{1/2} = P_{N+1/2} = 0, \\ \mathcal{D}_{\Upsilon,1/2} = \mathcal{D}_{\Upsilon,N+1/2} = 0, \quad \Upsilon \in \{\text{NO}_3, \text{S}, \text{N}_2\}. \end{aligned}$$

We then obtain the following semi-discretized ODE system for the PDEs:

$$\frac{dX_j}{dt} = -\frac{F_{j+1/2} - F_{j-1/2}}{\Delta z} + (\mu(S_{\text{NO}_3,j}, S_{\text{S},j}) - (1 - f_P)b) X_{\text{OHO},j}, \quad (2.21)$$

$$\frac{d(P_j X_j)}{dt} = -\frac{P_{j+1/2} F_{j+1/2} - P_{j-1/2} F_{j-1/2}}{\Delta z} + (\mu(S_{\text{NO}_3,j}, S_{\text{S},j}) - b) X_{\text{OHO},j}, \quad (2.22)$$

$$\frac{dS_{\text{NO}_3,j}}{dt} = \frac{\mathcal{D}_{\text{NO}_3,j+1/2} - \mathcal{D}_{\text{NO}_3,j-1/2}}{\Delta z} - \frac{1-Y}{2.86Y} \mu(S_{\text{NO}_3,j}, S_{\text{S},j}) X_{\text{OHO},j}, \quad (2.23)$$

$$\frac{dS_{\text{S},j}}{dt} = \frac{\mathcal{D}_{\text{S},j+1/2} - \mathcal{D}_{\text{S},j-1/2}}{\Delta z} - \left(\frac{\mu(S_{\text{NO}_3,j}, S_{\text{S},j})}{Y} - (1 - f_P)b \right) X_{\text{OHO},j}, \quad (2.24)$$

$$\frac{dS_{\text{N}_2,j}}{dt} = \frac{\mathcal{D}_{\text{N}_2,j+1/2} - \mathcal{D}_{\text{N}_2,j-1/2}}{\Delta z} + \frac{1-Y}{2.86Y} \mu(S_{\text{NO}_3,j}, S_{\text{S},j}) X_{\text{OHO},j}, \quad (2.25)$$

$$X_{\text{OHO},j} = P_j X_j,$$

$$X_{\text{U},j} = (1 - P_j) X_j,$$

where $j = 1, \dots, N$. These equations are thus exact conservation laws for each of the N layers. Note that $X_{\text{U},j}$ can be defined after the entire simulation.

2.3.2 Time discretization

Let t_n , $n = 0, 1, \dots$ denote the discrete time points and Δt the time step that should satisfy a certain Courant-Friedrichs-Lewy (CFL) condition depending on the chosen time-integration method. For explicit schemes, the right-hand sides of the equations are evaluated at time t_n . The value of a variable at time t_n is denoted by an upper index, e.g., P_j^n . The main restriction of the time step (for small Δz) is due to the

second-order spatial derivatives in the compression term [19, 27] and in the diffusion term for the solubles. Let X_{\max} denote the maximally possible particle concentration. The CFL condition for explicit Euler and batch sedimentation is

$$\Delta t \leq \frac{1}{\max\{k_1, k_2\}}, \quad (2.26)$$

with

$$\begin{aligned} k_1 &:= \frac{1}{\Delta z} \max_{0 \leq X \leq X_{\max}} |f'_b(X)| + \frac{1}{\Delta z^2} \max_{0 \leq X \leq X_{\max}} d_{\text{comp}}(X) \\ &\quad + \max\{\mu_{\max} - (1 - f_P)b, (1 - f_P)b\} + \max\left\{\frac{\rho_L \mu_{\max} X_{\max}}{\rho_X K_{\text{NO}_3}}, \mu_{\max} - b, b\right\}, \\ k_2 &:= \frac{2d_S}{\Delta z^2} + \frac{\mu_{\max} X_{\max}}{K_{\text{NO}_3}} \left(\frac{\rho_L}{\rho_X} + 1\right). \end{aligned}$$

For explicit Euler, the time derivatives on the left-hand side of (2.21)–(2.25) are approximated by the standard finite difference ratio and the right-hand side is evaluated at time t_n . First, Equation (2.21) gives the update X_j^{n+1} according to

$$X_j^{n+1} = X_j^n + \Delta t \left(-\frac{F_{j+1/2}^n - F_{j-1/2}^n}{\Delta z} + (\mu(S_{\text{NO}_3,j}^n, S_{\text{S},j}^n) - (1 - f_P)b) X_{\text{OHO},j}^n \right). \quad (2.27)$$

The equations for the substrates can be written in an analogous way, namely

$$S_{\text{NO}_3,j}^{n+1} = S_{\text{NO}_3,j}^n + \Delta t \left(\frac{\mathcal{D}_{\text{NO}_3,j+1/2}^n - \mathcal{D}_{\text{NO}_3,j-1/2}^n}{\Delta z} - \frac{1 - Y}{2.86Y} \mu(S_{\text{NO}_3,j}^n, S_{\text{S},j}^n) X_{\text{OHO},j}^n \right), \quad (2.28)$$

$$S_{\text{S},j}^{n+1} = S_{\text{S},j}^n + \Delta t \left(\frac{\mathcal{D}_{\text{S},j+1/2}^n - \mathcal{D}_{\text{S},j-1/2}^n}{\Delta z} - \left(\frac{\mu(S_{\text{NO}_3,j}^n, S_{\text{S},j}^n)}{Y} - (1 - f_P)b \right) X_{\text{OHO},j}^n \right), \quad (2.29)$$

$$S_{\text{N}_2,j}^{n+1} = S_{\text{N}_2,j}^n + \Delta t \left(\frac{\mathcal{D}_{\text{N}_2,j+1/2}^n - \mathcal{D}_{\text{N}_2,j-1/2}^n}{\Delta z} + \frac{1 - Y}{2.86Y} \mu(S_{\text{NO}_3,j}^n, S_{\text{S},j}^n) X_{\text{OHO},j}^n \right). \quad (2.30)$$

As for Equation (2.22), the approximation of the time derivative is

$$\frac{d(P_j X_j)}{dt} \approx \frac{P_j^{n+1} X_j^{n+1} - P_j^n X_j^n}{\Delta t}.$$

Note that if $X_j^{n+1} = 0$, then there is no particle in layer j , hence the value of P_j^{n+1} is irrelevant since $P_j^{n+1}X_j^{n+1} = 0$. We get the following update formula for P_j^{n+1} :

$$P_j^{n+1} = \begin{cases} P_j^n & \text{if } X_j^{n+1} = 0, \\ \frac{1}{X_j^{n+1}} \left[P_j^n X_j^n + \Delta t \left(-\frac{P_{j+1/2}^n F_{j+1/2}^n - P_{j-1/2}^n F_{j-1/2}^n}{\Delta z} + (\mu(S_{\text{NO}_3,j}^n, S_{\text{S},j}^n) - b) X_{\text{OHO},j}^n \right) \right] & \text{if } X_j^{n+1} > 0. \end{cases} \quad (2.31)$$

2.3.3 Numerical method in final form

For the ease of reference, we here summarize the information provided in this section and present the resulting numerical method for the approximate solution of the model (2.1)–(2.7), and thereby for the simulation of reactive settling.

1. Assume that the solution is sought at time $t = T > 0$. Choose $\Delta z = B/N$ and $\Delta t = T/n_{\max}$, N and n_{\max} being integers, such that the CFL condition (CFL) is satisfied.
2. Calculate the discrete initial values either by averaging

$$X_j^0 = \frac{1}{\Delta z} \int_{(j-1)\Delta z}^{j\Delta z} X^0(z) dz, \quad j = 1, \dots, N,$$

or by using the value in the mid of each layer:

$$X_j^0 = X^0((j-1/2)\Delta z), \quad j = 1, \dots, N.$$

Then set for $j = 1, \dots, N$:

$$P_j^0 = p_0, \quad X_{\text{OHO},j}^0 = p_0 X_j^0, \quad S_{\text{NO}_3,j}^0 = S_{\text{NO}_3}^0, \quad S_{\text{S},j}^0 = S_{\text{S}}^0, \quad S_{\text{N}_2,j}^0 = 0.$$

3. For $n = 0, 1, \dots, n_{\max} - 1$, update the discrete solution values as follows:
 - (a) For $j = 0, \dots, N$, calculate the numerical fluxes $G_{j+1/2}^n$ and $J_{j+1/2}^n$ from (3.33) and (2.18), respectively, where $X_j = X_j^n$, $X_{j+1} = X_{j+1}^n$, for $j = 1, \dots, N-1$; and set

$$G_{1/2}^n = G_{N+1/2}^n = J_{1/2}^n = J_{N+1/2}^n = 0.$$

- (b) Calculate the total numerical fluxes

$$F_{j+1/2}^n = G_{j+1/2}^n - J_{j+1/2}^n, \quad j = 0, \dots, N.$$

- (c) Calculate the percentage numerical fluxes

$$P_{j+1/2}^n = \begin{cases} P_{j+1}^n & \text{if } F_{j+1/2}^n \leq 0, \\ P_j^n & \text{if } F_{j+1/2}^n = 0, \end{cases} \quad j = 0, \dots, N.$$

- (d) Calculate X_j^{n+1} for $j = 1, \dots, N$ from the update formula (2.27).
 (e) Calculate P_j^{n+1} for $j = 1, \dots, N$ from the update formula (2.31).
 (f) Calculate $X_{\text{OHO},j}^{n+1} = P_j^{n+1} X_j^{n+1}$ for $j = 1, \dots, N$.
 (g) Calculate $X_{\text{U},j}^{n+1} = (1 - P_j^{n+1}) X_j^{n+1}$ for $j = 1, \dots, N$. (This step is optional).
 (h) For each soluble substrate $\Upsilon \in \{\text{NO}_3, \text{S}, \text{N}_2\}$, calculate the corresponding numerical diffusive fluxes $\mathcal{D}_{\Upsilon,j+1/2}^n$ from (2.20), where $S_{\Upsilon,j} = S_{\Upsilon,j}^n$ and $S_{\Upsilon,j+1} = S_{\Upsilon,j+1}^n$, for $j = 1, \dots, N-1$, and set

$$\mathcal{D}_{\Upsilon,1/2}^n = \mathcal{D}_{\Upsilon,N+1/2}^n = 0.$$

- (i) Calculate $S_{\text{NO}_3,j}^{n+1}$, $S_{\text{S},j}^{n+1}$ and $S_{\text{N}_2,j}^{n+1}$ from the update formulas (2.28)–(2.30).

All calculations are based on explicit evaluations of update formulas, so the numerical method can be readily implemented (for instance, in Fortran or any other programming language). No solution of linear or nonlinear systems is necessary; it is not necessary to appeal to any numerical solver or software (except, of course, for the visualization of results).

2.3.4 A theoretical result

The idea is that the CFL condition should imply that the right-hand side of the update formula for each variable is a monotone function of the same variables in all layers at the previous time point. For example, the CFL condition (CFL) implies that the right-hand side of (2.27) is a monotone function of the arguments X_{j-1}^n , X_j^n and X_{j+1}^n (note that $X_{\text{OHO},j}^n = P_j^n X_j^n$) for any values of the substrate concentrations and P_j^n appearing in the formula. A more comprehensive analysis can be found in [13], which also contains results that imply the following theorem.

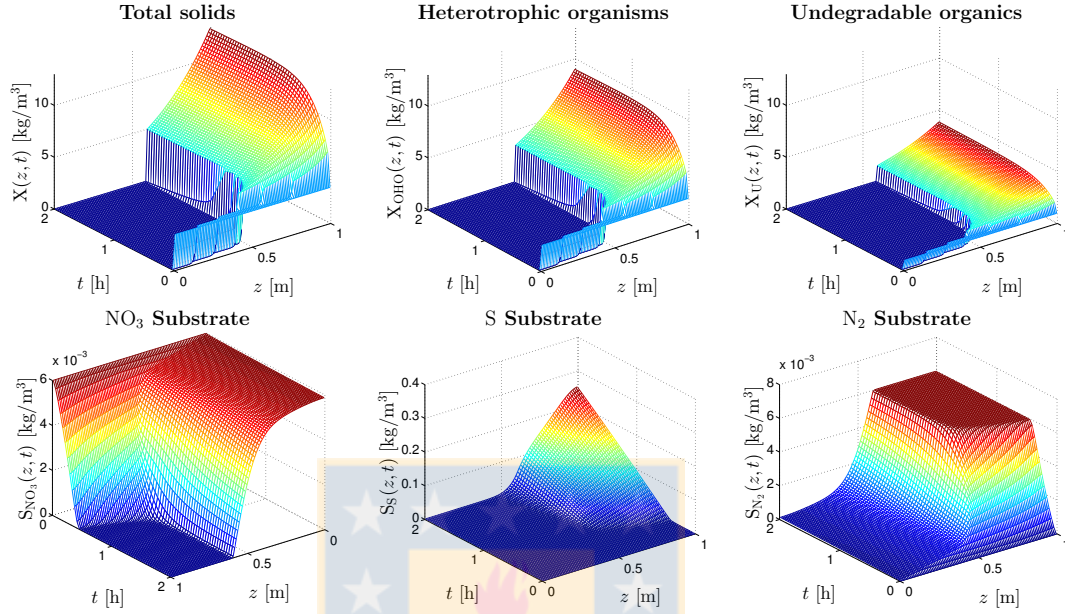


Figure 2.2: Example 1 (Kynch test, $d_S = 10^{-6} \text{ m}^2 \text{ s}^{-1}$). Here and in Figures 2.3 to 3.7, 2.9 and 2.10, the visual grid used to display the numerical solution is coarser than the computational grid, and the plot of the solution for S_{NO_3} has been rotated. Reprinted from [13].

Theorem 2.3.1. Assume that the numerical scheme in Section 2.3.3 produces

$$X_j^n \leq X_{\max}, \quad \text{for all } j = 1, \dots, N \text{ and } n = 1, \dots, n_{\max},$$

and that the CFL condition (CFL) holds. Then the following holds ($j = 1, \dots, N$ and $n = 1, \dots, n_{\max}$):

$$\begin{cases} 0 \leq X_j^n, S_{\text{NO}_3,j}^n, S_{\text{S},j}^n, S_{\text{N}_2,j}^n, \\ 0 \leq P_j^n \leq 1 \end{cases} \implies \begin{cases} 0 \leq X_j^{n+1}, S_{\text{NO}_3,j}^{n+1}, S_{\text{S},j}^{n+1}, S_{\text{N}_2,j}^{n+1}, \\ 0 \leq P_j^{n+1} \leq 1. \end{cases}$$

The theorem guarantees that if the variables are positive (rather, non-negative) initially, the numerical method will keep them positive. Likewise, percentage values P_j^n will stay between zero and one.

2.4 Numerical results

For all tests we employ the hindered settling velocity function v_{hs} and effective stress function σ_e given by (2.10) and (2.11), respectively. The heterotrophic specific growth rate μ is given in (2.8), and all other parameters are indicated in Table 3.1 (unless otherwise stated). For the KT we simulated three different scenarios differing in the choice of the diffusion coefficient d_S (Examples 1 to 3), while the two scenarios considered for each of the DT (Examples 4 and 5) and OT (Examples 6 and 7) differ in the initial concentration of particles.

In all numerical examples, we employ the explicit scheme with $N = 100$ layers for a column of height $B = 1$ m. To properly represent the reaction dynamics we present simulations up to $t = T = 2$ h, except for one long simulation of the KT, which is run to $T = 100$ h. (This final time is quite unrealistic since the settling phase in an SBR takes at most one hour. However, in this case we are interested in the long-time predictions of the model and the numerical algorithm.) The time step Δt is chosen by 98% of the bound given in the right-hand side of (CFL).

The initial values common to all examples are

$$S_S^0 = 9.00 \times 10^{-4} \text{ kg m}^{-3} \quad \text{and} \quad S_{\text{NO}_3}^0 = 6.00 \times 10^{-3} \text{ kg m}^{-3},$$

while we recall that by (2.6), the initial value of S_{N_2} is zero.

2.4.1 Examples 1 to 3: Kynch test (batch settling of an initially homogeneous suspension)

In Examples 1–3, we simulate the settling of an initially homogeneous suspension of initial density $X_0 = 3.5 \text{ kg m}^{-3}$, which is divided into heterotrophs and undegradable organics by $p_0 = 5/7 \approx 0.7143$, so that

$$X_{\text{OHO}}(z, 0) = 2.5 \text{ kg m}^{-3}, \quad X_{\text{U}}(z, 0) = 1.0 \text{ kg m}^{-3} \quad \text{for } 0 < z < B.$$

We employ this configuration to assess the influence of the substrate diffusion coefficient d_S . Example 1 has been obtained by employing the default value $d_S = 10^{-6} \text{ m}^2 \text{ s}^{-1}$ informed in Table 3.1. Figure 2.2 and 2.3 show the numerical results for all unknowns for $T = 2$ h and $T = 100$ h, respectively. We observe that the solids settle downwards to the bottom rapidly and form a sludge blanket with a sharp interface at $X_c = 5 \text{ kg m}^{-3}$. Moreover, the concentration increases downwards gradually until

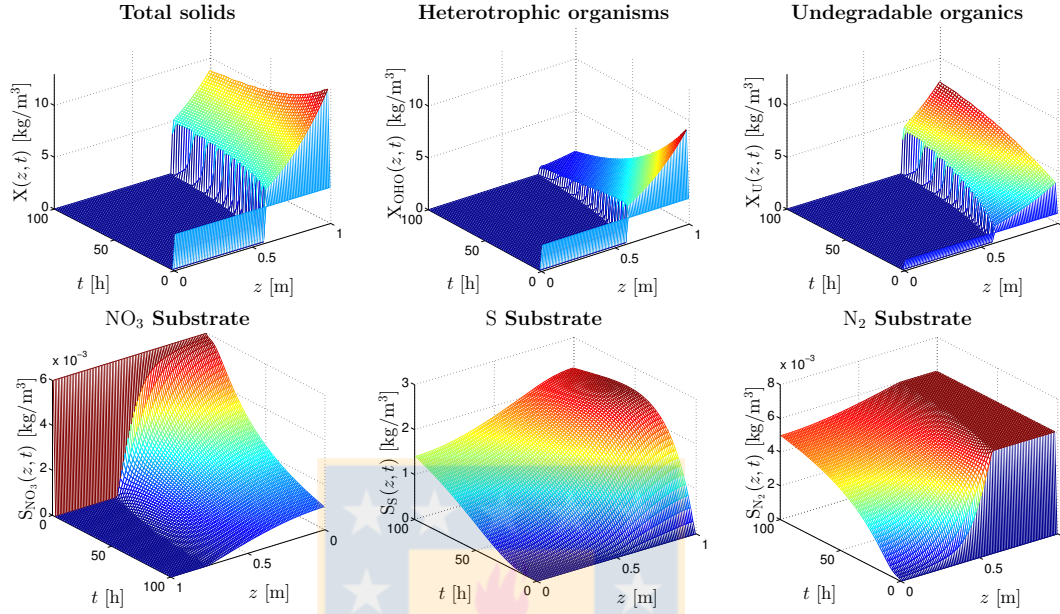


Figure 2.3: Example 1 (Kynch test, $d_S = 10^{-6} \text{ m}^2 \text{ s}^{-1}$): long-time simulation ($T = 100 \text{ h}$). Reprinted from [13].

reaching about 20 kg m^{-3} at the bottom. Here, and in Examples 2 to 7, the solutions for all quantities are bounded and non-negative. The S_{NO_3} plot indicates a very rapid degradation of nitrate within the sludge blanket while that same quantity decays only very slowly within the supernatant clear liquid. We observe the formation of readily biodegradable substrate (of concentration S_S) at the bottom of the column through decay of heterotrophs. This is no longer degraded when all nitrate is depleted. Furthermore, the solution for S_{N_2} has a plateau at $6 \times 10^{-3} \text{ kg m}^{-3}$, which is equal to the initial value of S_{NO_3} . This suggests that within the sludge blanket, almost all soluble nitrate has been converted into nitrogen.

For this particular case we also present a simulation until $T = 100 \text{ h}$ to study the long-time behaviour of the model. The results shown in Figure 2.3 illustrate that the total solids concentration attains a maximum of about 20 kg m^{-3} at the bottom but that this maximum, as well as the total solids mass, decay in time. Moreover, the proportion of undegradable organics increases in time (as expected). The substrates

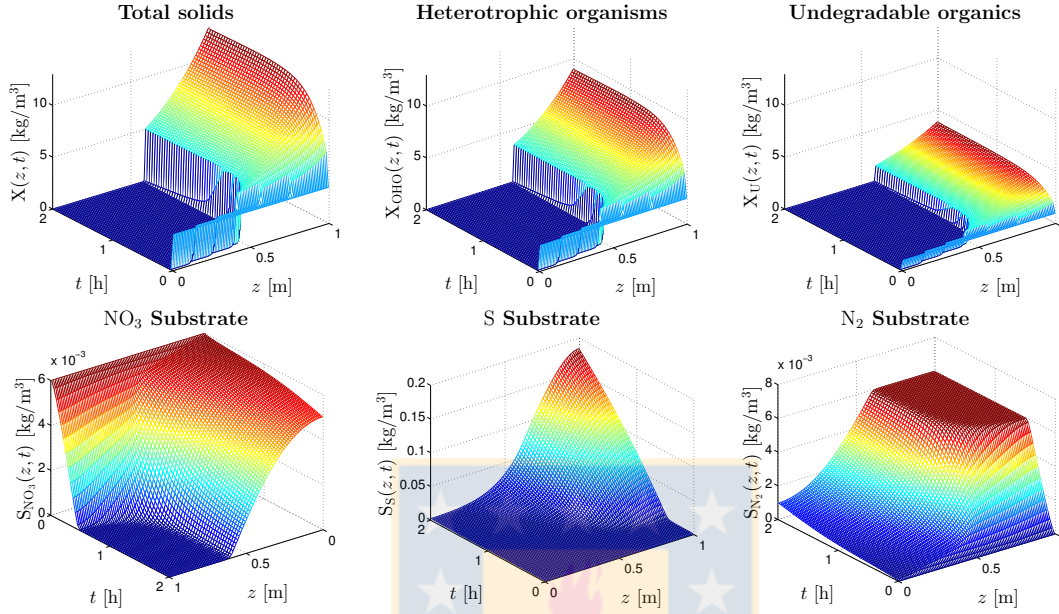


Figure 2.4: Example 2 (Kynch test, $d_S = 9 \times 10^{-6} \text{ m}^2 \text{ s}^{-1}$). Reprinted from [13].

slowly approach an equilibrium concentration as a consequence of their slow diffusive movement.

Figures 2.4 and 2.5 show the corresponding results for the same scenario but with increased values of the substrate diffusion parameter, namely $d_S = 9 \times 10^{-6} \text{ m}^2 \text{ s}^{-1}$ (Figure 2.4) and $d_S = 1.3 \times 10^{-5} \text{ m}^2 \text{ s}^{-1}$ (Figure 2.5). We observe that the changes in this parameter practically do not affect the solids settling behaviour; the solutions for X , X_U and X_{OH_O} are virtually the same as in Example 1. However, differences in the solution behaviour of the substrates are appreciable as can be seen for example by the reduction in S_{NO_3} at the top of the settling column at time $t = 2 \text{ h}$ when d_S increases. Roughly speaking, since increasing d_S means increasing the diffusive flux of each substrate, that is, the flow rate from regions of high concentration to those of low concentration, we observe that the flux of nitrate into the sludge zone consistently increases when comparing the results of Examples 1, 2, and 3. Since the degradation of nitrate takes place due to reactions in that zone, we obtain that for this test, increasing d_S produces an overall more rapid denitrification. Corresponding differences in solution behaviour are visible with the two other substrates.

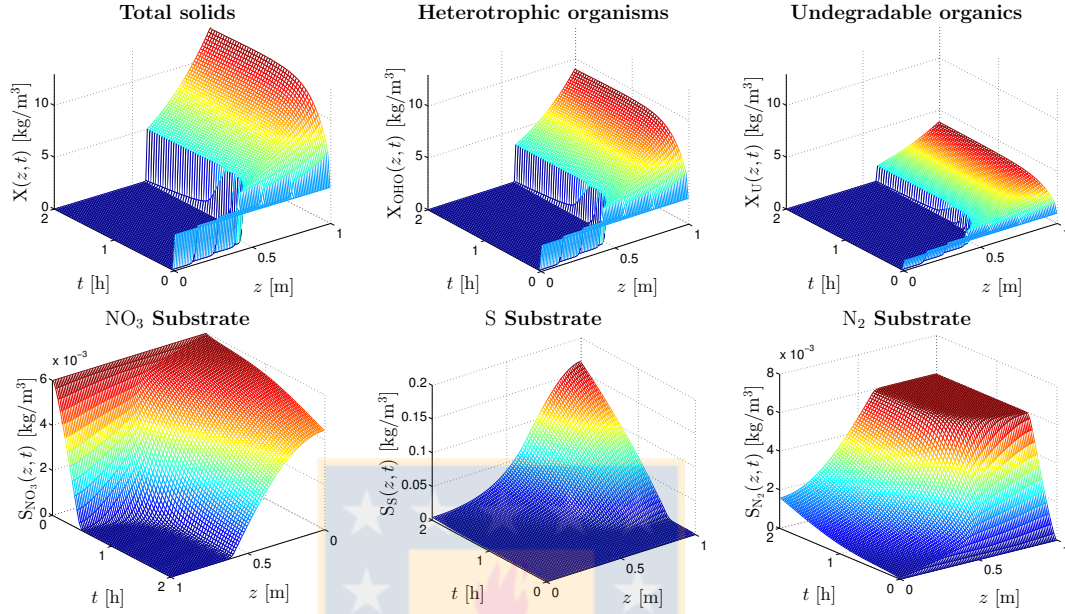


Figure 2.5: Example 3 (Kynch test, $d_S = 1.3 \times 10^{-5} \text{ m}^2 \text{ s}^{-1}$). Reprinted from [13].

2.4.2 Examples 4 and 5: Diehl test (batch settling of suspension initially located above clear liquid)

We here choose the following initial distribution of the solids:

$$X_0(z) = \begin{cases} 7 \text{ kg m}^{-3} & \text{for } 0 \text{ m} < z \leq 0.5 \text{ m,} \\ 0 & \text{for } 0.5 \text{ m} < z \leq 1 \text{ m} \end{cases}$$

for Example 4, and

$$X_0(z) = \begin{cases} 14 \text{ kg m}^{-3} & \text{for } 0 \text{ m} < z \leq 0.25 \text{ m,} \\ 0 & \text{for } 0.25 \text{ m} < z \leq 1 \text{ m} \end{cases}$$

for Example 5. All other parameters are chosen as in Example 1. Since the initial total solids mass is the same as in Examples 1 to 3, results can be compared. The numerical solutions are shown in Figures 3.6 and 3.7. We observe in both examples that the initial body of sludge dilutes, forming a so-called rarefaction wave, the solids

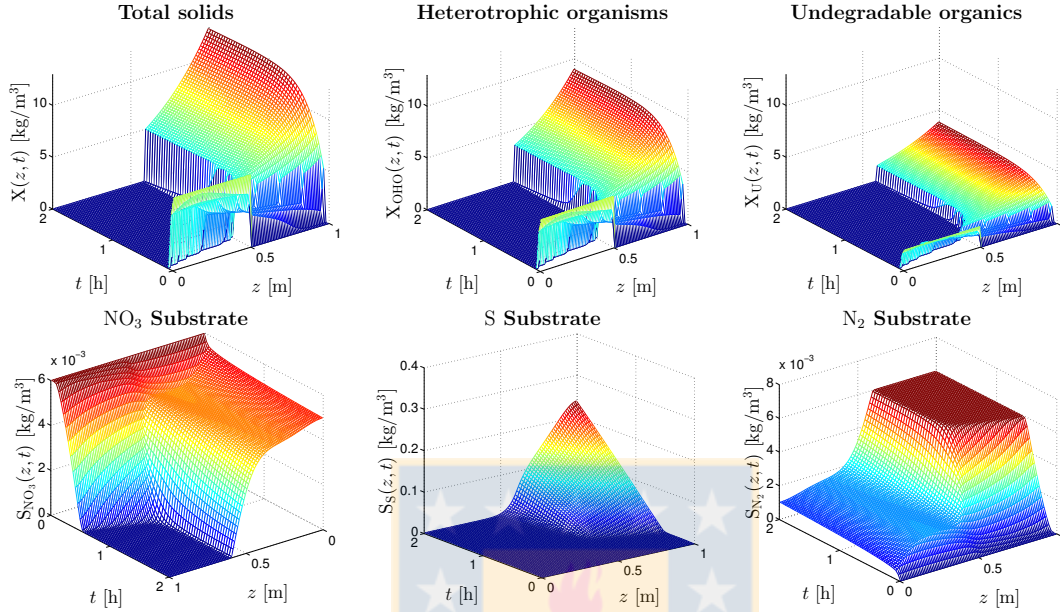


Figure 2.6: Example 4 (Diehl test, $X(z, 0) = 7 \text{ kg m}^{-3}$ above $z = 0.5 \text{ m}$). Reprinted from [13].

settle downward, and accumulate at the bottom to form a sludge layer. Under suitable choices of parameters and initial concentrations, the solution behaviour of a Diehl test produces a curved trajectory of the suspension-supernatant interface that does not arise with a Kynch test, and that can be converted into certain portions of the function f_b . While this property has led us to propose a Diehl test as a device for identification of f_b [8, 18, 45], we use this configuration basically to test the numerical method. We see that the solution for S_{NO_3} is non-monotone (as a function of z for fixed t), which is also reflected in the solution for S_{N_2} . Comparing the S_{NO_3} plot of Figure 3.7 with that of Figure 2.2 shows that the total amount of nitrate at $T = 2 \text{ h}$ is significantly smaller in Examples 4 and 5 than in Example 1. Consequently, the total amount of dissolved nitrogen gas shows the opposite behaviour.

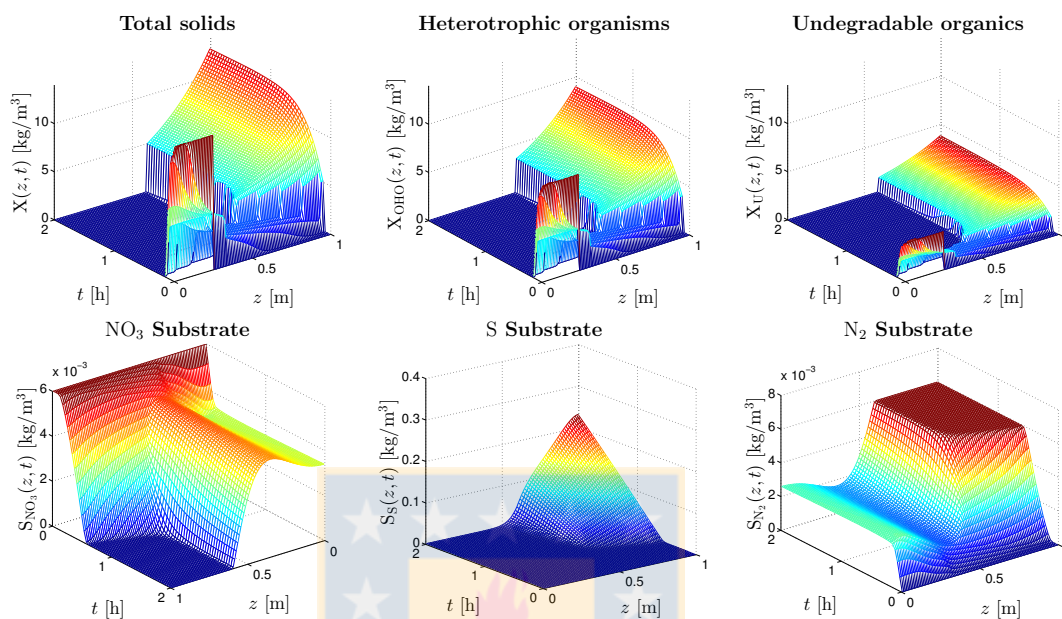


Figure 2.7: Example 5 (Diehl test, $X(z, 0) = 14 \text{ kg m}^{-3}$ above $z = 0.25 \text{ m}$). Reprinted from [13].

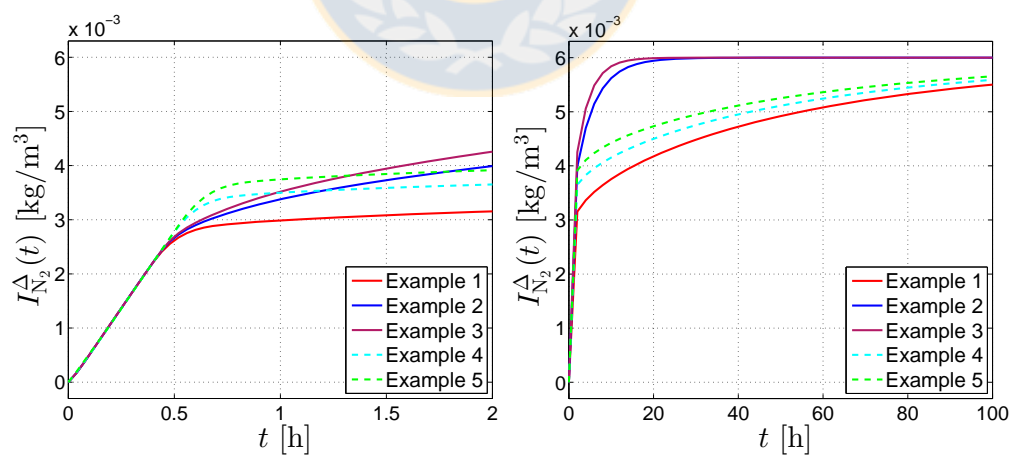


Figure 2.8: Comparison between different examples. Examples 1 to 5: evolution of the approximate normalized nitrate inventory $I_{\text{N}_2}^{\Delta}(t)$. Examples 1–3 show results of three KT with increasing diffusion coefficient d_S , while Examples 4–5 show results of two DT with the same value on d_S as in Ex. 1. Properly elaboration, published in [13].

In light of the latter observation we quantify the evolution of N_2 in the system by measuring the time-dependent average N_2 concentration, defined by

$$I_{N_2}(t) := \frac{1}{B} \int_0^B S_{N_2}(z, t) dz.$$

For a given discretization $\Delta := (\Delta z, \Delta t)$ and $t = n\Delta t$ this quantity is approximated by

$$I_{N_2}^\Delta(t) := \frac{1}{B} \sum_{j=1}^N S_{N_2,j}^n \Delta z = \frac{1}{N} \sum_{j=1}^N S_{N_2,j}^n.$$

Figure 2.8 displays the evolution of $I_{N_2}^\Delta(t)$ for Examples 1 to 5. Comparing the curves for Examples 1, 2 and 3, we find confirmed that an increased value of the substrate diffusion coefficient d_S accelerates the denitrification process in the setup of the Kynch test. However, d_S is a model parameter that is not possible to control, so it is of more practical interest to compare the results of Example 1 (KT) with those of Examples 4 and 5 (DT) (calculated with the same value of d_S). Here we observe that the initial rate of fairly rapid denitrification is the same in all of these three examples up to 30 minutes, but is maintained slightly longer in case of the DT, with the effect that the portions of the curves corresponding to slow rates of denitrification (produced in the consolidation stage after 30 mins) lie about 10% and 15%, in the respective cases of the DT Examples 4 and 5, above that of the KT Example 1 for a couple of hours. This result illustrates how the initial placement of solids mass may influence the rate of denitrification. For long times, the right plot in Figure 2.8 shows that the curves approach each other, which means that also a small diffusion d_S makes the nitrate slowly move down into the sediment where it is converted to nitrogen gas.

2.4.3 Examples 6 and 7: overcompressed test (expansion of compressed sludge)

We utilize the same parameters as in Example 1 and place a highly compressed body of sludge near the bottom of the column. Specifically, we choose

$$X(z, 0) = \begin{cases} 0 & \text{for } 0 \text{ m} < z \leq 0.7 \text{ m}, \\ 20 \text{ kg m}^{-3} & \text{for } 0.7 \text{ m} < z \leq 1 \text{ m} \end{cases}$$

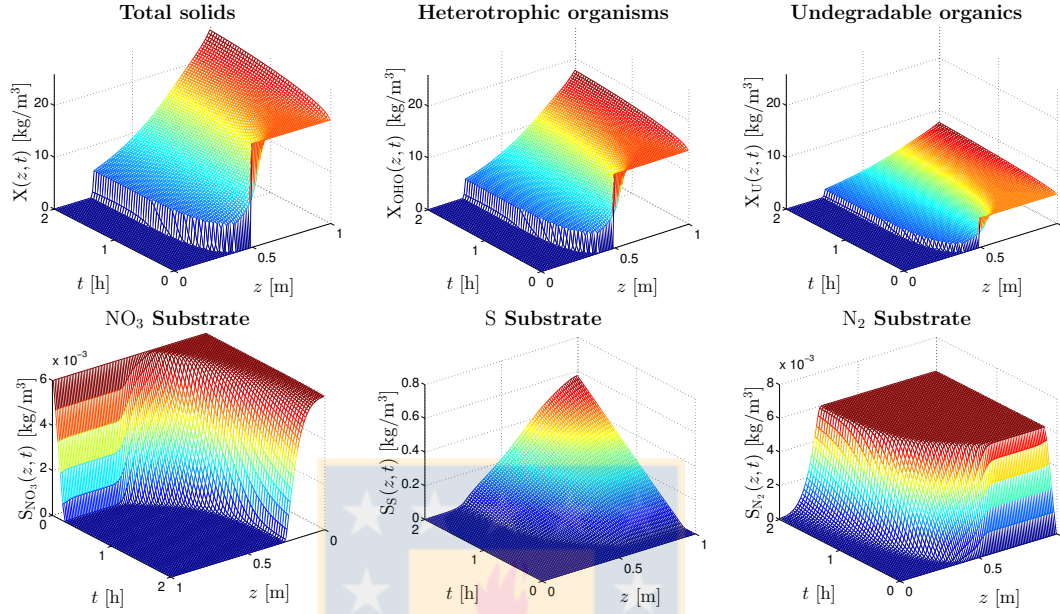


Figure 2.9: Example 6 (overcompressed test, $X(z, 0) = 20 \text{ kg m}^{-3}$ below $z = 0.5 \text{ m}$). Reprinted from [13].

for Example 6 and

$$X_{\text{OHO}}(z, 0) = \begin{cases} 0 & \text{for } 0 \text{ m} < z \leq 0.9 \text{ m}, \\ 25 \text{ kg m}^{-3} & \text{for } 0.9 \text{ m} < z \leq 1 \text{ m} \end{cases}$$

for Example 7. The respective numerical results are shown in Figures 2.9 and 2.10. In both cases, the compressed layer expands once the system starts to evolve. These simulations alert to the limitations of modelling sediment compressibility by a nonlinear diffusion term $\partial^2 D(\phi)/\partial z^2$. This approach corresponds to elastic and in a sense reversible material behaviour which is usually not observed with activated sludge in reality. Describing this behaviour in an anomalous situation with more realism calls for an improvement of the constitutive assumptions concerning sediment compressibility. We emphasize, however, that this test produces an upward movement of solid particles, which is associated with negative values of the velocity v defined in (2.9) allowing to test the numerical scheme under different conditions. The case discrimination in (2.19), which goes back to the method by [43], has precisely been devised to handle

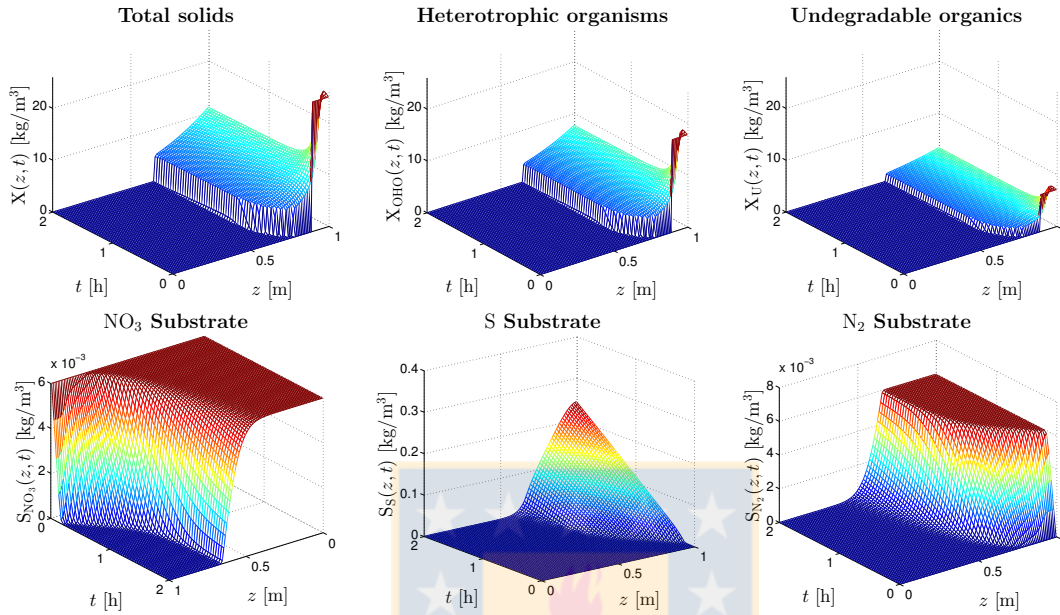


Figure 2.10: Example 6 (overcompressed test, $X(z,0) = 25 \text{ kg m}^{-3}$ below $z = 0.9 \text{ m}$). Reprinted from [13].

this situation. Thus, Figures 2.9 and 2.10 demonstrate that the model is sound, and the numerical scheme works properly, even for settling velocities of variable sign.

2.4.4 Numerical solution versus discretization

To illustrate the accuracy of the method, we plot in Figures 2.11 and 2.12 solutions of Examples 1 and 4 obtained at two different times with fairly coarse discretizations, $N = 20$ and $N = 50$, against a reference solution obtained with $N = 3200$ subintervals. We observe that smooth portions of the solution profiles are approximated quite well by approximate solutions at these coarse discretizations. Nevertheless, discontinuities appear smeared out. Furthermore, to gain some systematic insight into how the numerical solution behaves versus discretization, we calculated the approximate relative error, defined at a fixed time point T , by adding the relative errors of the individual components. The latter are obtained by dividing with the average masses at times

zero and T for the reference solution:

$$m_{\text{OHO}}^{\text{ref}}(T) := \frac{1}{2} (\|X_{\text{OHO}}^{\text{ref}}(\cdot, 0)\|_{L^1} + \|X_{\text{OHO}}^{\text{ref}}(\cdot, T)\|_{L^1}), \quad \text{where} \quad \|h\|_{L^1} := \int_0^B h(z) \, dz,$$

and similarly for the other variables. Both the masses at times zero and T are used as some component may be zero at either of those two time points because of the reactions. We define the normalized relative error

$$\begin{aligned} e_N^{\text{rel}}(T) := & \frac{\|(X_{\text{OHO}} - X_{\text{OHO}}^{\text{ref}})(\cdot, T)\|_{L^1}}{m_{\text{OHO}}^{\text{ref}}(T)} + \frac{\|(X_{\text{U}} - X_{\text{U}}^{\text{ref}})(\cdot, T)\|_{L^1}}{m_{\text{U}}^{\text{ref}}(T)} \\ & + \frac{\|(S_{\text{NO}_3} - S_{\text{NO}_3}^{\text{ref}})(\cdot, T)\|_{L^1}}{m_{\text{NO}_3}^{\text{ref}}(T)} + \frac{\|(S_{\text{N}_2} - S_{\text{N}_2}^{\text{ref}})(\cdot, T)\|_{L^1}}{m_{\text{N}_2}^{\text{ref}}(T)} \\ & + \frac{\|(S_{\text{S}} - S_{\text{S}}^{\text{ref}})(\cdot, T)\|_{L^1}}{m_{\text{S}}^{\text{ref}}(T)}, \end{aligned}$$

and the observed convergence rate between two discretizations with $N = N_1$ and $N = N_2$

$$\theta := -\log(e_{N_1}^{\text{rel}}/e_{N_2}^{\text{rel}})/\log(N_1/N_2).$$

Our results, collected in Table 2.2, are consistent with the fact that the scheme is formally first-order accurate in space and time, and moreover the approximate solutions exhibit discontinuities. Of course, while these results suggest that the scheme converges to a definite limit function, a rigorous convergence proof is still lacking. Furthermore, the CFL condition (CFL), which determines the admissible time step Δt for a given spatial discretization Δz , essentially imposes that $\Delta t \sim \Delta z^2$. This means that if one halves the spatial discretization Δz , or equivalently, doubles N (to increase accuracy) and chooses Δt according to (CFL), then one should expect that the total CPU time to solve the problem to a final time increases by a factor of eight. The CPU times reported in Table 2.2 indicate that this is indeed the case.

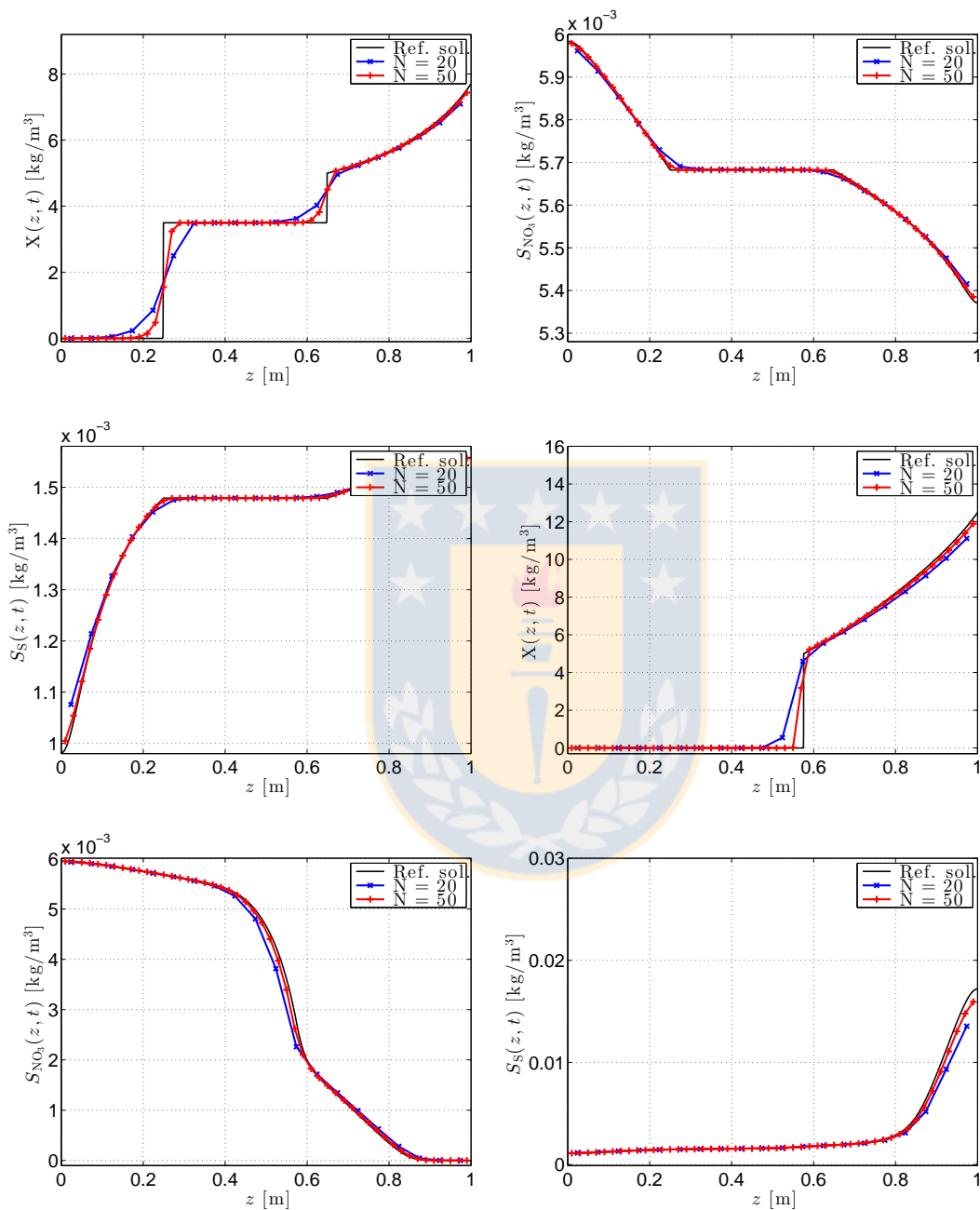


Figure 2.11: Example 1 (Kynch test): comparison between a reference solution ($N = 3200$) and two fastly obtained simple numerical solutions ($N = 20$ and $N = 50$) at simulated times $T = 4$ min (top row and half of second row) and $T = 30$ min (half of second row and bottom row), showing results (in order) for X , S_{NO_3} and S_{S} . Properly elaboration, published in [13].

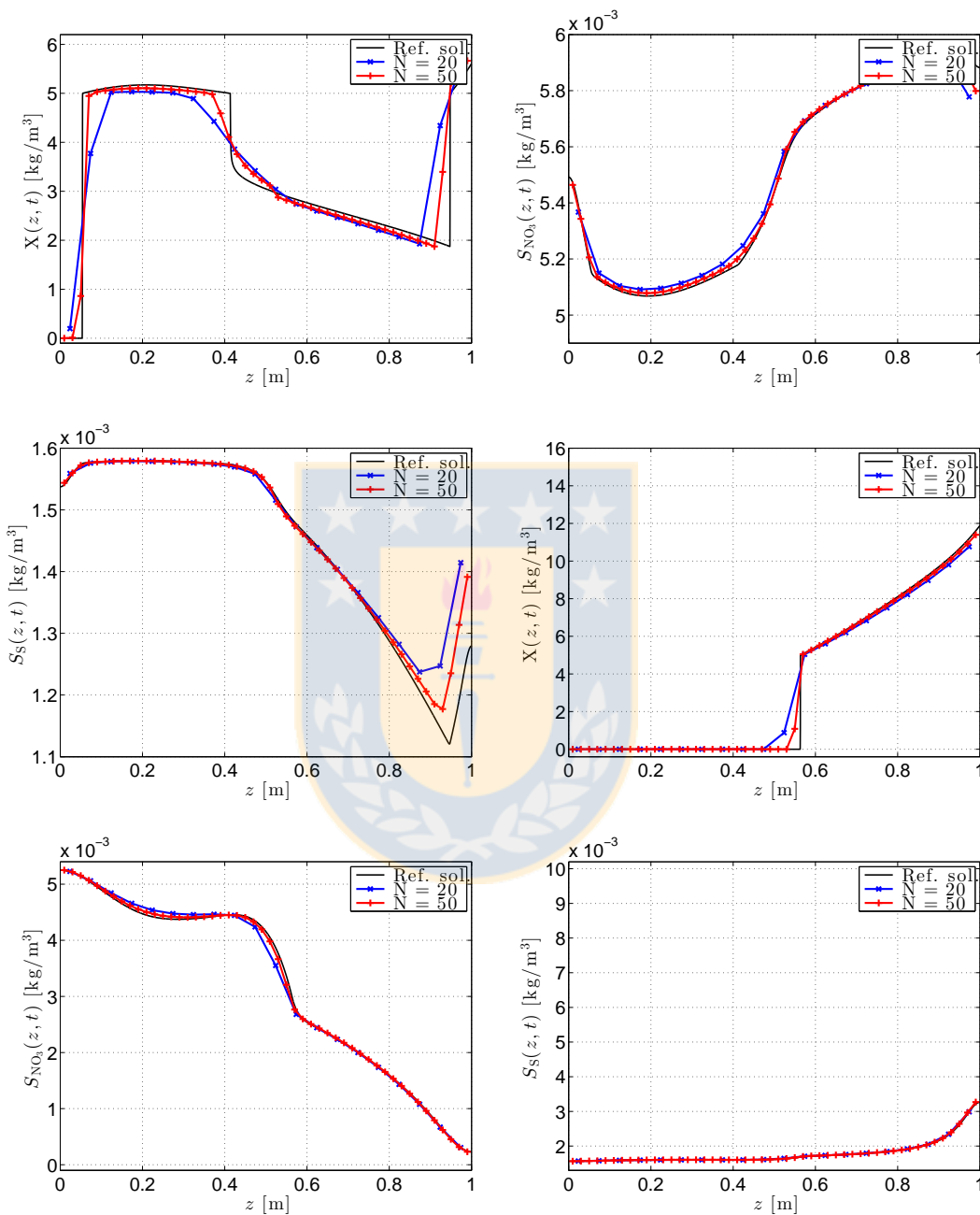


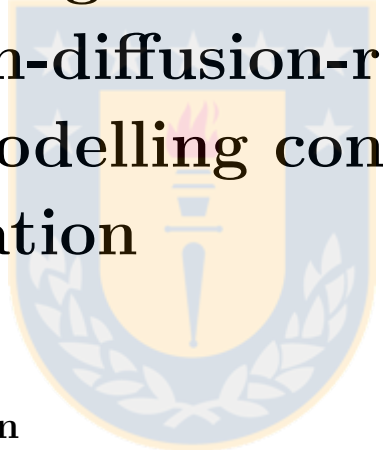
Figure 2.12: Example 4 (Diehl test): comparison between a reference solution ($N = 3200$) and two fast obtained simple numerical solutions ($N = 20$ and $N = 50$) at simulated times $T = 6$ min (top row and half of second row) and $T = 30$ min (half of second row and bottom row), showing results (in order) for X , S_{NO_3} and S_{S} . Properly elaboration, published in [13].

Table 2.2: Error table of Examples 1 and 4. Approximate relative errors e_N^{rel} , convergence rates θ (calculated between neighboring values of N) and CPU times for two different simulated times (cf. Figures 2.11 and 2.12). Properly elaboration, published in [13].

Example 1, $T = 4$ min				Example 1, $T = 30$ min		
N	e_N^{rel}	θ	CPU [s]	e_N^{rel}	θ	CPU [s]
20	0.066	—	0.0076	0.195	—	0.0163
50	0.020	1.765	0.0255	0.073	1.423	0.1533
100	0.011	0.788	0.1770	0.037	0.980	1.2127
200	0.005	1.262	1.3987	0.017	1.117	8.8516
400	0.002	1.191	9.5642	0.008	1.077	56.3849
800	0.001	0.783	63.8714	0.003	1.210	432.2561
Example 4, $T = 6$ min				Example 4, $T = 30$ min		
N	e_N^{rel}	θ	CPU [s]	e_N^{rel}	θ	CPU [s]
20	0.147	—	0.0016	0.087	—	0.0132
50	0.077	0.925	0.0148	0.035	1.309	0.1512
100	0.047	0.727	0.1141	0.021	0.777	1.1988
200	0.028	0.759	0.8956	0.011	0.944	9.8084
400	0.015	0.868	7.1999	0.006	0.916	55.8816
800	0.008	1.003	39.6432	0.003	1.127	423.4776

Chapter 3

A difference scheme for a degenerating convection-diffusion-reaction system modelling continuous sedimentation



3.1 Introduction

The separation of fine solid particles from a liquid by gravity under continuous flows in and out of large tanks is a unit operation in wastewater treatment, mineral processing, hydrometallurgy, and other applications. Since gravity acts in one dimension and computational resources for simulations are limited, spatially one-dimensional models are common. The continuous sedimentation of a suspension subject to applied feed and bulk flows, hindered settling and sediment compressibility can be modelled by a nonlinear, strongly degenerate parabolic PDE for the solids concentration $X = X(z, t)$ as a function of depth z and time t [27]. This PDE is based on the solid and liquid mass balances, and its coefficients depend discontinuously on z .

Important applications also involve chemical reactions between different components of the solid and liquid phases. In wastewater treatment, there are biokinetic reactions between flocculated activated sludge (bacteria) and substrates (nutrients) dissolved in

the liquid. This work combines the model of continuous sedimentation with compression [27] with a description of the transport and reaction of these components. The final model can be written as the system of PDEs

$$\frac{\partial X}{\partial t} + \frac{\partial}{\partial z} (\mathcal{F}(X, z, t) - \gamma(z) \partial_z D(X)) = \mathcal{A}_X(X, \mathbf{p}_X, \bar{\mathbf{p}}_L, z, t), \quad (3.1a)$$

$$\frac{\partial(\mathbf{p}_X X)}{\partial t} + \frac{\partial}{\partial z} (\mathbf{p}_X (\mathcal{F}(X, z, t) - \gamma(z) \partial_z D(X))) = \mathcal{A}_X(X, \mathbf{p}_X, \bar{\mathbf{p}}_L, z, t), \quad (3.1b)$$

$$\frac{\partial(\bar{\mathbf{p}}_L l_1(X))}{\partial t} + \frac{\partial}{\partial z} (\bar{\mathbf{p}}_L l_2 (\mathcal{F}(X, z, t) - \gamma(z) \partial_z D(X), z, t)) = \mathcal{A}_L(X, \mathbf{p}_X, \bar{\mathbf{p}}_L, z, t) \quad (3.1c)$$

for $z \in \mathbb{R}$ and $t > 0$, along with suitable initial conditions. The convective flux function \mathcal{F} describes the bulk flow and hindered settling, while the function D accounts for sediment compressibility. The characteristic function γ distinguishes between the interior and the exterior of the settling tank, i.e., $\gamma(z) = 1$ if $-H < z < B$ and $\gamma(z) = 0$ outside; see Figure 3.1 (a). Both \mathcal{F} and D depend nonlinearly on X and discontinuously on z , and it is assumed that $D = 0$ on an X -interval of positive length, so the model is strongly degenerate and its solutions will, in general, be discontinuous. Moreover, $\mathbf{p}_X = \mathbf{p}_X(z, t)$ and $\bar{\mathbf{p}}_L = \bar{\mathbf{p}}_L(z, t)$ are vectors of unknown (mass) percentages of components of the solid and liquid phases, l_1 and l_2 are certain given functions, and \mathcal{A}_X , \mathcal{A}_X and \mathcal{A}_L are algebraic expressions that stand for given feed and reaction terms. (Precise definitions and assumptions are provided in Section 3.2.)

We herein derive the new model (3.1) from volume and mass balances and common constitutive assumptions on the relative velocity between the two phases and on the reactions between components. One can insert any suitable constitutive functions that model the effects of hindered settling, compression and biochemical reactions. The model equations are written in a form suitable for explicit numerical methods where the equations in (3.1) are solved consecutively. We derive a difference scheme that combines the approach of [20, 27] for the non-reactive case (i.e., suitable for (3.1a) in the absence of reactions) with the numerical percentage transport introduced in [43] for a related multi-component, non-reactive model. The main mathematical result is an invariant-region principle proved under a suitable CFL condition. This result ensures that numerical solutions are physically relevant and, in particular, non-negative. Several examples illustrate the predictions of the new model and the convergence property of the scheme.

The results of this Chapter are published in:

- R. Bürger, S. Diehl, and C. Mejías. A difference scheme for a degenerating convection-diffusion-reaction system modelling continuous sedimentation. *ESAIM: Mathematical Modelling and Numerical Analysis*, 52(2): 365 – 392, 2018.
- R. Bürger, S. Diehl, and C. Mejías. A model for continuous sedimentation with reactions for wastewater treatment. In G. Mannia, editor, *Frontiers in Wastewater Treatment and Modelling (FICWTM 2017), Lecture Notes in Civil Engineering*, volume 4, pages 596 – 601, Cham, Switzerland, 2017. Springer International Publishing.
- R. Bürger, J. Careaga, S. Diehl, C. Mejías, and R. Ruiz-Baier. Convection-diffusion-reaction and transport-flow problems motivated by models of sedimentation: some recent advances. In P.N. de Souza and M. Viana, editors, *Proceedings of the International Congress of Mathematicians, Rio de Janeiro 2018 Vol. IV: Invited Lectures*, Singapore. World Scientific, in press.

3.1.1 Related work

For the non-reactive case, the first model for the hyperbolic case ($D \equiv 0$) [41] described hindered settling, and was extended in [27] by a strongly degenerating diffusion function $D \neq 0$ to include sediment compression at high solids concentrations. The discontinuous dependence of \mathcal{F} on z and the presence of $\gamma(z)$ arise from the description of the inlet and outlet streams of the sedimentation tank. Therefore, in the non-reactive case, (3.1a) represents an application of the theory of first-order conservation laws with discontinuous flux and its extensions to degenerate parabolic PDEs. It is well known that solutions of such equations are in general discontinuous and need to be defined as weak solutions along with a selection criterion or entropy condition to ensure uniqueness. The main mathematical issues posed by (3.1a) are to find suitable uniqueness conditions and establish well-posedness [27, 40, 46, 62], as well as to define numerical schemes that provably converge to the unique solution [25]. The well-posedness and numerical analysis of [27] is strongly based on the work by Karlsen, Risebro and Towers [79, 81, 82]. Versions of the scalar equation (3.1a) are still topic of current research in numerical analysis: adaptive resolution schemes for the case $\mathcal{A}_X \equiv 0$ can be found in [30], monotone entropy stable schemes for the case $D \equiv 0$ and $\mathcal{A}_X \equiv 0$ in [1], and a convergence rate in the case $\mathcal{A}_X \equiv 0$ with several spatial variables is derived in [80].

The well-posedness and numerical analysis of the non-reactive version of (3.1a) has led to a recent simulation model for secondary settling tanks (SSTs) in wastewater treatment and an adhering numerical scheme [20, 24]. That model has shown to give more realistic predictions than previous standard models [92, 120].

There are several motivations for extending our previous non-reactive model to the system (3.1). In both mineral processing and wastewater treatment, liquid flocculant added to the suspension sticks to the small particles so that larger flocs are formed and thereby their settling velocity increased. The importance of reactive sedimentation in wastewater treatment has been demonstrated in [3, 57, 60, 65, 67, 93, 100]. Similar phenomena modelled by PDEs are flocculation in mineral processing [110], multi-component two-phase flow in porous media [4, 10] and particle-size segregation in granular avalanches [64]. Another application with potential modelling advantages is counter-current “washing” of solids, a process of solvent extraction in hydrometallurgy by coupling a series of clarifier-thickeners [116]. A system of PDEs modelling two-dimensional hydrodynamics coupled to biological reactions for algal growth and a numerical scheme can be found in [11].

A PDE model and numerical scheme for batch sedimentation (closed vessel) of two particulate components including a reduced biokinetic model were presented in [13]. The movements of the substrates were only modelled by simple diffusion. In the examples herein we use the same biokinetic denitrification reactions as in [13].

Positivity preservation of numerical scheme for conservation laws [5, 101] is a challenge in itself. Standard numerical fluxes for finite volume schemes do not preserve the fundamental requirements that the mass percentages belong to the interval $[0, 1]$ and their sum is always equal to one [74]. This is, however, handled by our numerical scheme.

3.1.2 Outline of the remainder of this chapter

In Section 3.2, the model is derived. To this end, we introduce in Section 3.2 the concept of an ideal secondary settling tank (SST) (see Figure 3.1), the model variables and some fundamental assumptions. Simplifying assumptions typical of wastewater treatment are collected in Section 3.2.1. The mathematical model, based on conservation laws, is stated in Section 3.2.2. To convert it into an equivalent model suitable for simulation, we first replace (in Section 3.2.3) the abstract solid and fluid phase velocities by a mixture bulk velocity, expressed by the given volumetric flows and model variables, and a solid-fluid relative velocity, prescribed by constitutive functions. Next, in Section 3.2.4 we derive explicit expressions for the total fluxes of the solid and liquid phases, and after further reformulations arrive in Section 3.2.5 at the model in final, solvable form akin to (3.1). To close the model we introduce in Section 3.2.6 constitutive functions for hindered and compressive settling, and address in Section 3.2.7 the choice of initial data and feed input functions for a reactive model of denitrification. In

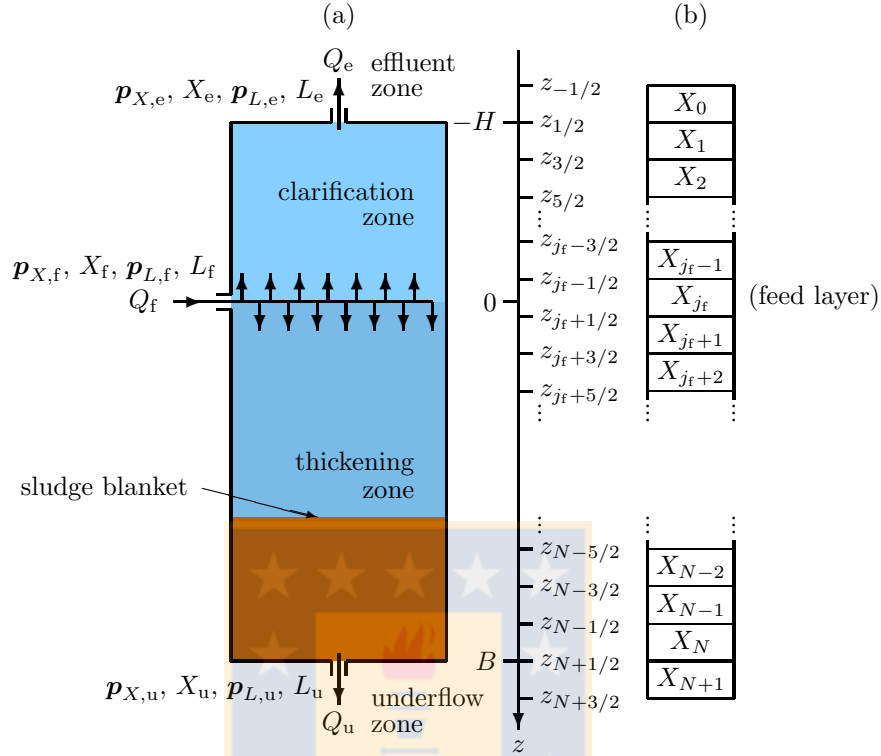


Figure 3.1: Schematic view of secondary settling tank (SST) with variables and numerical discretization. (a) An ideal (SST) with variables of the feed inlet, effluent and underflow indexed with f, e and u, respectively. The effluent, clarification, thickening, and underflow zones correspond to the respective intervals $z < -H$, $-H < z < 0$, $0 < z < B$, and $z > B$. The sludge blanket (concentration discontinuity) separates the hindered settling zone and the compression zone. (b) Aligned illustration of the subdivision of the SST into layers (see Section 3.3). The SST is divided into N internal computational cells, or layers, of depth $\Delta z = (B + H)/N$. Reprinted from [23].

Section 3.3, a numerical scheme is derived along with a CFL condition and an invariant region property. This is done via a method-of-lines discretization (Section 3.3.1) that combines ingredients from [24] and [48]. A time discretization leading to a fully discrete scheme is introduced in Section 3.3.2, and the corresponding CFL condition is stated in Section 3.3.3. Section 3.3.4 is devoted to the proof, via several lemmas that appeal to monotonicity arguments, of the main mathematical result, Theorem 3.3.1, which states that the scheme satisfies an invariant-region principle. In Section 3.4, we present numerical examples for a reaction model of denitrification. These illustrate the response of the SST to variations of the feed inputs and the impact of different constitutive assumptions. Section 3.4.4 contains estimations of the corresponding error and convergence rate.

3.2 Model formulation

In mineral processing and hydrometallurgy, continuously operated sedimentation tanks are usually referred to as “clarifier-thickeners” or simply “thickeners”, and in wastewater treatment (our main motivation) as “secondary clarifiers” or “secondary settling tanks” (SSTs). The ideal SST, shown in Figure 3.1 (a), has a constant cross-sectional area A . The concentration of each component is assumed to depend only on time t and depth z measured from the feed inlet located at $z = 0$. The balance laws that make up the model hold for $z \in \mathbb{R}$, have coefficients that are spatially discontinuous at $z = -H, 0$ and B , and need no boundary condition. The suspension is constituted by the solid phase that consists of particles and the liquid phase that consists of substrates dissolved in water.

The total concentration of particles (or the solid phase) is denoted by $X(z, t)$. Each (floculated) multi-component particle is assumed to consist of a number k_X of components described by the (mass) percentage vector

$$\mathbf{p}_X = (p_X^{(1)}, p_X^{(2)}, \dots, p_X^{(k_X)})^T, \quad \text{where } p_X^{(1)} + \dots + p_X^{(k_X)} = 1. \quad (3.2)$$

The effluent concentration is $X_e(t) := \lim_{\varepsilon \rightarrow 0^+} X(-H - \varepsilon, t)$. The underflow concentration X_u and the percentage vectors $\mathbf{p}_{X,e}$ and $\mathbf{p}_{X,u}$ are defined analogously. The concentrations of all solid components are

$$\mathbf{p}_X X =: \mathbf{C} = (C^{(1)}, \dots, C^{(k_L)})^T.$$

For $X = 0$ the values of \mathbf{p}_X are irrelevant; however, they should always satisfy (3.2).

The total concentration of the liquid phase is denoted by $L(z, t)$. The percentage vector \mathbf{p}_L and the concentrations at the in- and outlets are defined in the same way as for the solid phase. We assign the last percentage $p_L^{(k_L)}$ for the water component, which is much larger than the percentages of the soluble components $p_L^{(i)}$, $i = 1, \dots, k_L - 1$. If the concentrations of the soluble components are contained in the vector

$$\mathbf{S} = (S^{(1)}, \dots, S^{(k_L-1)})^T$$

and W denotes the water component, then

$$\mathbf{p}_L L = \begin{pmatrix} \mathbf{S} \\ W \end{pmatrix}, \quad \text{where } W = p_L^{(k_L)} L = \left(1 - \sum_{i=1}^{k_L-1} p_L^{(i)}\right) L = L - \sum_{i=1}^{k_L-1} S^{(i)}. \quad (3.3)$$

The concentrations X_f , L_f , percentage vectors $\mathbf{p}_{X,f}$, $\mathbf{p}_{L,f}$, and volumetric flows $Q_f \geq Q_u > 0$ are given functions of t . It turns out that the effluent volumetric flow $Q_e(t; \mathbf{C}, \mathbf{S})$ generally depends on unknown variables via the reaction terms; see Section 3.2.3. We define $q_f := Q_f/A$, $q_e := Q_e/A$ and $q_u := Q_u/A$.

The density of the solid phase ρ_X is assumed to be constant and much greater than the maximum packing concentration of the solids X_{\max} .

The (unknown) solid and liquid phase velocities are denoted by $v_X = v_X(z, t)$ and $v_L = v_L(z, t)$, respectively. Inside the SST, the particles undergo hindered settling and compression according to some constitutive function (see Section 3.2.6) for the relative velocity

$$v_X - v_L =: v_{\text{rel}} = v_{\text{rel}}(X, \partial X / \partial z). \quad (3.4)$$

In the effluent and underflow zones, both phases move at the same velocity, i.e.,

$$v_{\text{rel}} := 0 \quad \text{for } z < -H \text{ and } z \geq B. \quad (3.5)$$

The reaction terms for all particulate and soluble components are collected in the vectors $\mathbf{R}_X(\mathbf{C}, \mathbf{S})$ of length k_X and $\mathbf{R}_L(\mathbf{C}, \mathbf{S})$ of length k_L . We define

$$\tilde{\mathbf{R}}_X(\mathbf{C}, \mathbf{S}) := \sum_{i=1}^{k_X} R_X^{(i)}(\mathbf{C}, \mathbf{S}), \quad \tilde{\mathbf{R}}_L(\mathbf{C}, \mathbf{S}) := \sum_{i=1}^{k_L} R_L^{(i)}(\mathbf{C}, \mathbf{S}).$$

We assume that every volume of the suspension initially contains either of the two phases in the SST and always for the feed input. For a small volume $V = V_X + V_L$ of suspension, where V_X and V_L are the respective volume of each phase, the masses of the two phases in V can be expressed as $\rho_X V_X = XV$ and $\rho_L V_L = LV$, respectively.

Remark 3.2.1. *To allow for defining local values of density, concentration and volume fraction, the volume V should be sufficiently small but contain enough particles to be representative. We refer to [53] for a discussion including different definitions involving, e.g., the average or expected values of V_X and the mass m_X such that the limit $\lim_{V \rightarrow 0^+} m_X/V_X$ exists and can define the density ρ_X .*

3.2.1 Specific assumptions for wastewater treatment

The assumptions stated so far refer to any application. The further analysis will, however, rely on some simplifying assumptions typical of wastewater treatment with

biological reactions. Since the liquid phase in the feed inlet consists almost entirely of water, the density of the liquid phase ρ_L is assumed to be constant.

The water concentration $W = p_L^{(kL)} L$ does not influence, nor is influenced by, any reaction, so that $R_L^{(kL)} = 0$. We assume zero growth of bacteria when there is no, i.e., $\mathbf{R}_{X,j}(\mathbf{0}, \mathbf{S}) = \mathbf{0}$, and allow that a zero soluble substrate concentration may increase due to decay of bacteria, that is, $\mathbf{R}_{L,j}(\mathbf{C}, \mathbf{0}) \geq 0$ (non-negative components). We also assume that that if one component is not present, i.e. $p_X^{(k)} = 0$, then there cannot vanish any such material, i.e.,

$$R_X^{(k)}(\mathbf{p}_X X, \mathbf{S}) \Big|_{p_X^{(k)}=0} \geq 0, \quad (3.6)$$

and similarly for the substrate reaction functions \mathbf{R}_L . Furthermore, we assume that there is no reaction in the effluent and underflow regions. Finally, the following assumptions are technical but not restrictive for the application:

$$\tilde{R}_X(\mathbf{p}_X X_{\max}, \mathbf{S}) = 0, \quad v_{\text{rel}}(X_{\max}, \partial_z X) = 0. \quad (3.7)$$

The former states that the bacteria cannot grow when they have reached the maximum concentration X_{\max} and the latter that the particles follow the liquid flow at X_{\max} .

3.2.2 Balance equations

The fundamental equation that every volume of the suspension contains either of the two phases can be written as

$$V_X + V_L = V \quad \Leftrightarrow \quad \frac{X}{\rho_X} + \frac{L}{\rho_L} = 1 \quad \Leftrightarrow \quad L = \rho_L - rX, \quad \text{where } r := \frac{\rho_L}{\rho_X}. \quad (3.8)$$

We assume that this is satisfied at $t = 0$ within the SST and always for the given feed concentrations; $X_f/\rho_X + L_f/\rho_L = 1$. The assumption $\rho_X > X_{\max}$ implies that always $L > 0$.

The conservation of mass for each particulate and soluble/liquid component and the requirements of the percentages imply the following system of equations for $z \in \mathbb{R}$ and

$t > 0$, where $\delta(z)$ is the delta function:

$$\frac{\partial(\mathbf{p}_X X)}{\partial t} + \frac{\partial(\mathbf{p}_X X v_X)}{\partial z} = \delta(z) \mathbf{p}_{X,f} X_f q_f + \gamma(z) \mathbf{R}_X(\mathbf{C}, \mathbf{S}), \quad (3.9a)$$

$$\frac{\partial(\mathbf{p}_L L)}{\partial t} + \frac{\partial(\mathbf{p}_L L v_L)}{\partial z} = \delta(z) \mathbf{p}_{L,f} L_f q_f + \gamma(z) \mathbf{R}_L(\mathbf{C}, \mathbf{S}), \quad (3.9b)$$

$$p_X^{(1)} + \dots + p_X^{(k_X)} = 1, \quad (3.9c)$$

$$p_L^{(1)} + \dots + p_L^{(k_L)} = 1. \quad (3.9d)$$

3.2.3 Phase, bulk and relative velocities

The full set of $k_X + k_L + 4$ balance equations are (3.4), (3.8) and (3.9), and the unknowns are \mathbf{p}_X , X , v_X , \mathbf{p}_L , L and v_L . We now reduce the number of equations by eliminating the variables v_X and v_L . To this end, we first replace them by v_{rel} and the average bulk velocity of the suspension q , and then express q in terms of the rest of the unknowns.

Lema 3.2.1. *Equations (3.9a) and (3.9c) are equivalent to (3.9a) and*

$$\frac{\partial X}{\partial t} + \frac{\partial(X v_X)}{\partial z} = \delta(z) X_f q_f + \gamma(z) \tilde{R}_X. \quad (3.10)$$

Analogously, (3.9b) and (3.9d) are equivalent to (3.9b) and

$$\frac{\partial L}{\partial t} + \frac{\partial(L v_L)}{\partial z} = \delta(z) L_f q_f + \gamma(z) \tilde{R}_L. \quad (3.11)$$

Proof. Summing all equations in (3.9a), using (3.9c) and that $\mathbf{p}_{X,f}$ satisfies (3.2), we get (3.10). Conversely, summing all equations in (3.9a) and subtracting (3.10) implies (3.9c).

Second part is solved similarly to the first part. □

With the volume fraction of the solid phase $\phi := V_X/V$, we have $X = \rho_X \phi$ and $L = \rho_L(1 - \phi)$, cf. (3.8). Analogously, the feed inlet concentrations can be written as $X_f = \rho_X \phi_f$ and $L_f = \rho_L(1 - \phi_f)$. Substituting these expressions into (3.10) and (3.11) and dividing by the constant densities ρ_X and ρ_L , respectively, we get

$$\begin{aligned} \frac{\partial \phi}{\partial t} + \frac{\partial(\phi v_X)}{\partial z} &= \delta(z) \phi_f q_f + \gamma(z) \frac{\tilde{R}_X}{\rho_X}, \\ \frac{\partial(1 - \phi)}{\partial t} + \frac{\partial((1 - \phi) v_L)}{\partial z} &= \delta(z) (1 - \phi_f) q_f + \gamma(z) \frac{\tilde{R}_L}{\rho_L}. \end{aligned}$$

Adding these two equations and defining the average bulk velocity and a weighted reaction function:

$$q(z, t) := \phi v_X(z, t) + (1 - \phi)v_L(z, t), \quad (3.12)$$

$$\mathcal{R}(\mathbf{C}, \mathbf{S}) := \frac{\tilde{R}_X(\mathbf{C}, \mathbf{S})}{\rho_X} + \frac{\tilde{R}_L(\mathbf{C}, \mathbf{S})}{\rho_L}, \quad (3.13)$$

we get an equation without any time derivative:

$$\partial_z q = \delta(z)q_f + \gamma(z)\mathcal{R}(\mathbf{C}, \mathbf{S}). \quad (3.14)$$

We can express v_X and v_L in terms of q and v_{rel} since (3.4) and (3.12) are equivalent to

$$v_X = q + v, \quad \text{where } v := (1 - \phi)v_{\text{rel}}, \quad (3.15)$$

$$v_L = q - \phi v_{\text{rel}}. \quad (3.16)$$

We now derive an explicit expression for q . In view of (3.5), (3.12) implies:

$$q(z, t) = \begin{cases} v_X(z, t) = v_L(z, t) = -q_e(t) & \text{for } z \leq -H, \\ v_X(z, t) = v_L(z, t) = q_u(t) & \text{for } z \geq B, \end{cases} \quad (3.17)$$

where q_u is known and q_e is unknown. We integrate (3.14) from z to B to get

$$q(z, t; \mathbf{C}, \mathbf{S}) = q(B, t) - \int_z^B \left(\delta(\xi)q_f(t) + \gamma(\xi)\mathcal{R}(\mathbf{C}(\xi, t), \mathbf{S}(\xi, t)) \right) d\xi. \quad (3.18)$$

The following function describes the additional bulk velocity due to the reactions:

$$q^{\text{reac}}(z; \mathbf{C}, \mathbf{S}) := \int_z^B \gamma(\xi)\mathcal{R}(\mathbf{C}, \mathbf{S}) d\xi. \quad (3.19)$$

Since by (3.17), $q(B, t) = q_u(t)$, we may express q in terms of the unknowns as follows:

$$q(z, t; \mathbf{C}, \mathbf{S}) := \begin{cases} q_u(t) - q_f(t) - q^{\text{reac}}(-H; \mathbf{C}, \mathbf{S}) & \text{for } z \leq -H, \\ q_u(t) - q_f(t) - q^{\text{reac}}(z; \mathbf{C}, \mathbf{S}) & \text{for } -H < z < 0, \\ q_u(t) - q^{\text{reac}}(z; \mathbf{C}, \mathbf{S}) & \text{for } 0 < z < B, \\ q_u(t) & \text{for } z \geq B. \end{cases} \quad (3.20)$$

Moreover, (3.17) states that $q(z, t) = -q_e(t)$ for $z \leq -H$, so (3.20) defines the effluent bulk velocity in terms of the unknowns: $q_e(t; \mathbf{C}, \mathbf{S}) = q_f(t) - q_u(t) + q^{\text{reac}}(-H; \mathbf{C}, \mathbf{S})$.

3.2.4 Solid and liquid total fluxes

The flux functions of the PDEs (3.10) for X and (3.11) for L can, by means of (3.15) and (3.16), be written as

$$Xv_X = Xq + Xv, \quad (3.21)$$

$$Lv_L = \rho_L(1 - \phi)(q - \phi v_{\text{rel}}) = \rho_L((1 - \phi)q - \phi v) = \rho_L \left(q - \frac{Xq + Xv}{\rho_X} \right). \quad (3.22)$$

Thus, we define the total fluxes in terms of q and $v = (1 - \phi)v_{\text{rel}}$ as follows:

$$F_X := Xq + Xv = Xq + X \left(1 - \frac{X}{\rho_X} \right) v_{\text{rel}}, \quad (3.23)$$

$$F_L := \rho_L q - r F_X \Leftrightarrow \frac{F_X}{\rho_X} + \frac{F_L}{\rho_L} = q. \quad (3.24)$$

With q defined by (3.20), F_X by (3.23) and F_L by (3.24) we get the following governing equations, which neither contain v_X nor v_L :

$$\frac{\partial(\mathbf{p}_X X)}{\partial t} + \frac{\partial(\mathbf{p}_X F_X)}{\partial z} = \delta(z) \mathbf{p}_{X,f} X_f q_f + \gamma(z) \mathbf{R}_X(\mathbf{C}, \mathbf{S}), \quad (3.25a)$$

$$\frac{\partial(\mathbf{p}_L L)}{\partial t} + \frac{\partial(\mathbf{p}_L F_L)}{\partial z} = \delta(z) \mathbf{p}_{L,f} L_f q_f + \gamma(z) \mathbf{R}_L(\mathbf{C}, \mathbf{S}), \quad (3.25b)$$

$$p_X^{(1)} + \dots + p_X^{(k_X)} = 1, \quad (3.25c)$$

$$p_L^{(1)} + \dots + p_L^{(k_L)} = 1. \quad (3.25d)$$

The proof of the following lemma is analogous to that of Lemma 3.2.1.

Lema 3.2.2. *Equations (3.25a) and (3.25c) are equivalent to (3.25a) and*

$$\frac{\partial X}{\partial t} + \frac{\partial F_X}{\partial z} = \delta(z) X_f q_f + \gamma(z) \tilde{\mathbf{R}}_X. \quad (3.26)$$

Analogously, (3.25b) and (3.25d) are equivalent to (3.25b) and

$$\frac{\partial L}{\partial t} + \frac{\partial F_L}{\partial z} = \delta(z) L_f q_f + \gamma(z) \tilde{\mathbf{R}}_L. \quad (3.27)$$

Lema 3.2.3. *Equations (3.26) and (3.27) are equivalent to (3.26) and (3.8).*

Proof. Dividing (3.26) by ρ_X , (3.27) by ρ_L and summing these two equations, we get the following equation which can replace (3.27) (with maintained equivalence):

$$\frac{\partial}{\partial t} \left(\frac{X}{\rho_X} + \frac{L}{\rho_L} \right) + \frac{\partial}{\partial z} \left(\frac{F_X}{\rho_X} + \frac{F_L}{\rho_L} \right) = \delta(z) q_f \left(\frac{X_f}{\rho_X} + \frac{L_f}{\rho_L} \right) + \gamma(z) \left(\frac{\tilde{R}_X}{\rho_X} + \frac{\tilde{R}_L}{\rho_L} \right)$$

All terms except the first cancel. This is because of the equality (3.24), the expression (3.18) for q and the definition of \mathcal{R} in (3.13). The remaining equation is

$$\frac{\partial}{\partial t} \left(\frac{X}{\rho_X} + \frac{L}{\rho_L} \right) = 0 \quad \Leftrightarrow \quad \frac{\partial}{\partial t} \left(\frac{V_X}{V} + \frac{V_L}{V} \right) = 0 \quad \Leftrightarrow \quad \frac{V_X}{V} + \frac{V_L}{V} = g(z),$$

where the function $g(z)$ must be equal to one, since it is at time $t = 0$ by assumption. Hence, the remaining equation is equivalent to (3.8). \square

Lema 3.2.4. *Equations (3.4), (3.8) and (3.9) are equivalent to the governing equations (3.25).*

Proof. Lemma 3.2.1 states that (3.9c) and (3.9d) can be replaced (keeping the equivalence) by (3.10) and (3.11). Equations (3.4) and (3.8) imply via (3.21)–(3.24) that $Xv_X = F_X$ and $Lv_L = F_L$. Hence, (3.10) and (3.11) are equivalent to (3.26) and (3.27), which by Lemma 3.2.2 can be replaced by (3.25c) and (3.25d). For the other implication, we should prove that (3.4), (3.8), $F_X = Xv_X$ and $F_L = Lv_L$ hold. Lemma 3.2.2 implies first that (3.25c) and (3.25d) can be replaced by (3.26) and (3.27). Then Lemma 3.2.3 implies (3.8). By (3.15) and (3.16), (3.4) is directly satisfied and $F_X = X(q + v) = Xv_X$. With this equality and $\phi = X/\rho_X$, we obtain from (3.12) $F_X/\rho_X + (1 - X/\rho_X)v_L = q$. Substituting this into the definition of F_L (3.24), we get $F_L = \rho_L(q - rF_X) = (\rho_L - rX)v_L = Lv_L$, where the last equality follows from (3.8). \square

3.2.5 Model equations in final form

We observe that the last scalar equation of (3.25b) determines $p_L^{(k_L)}$ for the water component of the liquid. This variable does not appear in any other equation. A simpler equation to determine $p_L^{(k_L)}$ is (3.25d). Let the notation with a bar $\bar{\mathbf{p}}_L$ denote the first $k_L - 1$ components of \mathbf{p}_L .

Theorem 3.2.1. *The balance equations (3.4) and (3.9) are equivalent to the following set of model equations defined for $z \in \mathbb{R}$ and $t > 0$:*

$$\frac{\partial X}{\partial t} + \frac{\partial F_X}{\partial z} = \delta(z)X_f q_f + \gamma(z)\tilde{R}_X, \quad (3.28a)$$

$$\frac{\partial(\mathbf{p}_X X)}{\partial t} + \frac{\partial(\mathbf{p}_X F_X)}{\partial z} = \delta(z)\mathbf{p}_{X,f} X_f q_f + \gamma(z)\mathbf{R}_X, \quad (3.28b)$$

$$L = \rho_L - rX, \quad (3.28c)$$

$$\frac{\partial(\bar{\mathbf{p}}_L L)}{\partial t} + \frac{\partial(\bar{\mathbf{p}}_L F_L)}{\partial z} = \delta(z)\bar{\mathbf{p}}_{L,f} L_f q_f + \gamma(z)\bar{\mathbf{R}}_L, \quad \text{where } F_L = \rho_L q - rF_X, \quad (3.28d)$$

$$p_L^{(k_L)} = 1 - (p_L^{(1)} + \dots + p_L^{(k_L-1)}). \quad (3.28e)$$

Proof. We apply Lemmas 3.2.4, 3.2.2 and 3.2.3 (in that order) to obtain equivalently (3.28a)–(3.28c) and (3.25b). It remains to prove that (3.25b) can be split into (3.28d) and (3.28e). Lemma 3.2.3 states that we can replace (3.28c) by (3.27), which in turn by Lemma 3.2.2 can be replaced by (3.28e). Conversely, summing the equations in (3.28d), recalling that $R_L^{(k_L)} = 0$ and using (3.28e), we get

$$\frac{\partial}{\partial t}((1 - p_L^{(k_L)})L) + \frac{\partial}{\partial z}((1 - p_L^{(k_L)})F_L) = \delta(z)(1 - p_{L,f}^{(k_L)})L_f q_f + \gamma(z)\tilde{R}_L$$

Now subtract (3.27) to obtain the last equation of (3.25b). \square

The formulation (3.28) has two advantages. Firstly, for a numerical method with explicit time stepping, the new value of X is obtained by solving (3.28a) only. Then \mathbf{p}_X is updated by (3.28b), etc. Secondly, this form of the governing equations yields the invariant-region property of the numerical scheme (see Theorem 3.3.1), which states that the solution stays in the following region (vectors in inequalities should be interpreted component-wise):

$$\Omega := \{\mathbf{u} \in \mathbb{R}^{k_X+k_L+2} : 0 \leq \mathbf{p}_X, \mathbf{p}_L \leq 1, 0 \leq X \leq X_{\max}, \\ \rho_L - rX_{\max} \leq L \leq \rho_L, p_X^{(1)} + \dots + p_X^{(k_X)} = 1, p_L^{(1)} + \dots + p_L^{(k_L)} = 1\}.$$

We have no proof that an *exact* solution of system (3.28) stays in Ω if the initial datum does since the well-posedness (existence and uniqueness) analysis of the model is not yet concluded, and a suitable concept of a (discontinuous) exact solution is not yet established. However, it is reasonable to expect that an exact solution of (3.28) should also assume values within Ω . To support this conjecture, we mention first that the invariant region property proved herein holds uniformly for approximate solutions, and therefore will hold for any limit to which the scheme converges as discretization

parameters tend to zero. In fact, in some previous work on related models the existence of an exact solution is proved by convergence of a suitable numerical scheme [25, 27, 81], where the convergence proofs involve a uniform L^∞ bound, that is, a simple form of an invariant-region principle. For instance, consider the Cauchy problem for the scalar equation (3.28a) without the reaction term ($\bar{R}_X \equiv 0$). Bürger et al. [27] proved the existence of a solution $X = X(z, t)$, which has the interval $[0, X_{\max}]$ as invariant region, via the convergence of an explicit numerical scheme. With the properties of the reaction term here, namely that $\bar{R}_X = 0$ if $X = 0$ or $X = X_{\max}$, the invariance property of the numerical scheme follows with the arguments of the proof of Lemma 3.3.3 (in Section 3.3.4). The convergence of that scheme with a reaction term being a function of X only (and utilizing that it is zero for $X = 0$ or $X = X_{\max}$) can be established by modifying the proof in [27].

Another important property of (3.28) is its hyperbolicity, that is, in those regions where the governing system of PDEs reduces to a first-order system of conservation laws, the corresponding flux Jacobian should have real eigenvalues only. To verify satisfaction of this property here, we assume for a moment that F_X is a convective flux function, i.e., a function of X only (v_{rel} is a function of X only; see (3.23)). Then the system (3.28) is of first order where the Jacobian is the same as for the homogeneous system

$$\frac{\partial}{\partial t} \begin{pmatrix} X \\ \mathbf{p}_X X \\ \bar{\mathbf{p}}_L L \end{pmatrix} + \frac{\partial}{\partial z} \begin{pmatrix} F_X \\ (\mathbf{p}_X X) \frac{F_X}{X} \\ (\bar{\mathbf{p}}_L L) \frac{F_L}{L} \end{pmatrix} = \mathbf{0},$$

that is, since F_X , F_L and L are functions of X , its Jacobian is a lower triangular matrix with the diagonal

$$\left(F'_X(X), \frac{F_X(X)}{X}, \dots, \frac{F_X(X)}{X}, \frac{F_L(X)}{L}, \dots, \frac{F_L(X)}{L} \right).$$

Since these entries are real, the system is hyperbolic. In the next subsection, we will assume a constitutive assumption that implies that the system (3.28) in addition to the convective flux has second-order derivatives.

3.2.6 Constitutive assumptions for hindered and compressive settling

Consistently with [13, 24, 27] we assume that $v_{\text{rel}} = v/(1 - \phi)$, where

$$v = v(X, \partial X/\partial z, z) := \gamma(z)v_{\text{hs}}(X) \left(1 - \frac{\rho_X \sigma'_e(X)}{Xg(\rho_X - \rho_L)} \frac{\partial X}{\partial z} \right).$$

Here, v_{hs} is the hindered settling velocity and σ_e the effective solids stress, for which constitutive functions are needed; see Section 3.4. We require that $\sigma_e(X) = 0$ for $X < X_c$, where X_c is a critical concentration above which the particles form a network, and $\sigma'_e(X) \geq 0$ for $X > X_c$ (see [27]). It is convenient to define

$$f_b(X) := Xv_{\text{hs}}(X), \quad d(X) := v_{\text{hs}}(X) \frac{\rho_X \sigma'_e(X)}{g(\rho_X - \rho_L)}, \quad D(X) := \int_{X_c}^X d(s) ds.$$

With the batch settling flux function $f_b(X)$, the total particulate flux (3.23) becomes

$$F_X(X, \partial X/\partial z, z, t) = Xq(z, t) + \gamma(z) \left(f_b(X) - \frac{\partial D(X)}{\partial z} \right). \quad (3.29)$$

Remark 3.2.2. We verify that the final model can be expressed as (3.1) when the reactive bulk velocity is neglected, i.e., $q^{\text{reac}} := 0$. Then (3.20) implies that $q = q(z, t)$, and comparing (3.1a) with (3.28a) and (3.29), we get $\mathcal{F}(X, z, t) = Xq(z, t) + \gamma(z)f_b(X)$. Moreover, by (3.8) we can express $L = l_1(X) := \rho_L - rX$. Thus, all variables \mathbf{p}_X , X , \mathbf{p}_L , L , \mathbf{S} and \mathbf{C} can be expressed in terms of \mathbf{p}_X , $\bar{\mathbf{p}}_L$ and X , so that the right-hand sides of (3.28a), (3.28b) and (3.28d) can be written as functions \mathcal{A}_X , \mathcal{A}_X and \mathcal{A}_L , respectively, of $(X, \mathbf{p}_X, \bar{\mathbf{p}}_X, z, t)$. Finally, (3.24) gives $F_L = l_2(F_X, z, t) := \rho_L q(z, t) - rF_X$.

3.2.7 Initial data and feed input functions

Initial data at $t = 0$, namely

$$X(z, 0) = X^0(z), \quad \mathbf{p}_X(z, 0) = \mathbf{p}_X^0(z), \quad \mathbf{p}_L(z, 0) = \mathbf{p}_L^0(z), \quad L(z, 0) = L^0(z), \quad z \in \mathbb{R}$$

are obtained either from direct information on the particulate total concentration $X^0(z)$ and the percentage vector $\mathbf{p}_X^0(z)$, or from given component concentrations:

$$\mathbf{p}_X^0 X^0 = \mathbf{C}^0 = (C^{(1),0}, \dots, C^{(k_X),0})^T.$$

In the latter case, summation yields

$$X^0 = X^0(p_X^{(1),0} + \dots + p_X^{(k_X),0}) = C^{(1),0} + \dots + C^{(k_X),0} \quad \text{and} \quad \mathbf{p}_X^0 = \mathbf{C}^0/X^0.$$

If $\mathbf{S}^0 = (S^{(1),0}, S^{(2),0}, \dots, S^{(k_L-1),0})^T$ denotes the initial soluble concentrations, then (3.8) and (3.3) give $L^0 = \rho_L - rX^0$ and

$$\mathbf{p}_L^0 = \left(\begin{array}{c} \mathbf{S}^0/L^0 \\ 1 - \sum_{i=1}^{k_L-1} S^{(i),0}/L^0 \end{array} \right).$$

The feed input functions $\mathbf{p}_{X,f}(t)$, $X_f(t)$, $\mathbf{p}_{L,f}(t)$ and $L_f(t)$ are defined analogously.

3.3 A numerical scheme

As in [18], we divide the SST into N internal computational cells, or layers, of depth $\Delta z = (B + H)/N$; see Figure 3.1 (b). The midpoint of layer j is assumed to have the coordinate z_j , hence the layer is the interval $[z_{j-1/2}, z_{j+1/2}]$. Layer 1, the top layer in the clarification zone, is thus $[z_{1/2}, z_{3/2}] = [-H, -H + \Delta z]$, and the bottom location is $z = z_{N+1/2} = B$. We define j_f to be the smallest integer larger than or equal to $H/\Delta z$, i.e., $j_f := \lceil H/\Delta z \rceil$. Then the feed inlet ($z = 0$) is located in layer j_f (the feed layer). Layers -1 and $N + 1$ have been added to obtain the correct effluent and underflow concentrations, respectively. The average values of the unknowns in each layer j are denoted by $\mathbf{P}_{X,j} = \mathbf{P}_{X,j}(t)$, $X_j = X_j(t)$, etc. The unknown output functions at the effluent and underflow are $X_e(t) := X_0(t)$, $X_u(t) := X_{N+1}(t)$, etc. To simplify formulas below, we use two mirror cells and set $X_{-1} := X_0$, $X_{N+2} := X_{N+1}$ and analogously for the other variables.

3.3.1 Spatial discretization

The computational domain is composed of $N + 2$ intervals and one needs to define numerical fluxes for $N + 3$ layer boundaries. Except for the reaction term, (3.28a) is a model for which a working numerical scheme is available [18]. The reaction term depends on all variables, and is strongly coupled to the other equations via the total flux (3.29), which contains the bulk velocity $q = q(z, t, \mathbf{C}, \mathbf{S})$, which, in contrast to the non-reactive case, depends on the unknown concentrations via q^{reac} in (3.19) and (3.20). This function is well defined at $z_{j+1/2}$ because of the integration in (3.19). For piecewise constant functions in each layer, i.e. $X(z, t) = X_j$, $z \in (z_{j-1/2}, z_{j+1/2}]$, etc.,

we obtain

$$q_{j+1/2}^{\text{reac}} := q^{\text{reac}}(z_{j+1/2}) := \begin{cases} \sum_{i=j+1}^N \gamma_i \mathcal{R}_i \Delta z & \text{for } j = -1, \dots, N-1, \\ 0 & \text{for } j = N, N+1, \end{cases} \quad (3.30)$$

where we recall that $\mathcal{R} = 0$ outside the SST, and then define $q_{j+1/2} := q(z_{j+1/2}, t)$ in accordance with (3.20):

$$q_{j+1/2} = \begin{cases} q_u(t) - q_f(t) - \sum_{i=j+1}^N \mathcal{R}_i \Delta z & \text{for } j = -1, \dots, j_f - 1, \\ q_u(t) - \sum_{i=j+1}^N \mathcal{R}_i \Delta z & \text{for } j = j_f, \dots, N-1, \\ q_u(t) & \text{for } j = N, N+1. \end{cases} \quad (3.31)$$

The first bulk flow term qX of (3.29) can be handled by a standard upwind flux:

$$\mathcal{B}_{j+1/2} := \begin{cases} q_{j+1/2} X_{j+1} & \text{if } q_{j+1/2} \leq 0, \\ q_{j+1/2} X_j & \text{if } q_{j+1/2} > 0, \end{cases} \quad j = -1, \dots, N+1. \quad (3.32)$$

The rest of the terms of (3.29) are only non-zero (strictly) inside the SST. We define $\gamma_{j+1/2} := \gamma(z_{j+1/2})$ (recall that $\gamma(-H) = \gamma(B) = 0$) and define the numerical convective flux $G_{j+1/2}$ for $j = -1, \dots, N+1$ by means of the Godunov flux \mathcal{G} :

$$G_{j+1/2} := \gamma_{j+1/2} \mathcal{G}(X_j, X_{j+1}), \quad \text{where } \mathcal{G}(u, v) := \begin{cases} \min_{u \leq X \leq v} f_b(X) & \text{if } u \leq v, \\ \max_{u \geq X \geq v} f_b(X) & \text{if } u > v. \end{cases} \quad (3.33)$$

Analogously, the numerical diffusive flux (modelling compression in sedimentation) is

$$J_{j+1/2} := \gamma_{j+1/2} \frac{D(X_{j+1}) - D(X_j)}{\Delta z}, \quad j = -1, \dots, N+1.$$

Then the total flux (3.29) between cells j and $j+1$ is approximated by

$$F_{X,j+1/2} := \mathcal{B}_{j+1/2} + G_{j+1/2} - J_{j+1/2}, \quad j = -1, \dots, N+1.$$

The corresponding flux of (3.28b) is $\mathbf{P}_{X,j+1/2} F_{X,j+1/2}$, where $\mathbf{P}_{X,j+1/2}$ needs to be defined. If $F_{X,j+1/2} > 0$, then particles move in the direction of the z -axis over the boundary $z_{j+1/2}$, i.e. downwards. Then the values of $\mathbf{P}_{X,j+1/2}$ at the cell boundary are those coming from the left cell, i.e. $\mathbf{P}_{X,j}$. If $F_{X,j+1/2} \leq 0$, then the particles move

upwards and the values are $\mathbf{P}_{X,j+1}$. Consequently, following [43] we define

$$\mathbf{P}_{X,j+1/2} := \begin{cases} \mathbf{P}_{X,j+1} & \text{if } F_{X,j+1/2} \leq 0, \\ \mathbf{P}_{X,j} & \text{if } F_{X,j+1/2} > 0, \end{cases} \quad j = -1, \dots, N+1.$$

For the liquid percentage vector appearing in (3.28d), we use the same principle. By (3.24), we define $F_{L,j+1/2} := \rho_L q_{j+1/2} - r F_{X,j+1/2}$ for $j = -1, \dots, N+1$ and

$$\mathbf{P}_{L,j+1/2} := \begin{cases} \mathbf{P}_{L,j+1} & \text{if } F_{L,j+1/2} \leq 0, \\ \mathbf{P}_{L,j} & \text{if } F_{L,j+1/2} > 0, \end{cases} \quad j = -1, \dots, N+1.$$

We introduce the notation $[\Delta F]_j := F_{j+1/2} - F_{j-1/2}$ and let δ_{j,j_f} denote the Kronecker delta, which is 1 if $j = j_f$ and zero otherwise. The conservation of mass for each layer gives the following method-of-lines equations (for $j = 0, \dots, N+1$):

$$\frac{dX_j}{dt} = -\frac{[\Delta F_X]_j}{\Delta z} + \delta_{j,j_f} \frac{X_f q_f}{\Delta z} + \gamma_j \tilde{\mathbf{R}}_{X,j}, \quad (3.34a)$$

$$\frac{d(\mathbf{P}_{X,j} X_j)}{dt} = -\frac{[\Delta(\mathbf{P}_X F_X)]_j}{\Delta z} + \delta_{j,j_f} \frac{\mathbf{p}_{X,f} X_f q_f}{\Delta z} + \gamma_j \mathbf{R}_{X,j}, \quad (3.34b)$$

$$L_j = \rho_L - r X_j,$$

$$F_{L,j+1/2} = \rho_L q_{j+1/2} - r F_{X,j+1/2},$$

$$\frac{d(\mathbf{P}_{L,j} L_j)}{dt} = -\frac{[\Delta(\mathbf{P}_L F_L)]_j}{\Delta z} + \delta_{j,j_f} \frac{\mathbf{p}_{L,f} L_f q_f}{\Delta z} + \gamma_j \mathbf{R}_{L,j}, \quad (3.34c)$$

$$P_L^{(k_L)} = 1 - (P_L^{(1)} + \dots + P_L^{(k_L-1)}). \quad (3.34d)$$

If $X_j = 0$, i.e. there are no solids in layer j , then the value of $\mathbf{P}_{X,j}$ is irrelevant. Furthermore, note that in (3.34a) we have $\tilde{\mathbf{R}}_{X,j} = \tilde{\mathbf{R}}_X(\mathbf{C}_j, \mathbf{S}_j)$, where $\mathbf{C}_j = \mathbf{P}_{X,j} X_j$ and $\mathbf{S}_j = \bar{\mathbf{P}}_{L,j} L_j = \bar{\mathbf{P}}_{L,j} (\rho_L - r X_j)$, where $\bar{\mathbf{P}}_{L,j}$ is a vector containing the first $k_L - 1$ components of $\mathbf{P}_{L,j}$. The same holds for each component of $\mathbf{R}_{X,j}$ and $\mathbf{R}_{L,j}$. In (3.34c) and similar formulas below for the computation of \mathbf{P}_L we skip the notation with a bar over all vectors. It is understood that the last equation of (3.34c) is replaced by (3.34d).

3.3.2 Explicit fully discrete scheme

First, we recall that the initial data for any (one-step) time discretization method can be obtained as is shown in Section 3.2.7. If the final simulation time is T , we let t_n , $n = 0, 1, \dots, n_T$, denote the discrete time points and $\Delta t = T/n_T$ the time step

that should satisfy a certain CFL condition depending on the chosen time-integration method. Set $\lambda := \Delta t / \Delta z$. For explicit schemes, the right-hand sides of the equations are evaluated at time t_n . The value of a variable at time t_n is denoted by an upper index, e.g., X_j^n . For explicit Euler time integration of (3.34a)–(3.34c), we note in particular the approximation

$$\frac{d(\mathbf{P}_{X,j} X_j)}{dt} \approx \frac{\mathbf{P}_{X,j}^{n+1} X_j^{n+1} - \mathbf{P}_{X,j}^n X_j^n}{\Delta t},$$

which implies the following explicit scheme (recall that always $L_j^{n+1} > 0$):

$$X_j^{n+1} = X_j^n + \lambda \left(-[\Delta F_X^n]_j + \delta_{j,j_f} X_f^n q_f^n \right) + \Delta t \gamma_j \tilde{R}_{X,j}^n, \quad (3.35a)$$

$$\mathbf{P}_{X,j}^{n+1} = \begin{cases} \text{irrelevant, e.g. } \mathbf{P}_{X,j}^n, & \text{if } X_j^{n+1} = 0, \\ \frac{1}{X_j^{n+1}} \left[\mathbf{P}_{X,j}^n X_j^n + \lambda \left(\delta_{j,j_f} \mathbf{p}_{X,f}^n X_f^n q_f^n - [\Delta(\mathbf{P}_X^n F_X^n)]_j \right) + \Delta t \gamma_j \mathbf{R}_{X,j}^n \right], & \text{if not,} \end{cases} \quad (3.35b)$$

$$L_j^{n+1} = \rho_L - r X_j^{n+1}, \quad (3.35c)$$

$$F_{L,j+1/2}^n = \rho_L q_{j+1/2}^n - r F_{X,j+1/2}^n, \quad (3.35d)$$

$$\mathbf{P}_{L,j}^{n+1} = \frac{1}{L_j^{n+1}} \left[\mathbf{P}_{L,j}^n L_j^n + \lambda \left(-[\Delta(\mathbf{P}_L^n F_L^n)]_j + \delta_{j,j_f} \mathbf{p}_{L,f}^n L_f^n q_f^n \right) + \Delta t \gamma_j \mathbf{R}_{L,j}^n \right], \quad (3.35e)$$

$$P_{L,j}^{(k_L),n+1} = 1 - (P_{L,j}^{(1),n+1} + \dots + P_{L,j}^{(k_L-1),n+1}). \quad (3.35f)$$

The biological reactions do not only influence the variables locally via the reaction terms, but also globally via the additional bulk velocity term $q_{j+1/2}^{\text{react},n}$. In fact, a local volume increase or decrease at $z = z_0$ has an immediate influence for all $z < z_0$. In other words, the bulk velocity change $q^{\text{react}}(z; \mathbf{C}, \mathbf{S})$ given by (3.19) depends on the reactions in the interval $[z, B]$. For the numerical scheme, this means that the update formulas for the concentrations in a layer j_0 contain the other concentrations in all layers $j > j_0$; see (3.31). We will see in Section 3.3.4 that this unfortunately means that the scheme is not monotone. The terms \mathcal{R}_j , $j = 1, \dots, N$ in (3.30) destroy the monotonicity. Since these are negligible in wastewater treatment (see Section 3.4), we define $q_{j+1/2}^{\text{react}} := 0$ instead of (3.30).

3.3.3 CFL condition

We define the vector of unknowns $\mathbf{u} := (\mathbf{p}_X, X, \mathbf{p}_L, L)$ and the following bounds (which are assumed to be finite):

$$\begin{aligned} \|f_b\|_\infty &:= \max_{0 \leq X \leq X_{\max}} |f_b(X)|, & \|q\|_\infty &:= \max_{0 \leq t \leq T} q_f(t), \\ M_C &:= \sup_{\substack{\mathbf{u} \in \Omega \\ 1 \leq k \leq k_X}} \left| \frac{\partial \tilde{R}_X}{\partial C^{(k)}} \right|, & M_S &:= \sup_{\mathbf{u} \in \Omega, 1 \leq k \leq k_L - 1} \left| \frac{\partial \tilde{R}_X}{\partial S^{(k)}} \right|, \\ M_C^X &:= \sup_{\substack{\mathbf{u} \in \Omega \\ 1 \leq k \leq k_X}} \left| \frac{\partial R_X^{(k)}}{\partial C^{(k)}} \right|, & M_S^L &:= \sup_{\substack{\mathbf{u} \in \Omega \\ 1 \leq k \leq k_L - 1}} \left| \frac{\partial R_L^{(k)}}{\partial S^{(k)}} \right| \end{aligned}$$

along with $M := M_C + rM_S$. The CFL condition is

$$\Delta t \left(\frac{\|q\|_\infty}{\Delta z} + \max(\beta_X, \beta_{\mathbf{p}_X}, \beta_{\mathbf{p}_L}) \right) \leq 1, \quad (\text{CFL})$$

where

$$\begin{aligned} \beta_X &:= \frac{\|f_b'\|_\infty}{\Delta z} + \frac{2\|d\|_\infty}{\Delta z^2} + M, & \beta_{\mathbf{p}_X} &:= \frac{\|f_b'\|_\infty}{\Delta z} + \frac{2\|d\|_\infty}{\Delta z^2} + M_C^X, \\ \beta_{\mathbf{p}_L} &:= \frac{\|f_b\|_\infty}{\Delta z(\rho_X - X_{\max})} + \frac{2D(X_{\max})}{\Delta z^2(\rho_X - X_{\max})} + M_S^L. \end{aligned} \quad (3.36)$$

3.3.4 Properties of the numerical scheme

With $\eta := \lambda/\Delta z = \Delta t/\Delta z^2$ the update formula (3.35a) reads for each layer:

$$\begin{aligned} X_0^{n+1} &= X_0^n - \lambda[\Delta \mathcal{B}^n]_0, \\ X_1^{n+1} &= X_1^n - \lambda([\Delta \mathcal{B}^n]_1 + \mathcal{G}(X_1^n, X_2^n)) + \eta(D(X_2^n) - D(X_1^n)) + \Delta t \tilde{R}_{X,1}^n, \\ X_j^{n+1} &= X_j^n - \lambda([\Delta \mathcal{B}^n]_j + \mathcal{G}(X_j^n, X_{j+1}^n) - \mathcal{G}(X_{j-1}^n, X_j^n)) \\ &\quad + \eta(D(X_{j+1}^n) - 2D(X_j^n) + D(X_{j-1}^n)) \\ &\quad + \lambda \delta_{j,j_f} X_f^n q_f^n + \Delta t \tilde{R}_{X,j}^n, \quad j = 2, \dots, N-1, \\ X_N^{n+1} &= X_N^n - \lambda([\Delta \mathcal{B}^n]_N - \mathcal{G}(X_{N-1}^n, X_N^n)) - \eta(D(X_N^n) - D(X_{N-1}^n)) + \Delta t \tilde{R}_{X,N}^n \\ X_{N+1}^{n+1} &= X_{N+1}^n - \lambda[\Delta \mathcal{B}^n]_{N+1}. \end{aligned}$$

To be able to prove an invariant region property for each variable, we want every formula to be a monotone function of each argument, i.e., we wish to have $\partial X_j^{n+1}/\partial X_k^n \geq 0$ for all j, k . For $j = k$, this can be achieved by invoking (CFL). The problematic terms

above are $\lambda[\Delta\mathcal{B}^n]_j$ since they contain the bulk velocity reaction function q^{reac} in (3.19). To see this, we let the characteristic function χ_I be equal to 1 if the statement I is true, otherwise 0. Then

$$\mathcal{B}_{j+1/2} = X_{j+1}q_{j+1/2}\chi_{q_{j+1/2}\leq 0} + X_jq_{j+1/2}\chi_{q_{j+1/2}> 0} \quad (3.37)$$

and hence, for $j = 0, \dots, N-1$ and $k = j+2, \dots, N+1$, we have

$$\begin{aligned} \frac{\partial X_j^{n+1}}{\partial X_k} &= -\lambda \frac{\partial[\Delta\mathcal{B}]_j}{\partial X_k} \\ &= -\lambda \left((X_{j+1}\chi_{q_{j+1/2}\leq 0} + X_j\chi_{q_{j+1/2}> 0}) \frac{\partial q_{j+1/2}}{\partial X_k} \right. \\ &\quad \left. + (X_j\chi_{q_{j-1/2}\leq 0} + X_{j-1}\chi_{q_{j-1/2}> 0}) \frac{\partial q_{j-1/2}}{\partial X_k} \right). \end{aligned}$$

The derivatives of $q_{j+1/2}^n$ can have any sign due to the reaction terms. We therefore confine the analysis to the scheme when we set $\mathcal{R}_j := 0$, $j = 1, \dots, N$ in (3.30), i.e. $q_{j+1/2}^{\text{reac}} := 0$. Then $q_{j+1/2}$ depends only on time and (3.35) becomes a three-point scheme.

Lema 3.3.1. *Assume that $0 \leq X_j \leq X_{\max}$ for all j . Then the Godunov flux $\mathcal{G}_{j+1/2} = \mathcal{G}(X_j, X_{j+1})$, see (3.33), applied on $0 \leq f_b \in C^1$ satisfies*

$$\begin{aligned} -\|f'_b\|_\infty &\leq \frac{\partial \mathcal{G}_{j+1/2}}{\partial X_{j+1}} \leq 0 \leq \frac{\partial \mathcal{G}_{j+1/2}}{\partial X_j} \leq \|f'_b\|_\infty, \\ \left| \frac{\partial[\Delta\mathcal{G}]_j}{\partial X_j} \right| &\leq \|f'_b\|_\infty, \quad \frac{\mathcal{G}_{j+1/2}}{X_j} \leq \|f'_b\|_\infty, \quad \frac{\mathcal{G}_{j+1/2}}{X_{j+1}} \leq \|f'_b\|_\infty. \end{aligned}$$

Proof. If $X_j \leq X_{j+1}$, then

$$\mathcal{G}_{j+1/2} = \min\{f_b(X_j), f_b(\xi), f_b(X_{j+1})\},$$

where $\xi \in (X_j, X_{j+1})$ is a (possible) stationary point of f_b . If $\mathcal{G}_{j+1/2} = f_b(X_j)$, then X_j is the minimum point and the left endpoint of the interval, hence

$$\partial \mathcal{G}_{j+1/2} / \partial X_j = f'_b(X_j) \geq 0.$$

Otherwise, $\partial \mathcal{G}_{j+1/2} / \partial X_j = 0$ holds. Similarly, if $X_j > X_{j+1}$, then $\partial \mathcal{G}_{j+1/2} / \partial X_j = 0$ or $= f'_b(X_j) \geq 0$ (the right endpoint X_j is a maximum point). Analogously,

$\partial \mathcal{G}_{j+1/2} / \partial X_{j+1} = 0$ or $= f'_b(X_{j+1}) \leq 0$. Combining these results, we get

$$\frac{\partial [\Delta \mathcal{G}]_j}{\partial X_j} \in \{f'_b(X_j), 0, -f'_b(X_j)\}.$$

Assume again $X_j \leq X_{j+1}$, so that $\mathcal{G}_{j+1/2} = \min\{f_b(X_j), f_b(\xi), f_b(X_{j+1})\}$. Then $\mathcal{G}_{j+1/2}/X_j \leq f_b(X_j)/X_j$ and $\mathcal{G}_{j+1/2}/X_{j+1} \leq f_b(X_{j+1})/X_{j+1}$. If $X_j > X_{j+1}$, then $\mathcal{G}_{j+1/2} = \max\{f_b(X_j^n), f_b(\xi), f_b(X_{j+1}^n)\}$ where $\xi \in (X_{j+1}, X_j)$ is a possible stationary point. Then we have

$$\frac{\mathcal{G}_{j+1/2}}{X_{j+1}} \leq \frac{\mathcal{G}_{j+1/2}}{X_j} = \begin{cases} \text{either} & f_b(X_j)/X_j, \\ \text{or} & f_b(\xi)/X_j \leq f_b(\xi)/\xi, \\ \text{or} & f_b(X_{j+1})/X_j \leq f_b(X_{j+1})/X_{j+1}. \end{cases}$$

For any $X \in (0, X_{\max})$, take $\bar{\xi} \in (0, X)$ according to the mean-value theorem so that

$$\frac{f_b(X)}{X} = \frac{f_b(X) - f_b(0)}{X} = f'_b(\bar{\xi}) \leq \|f'_b\|_\infty.$$

□

We define the vector of unknown discrete variables $\mathbf{U}_j^n := (\mathbf{P}_{X,j}^n, X_j^n, \mathbf{P}_{L,j}^n, L_j^n)$.

Lema 3.3.2. Assume that $\mathbf{U}_j^n \in \Omega$ for all j . Then the following holds for $i = 1, \dots, k_X$:

$$\left| \frac{\partial \tilde{R}_{X,j}}{\partial X_k} \right| \begin{cases} \leq M & \text{if } k = j, \\ = 0 & \text{if } k \neq j, \end{cases} \quad \left| \frac{\partial \tilde{R}_{X,j}}{\partial P_{X,k}^{(i)}} \right| = X_k \left| \frac{\partial \tilde{R}_{X,j}}{\partial C_k^{(i)}} \right| \begin{cases} \leq X_j M_C & \text{if } k = j, \\ = 0 & \text{if } k \neq j. \end{cases}$$

Proof. The cases $k \neq j$ are trivial. Assume that $k = j$ and differentiate

$$\frac{\partial \tilde{R}_{X,j}}{\partial X_k} = \frac{\partial \tilde{R}_{X,j}}{\partial X_k} (\mathbf{P}_{X,j} X_j, \bar{\mathbf{P}}_{L,j} (\rho_L - r X_j)) = \mathbf{P}_{X,j}^T \nabla_C \tilde{R}_X - r \bar{\mathbf{P}}_{L,j}^T \nabla_S \tilde{R}_X,$$

where

$$|\mathbf{P}_{X,j}^T \nabla_C \tilde{R}_X| \leq \sum_{i=1}^{k_X} |P_{X,j}^{(i)}| \left| \frac{\partial \tilde{R}_{X,j}}{\partial C^{(i)}} \right| \leq M_C \sum_{i=1}^{k_X} |P_{X,j}^{(i)}| = M_C,$$

and the second term is estimated similarly. The derivative $|\partial \tilde{R}_{X,j} / \partial P_{X,k}^{(i)}|$ is handled similarly. □

We define $a^+ := \max\{a, 0\}$ and $a^- := \min\{a, 0\}$.

Lema 3.3.3. *If $\mathcal{U}_j^n \in \Omega$, $q_{j+1/2}^{\text{reac},n} := 0$ for all j and (CFL) holds, then $0 \leq X_j^{n+1} \leq 1$ for all j .*

Proof. We write the update formula (3.35a) for $j = 0, \dots, N+1$ as

$$X_j^{n+1} = \mathcal{H}_X(X_{j-1}^n, X_j^n, X_{j+1}^n),$$

and we shall show that \mathcal{H}_X is a monotone function in each of its variables. We can write (3.37) as

$$\mathcal{B}_{j+1/2}^n = X_{j+1} q_{j+1/2}^{n,-} + X_j q_{j+1/2}^{n,+},$$

so that

$$\begin{aligned} \frac{\partial[\Delta \mathcal{B}^n]_j}{\partial X_j^n} &= \frac{\partial}{\partial X_j^n} (\mathcal{B}_{j+1/2}^n - \mathcal{B}_{j-1/2}^n) \\ &= \frac{\partial}{\partial X_j^n} (X_{j+1}^n q_{j+1/2}^{n,-} + X_j^n q_{j+1/2}^{n,+} - X_j^n q_{j-1/2}^{n,-} - X_{j-1}^n q_{j-1/2}^{n,+}) \\ &= q_{j+1/2}^{n,+} - q_{j-1/2}^{n,-} \leq q_{j+1/2}^{n,+} - q_{j-1/2}^{n,-} = q_u^n + q_e^n = q_f^n \\ &\leq \|q\|_\infty. \end{aligned}$$

Differentiation of (3.35a) and utilization of (CFL) and Lemmas 3.3.1 and 3.3.2 imply

$$\begin{aligned}
\frac{\partial X_0^{n+1}}{\partial X_0^n} &= 1 - \lambda \frac{\partial[\Delta\mathcal{B}^n]_0}{\partial X_0^n} \geq 1 - \lambda\|q\|_\infty \geq 0, \\
\frac{\partial X_0^{n+1}}{\partial X_1^n} &= -\lambda q_{1/2}^{n,-} \geq 0, \\
\frac{\partial X_1^{n+1}}{\partial X_0^n} &= \lambda q_{1/2}^{n,+} \geq 0, \\
\frac{\partial X_1^{n+1}}{\partial X_1^n} &= 1 - \lambda \left(\frac{\partial[\Delta\mathcal{B}^n]_1}{\partial X_1^n} + \frac{\partial\mathcal{G}(X_1^n, X_2^n)}{\partial X_1^n} \right) - \eta d(X_1^n) + \Delta t \frac{\partial\tilde{R}_{X,1}^n}{\partial X_1^n} \\
&\geq 1 - (\lambda(\|q\|_\infty + \|f'_b\|_\infty) + \eta\|d\|_\infty + \Delta t M) \geq 0, \\
\frac{\partial X_1^{n+1}}{\partial X_2^n} &= \lambda \left(-q_{3/2}^{n,-} - \frac{\partial\mathcal{G}(X_1^n, X_2^n)}{\partial X_2^n} \right) + \eta d(X_2^n) \geq 0, \\
\frac{\partial X_j^{n+1}}{\partial X_{j-1}^n} &= \lambda \left(q_{j-1/2}^{n,+} + \frac{\partial\mathcal{G}(X_{j-1}^n, X_j^n)}{\partial X_{j-1}^n} \right) + \eta d(X_{j-1}^n) \geq 0, \quad j = 2, \dots, N-1, \\
\frac{\partial X_j^{n+1}}{\partial X_j^n} &= 1 - \lambda \left(\frac{\partial[\Delta\mathcal{B}^n]_j}{\partial X_j^n} + \frac{\partial[\Delta\mathcal{G}^n]_j}{\partial X_j^n} \right) - 2\eta d(X_j^n) + \Delta t \frac{\partial\tilde{R}_{X,j}^n}{\partial X_j^n} \\
&\geq 1 - (\lambda(\|q\|_\infty + \|f'_b\|_\infty) + 2\eta\|d\|_\infty + \Delta t M) \geq 0, \quad j = 2, \dots, N-1, \\
\frac{\partial X_j^{n+1}}{\partial X_{j+1}^n} &= -\lambda \left(q_{j+1/2}^{n,-} + \frac{\partial\mathcal{G}(X_j^n, X_{j+1}^n)}{\partial X_{j+1}^n} \right) + \eta d(X_{j+1}^n) \geq 0, \quad j = 2, \dots, N-1.
\end{aligned}$$

The remaining derivatives at the boundary $z = B$ are symmetric to those at $z = -H$. The proved monotonicity of \mathcal{H}_X and the assumptions (3.7) imply that, for $j \neq j_f$,

$$0 = \mathcal{H}_X(0, 0, 0) \leq X_j^{n+1} = \mathcal{H}_X(X_{j-1}^n, X_j^n, X_{j+1}^n) \leq \mathcal{H}_X(X_{\max}, X_{\max}, X_{\max}) = X_{\max}$$

and for $j = j_f$ we have

$$\begin{aligned}
0 &\leq \Delta t X_f q_f = \mathcal{H}_X(0, 0, 0) \leq X_j^{n+1} = \mathcal{H}_X(X_{j-1}^n, X_j^n, X_{j+1}^n) \leq \mathcal{H}_X(X_{\max}, X_{\max}, X_{\max}) \\
&= X_{\max} - \lambda(q_u X_{\max} - (q_u - q_f) X_{\max}) + \lambda X_f q_f = X_{\max} - \lambda q_f (X_{\max} - X_f) \leq X_{\max}.
\end{aligned}$$

□

Lema 3.3.4. *If $\mathcal{U}_j^n \in \Omega$, $q_{j+1/2}^{\text{reac},n} := 0$ for all j , and (CFL) holds, then $0 \leq \mathbf{P}_{X,j}^{n+1} \leq 1$ for all j .*

Proof. If $X_j^{n+1} = 0$, then $\mathbf{P}_{X,j}^{n+1} := \mathbf{P}_{X,j}^n \in [0, 1]$. We assume that $X_j^{n+1} > 0$ and write (3.35b) as

$$\mathbf{P}_{X,j}^{n+1} = \frac{\Psi_{X,j}^n}{X_j^{n+1}},$$

where $\Psi_{X,j}^n := \mathbf{P}_{X,j}^n X_j^n + \lambda \left(-[\Delta(\mathbf{P}_X^n F_X^n)]_j + \delta_{j,j_t} \mathbf{p}_{X,f}^n X_f^n q_f^n \right) + \Delta t \gamma_j \mathbf{R}_{X,j}^n$, and

$$\begin{aligned} [\Delta(\mathbf{P}_X^n F_X^n)]_j &= \mathbf{P}_{X,j+1/2}^n F_{X,j+1/2}^n - \mathbf{P}_{X,j-1/2}^n F_{X,j-1/2}^n \\ &= \mathbf{P}_{X,j+1}^n F_{X,j+1/2}^{n,-} + \mathbf{P}_{X,j}^n F_{X,j+1/2}^{n,+} - \mathbf{P}_{X,j}^n F_{X,j-1/2}^{n,-} - \mathbf{P}_{X,j-1}^n F_{X,j-1/2}^{n,+}. \end{aligned} \quad (3.38)$$

Consider $\Psi_{X,j}^{(k),n} = \Psi_{X,j}^{(k),n}(P_{X,j}^{(k),n})$. We have

$$(\Psi_{X,j}^{(k),n})'(P_{X,j}^{(k),n}) = X_j^n - \lambda \{ F_{X,j+1/2}^{n,+} - F_{X,j-1/2}^{n,-} \} + \Delta t \gamma_j \frac{\partial R_{X,j}^{(k),n}}{\partial P_{X,j}^{(k),n}}. \quad (3.39)$$

The last term here is estimated by

$$\Delta t \gamma_j \frac{\partial R_{X,j}^{(k),n}}{\partial P_{X,j}^{(i),n}} = X_j^n \Delta t \gamma_j \frac{\partial R_{X,j}^{(k),n}}{\partial C_j^{(i),n}} \geq -X_j^n \Delta t M_C^X,$$

cf. Lemma 3.3.2. To estimate the expression within curled brackets in (3.39), we note that $-a^- = (-a)^+$, $(a+b)^+ \leq a^+ + b^+$ and start with the first of three terms of $F_X = \mathcal{B} + G - J$:

$$\begin{aligned} \mathcal{B}_{j+1/2}^{n,+} + (-\mathcal{B}_{j-1/2}^n)^+ &= (X_{j+1}^n q_{j+1/2}^{n,-} + X_j^n q_{j+1/2}^{n,+})^+ + (-X_j^n q_{j-1/2}^{n,-} - X_{j-1}^n q_{j-1/2}^{n,+})^+ \\ &\leq X_j^n (q_{j+1/2}^{n,+} - q_{j-1/2}^{n,-}) \leq X_j^n (q_{j_t+1/2}^{n,+} - q_{j_t+1/2}^{n,-}) \\ &= X_j^n (q_u^n + q_e^n) = X_j^n q_f^n \leq X_j^n \|q\|_\infty. \end{aligned}$$

Since $\mathcal{G}(u, v) > 0$ whenever $f_b > 0$ we use Lemma 3.3.1 to obtain

$$G_{j+1/2}^{n,+} + (-G_{j-1/2}^n)^+ = G_{j+1/2}^{n,+} = G_{j+1/2}^n \leq X_j^n \|f'_b\|_\infty.$$

The term corresponding to $-J$ is estimated by utilizing that $D(X)$ is a non-decreasing function, which is zero for $X \leq X_c$:

$$\begin{aligned} (-J_{j+1/2}^{n,+})^+ + J_{j-1/2}^{n,+} &= \frac{1}{\Delta z} \left((D(X_j^n) - D(X_{j+1}^n))^+ + (D(X_j^n) - D(X_{j-1}^n))^+ \right) \\ &\leq \frac{1}{\Delta z} 2D(X_j^n) = \frac{2}{\Delta z} \int_{X_c}^{X_j^n} d(s) ds \leq X_j^n \frac{2\|d\|_\infty}{\Delta z}. \end{aligned} \quad (3.40)$$

The CFL condition (CFL) now implies that

$$(\Psi_{X,j}^{(k),n})'(P_{X,j}^{(i),n}) \geq X_j^n \left[1 - \left(\lambda(\|q\|_\infty + \|f'_b\|_\infty) + 2\eta\|d\|_\infty + \Delta t M_C^X \right) \right] \geq 0.$$

By assumption (3.6), we have

$$\begin{aligned} \Psi_{X,j}^{(k),n}(0) &= \lambda \left(-P_{X,j+1}^{(k),n} F_{X,j+1/2}^{n,-} + P_{X,j-1}^{(k),n} F_{X,j-1/2}^{n,+} + \delta_{j,j_f} P_{X,f}^{(k),n} X_f^n q_f^n \right) \\ &\quad + \Delta t \gamma_j R_{X,j}^{(k),n} \Big|_{P_{X,j}^{(k),n}=0} \\ &\geq 0. \end{aligned}$$

Hence, $\Psi_{X,j}^{(k),n} = \Psi_{X,j}^{(k),n}(P_{X,j}^{(k),n}) \geq 0$ holds for all $k = 1, \dots, k_X$, and since

$$\sum_{k=1}^{k_X} \Psi_{X,j}^{(k),n} = X_j^{n+1},$$

it follows that $\Psi_{X,j}^{(k),n} \leq X_j^{n+1}$. We have proved that $0 \leq \mathbf{P}_{X,j}^{n+1} \leq 1$. \square

Lema 3.3.5. *If $\mathbf{U}_j^n \in \Omega$, $q_{j+1/2}^{\text{reac},n} := 0$ for all j and (CFL) holds, then $0 \leq \mathbf{P}_{L,j}^{n+1} \leq 1$ for all j .*

Proof. We follow the proof of Lemma 3.3.4 and write (3.35e) as

$$\mathbf{P}_{L,j}^{n+1} = \frac{\Psi_{L,j}^n}{L_j^{n+1}},$$

where $\Psi_{L,j}^n := \mathbf{P}_{L,j}^n L_j^n + \lambda \left(-[\Delta(\mathbf{P}_L^n F_L^n)]_j + \delta_{j,j_f} \mathbf{p}_{L,f}^n L_f^n q_f^n \right) + \Delta t \gamma_j \mathbf{R}_{L,j}^n$. We consider $\Psi_{L,j}^{(k),n} = \Psi_{L,j}^{(k),n}(P_{L,j}^{(k),n})$ and calculate

$$(\Psi_{L,j}^{(k),n})'(P_{L,j}^{(i),n}) = L_j^n - \lambda \{ F_{L,j+1/2}^{n,+} - F_{L,j-1/2}^{n,-} \} + \Delta t \gamma_j \frac{\partial R_{L,j}^{(k),n}}{\partial P_{L,j}^{(k),n}}. \quad (3.41)$$

For the expression within curled bracket of (3.41), we note that

$$\begin{aligned} F_{L,j+1/2}^{n,+} &= (q_{j+1/2}^n \rho_L - r F_{X,j+1/2}^n)^+ \\ &= (q_{j+1/2}^n \rho_L - r \mathcal{B}_{j+1/2}^n - r G_{j+1/2}^n + r J_{j+1/2}^n)^+ \leq \mathcal{T}_1 + r J_{j+1/2}^{n,+}, \end{aligned}$$

where $\mathcal{T}_1 := (q_{j+1/2}^n \rho_L - r \mathcal{B}_{j+1/2}^n)^+$. Similarly, we obtain

$$(-F_{L,j-1/2}^{n,+})^+ \leq \mathcal{T}_2 + r G_{j-1/2}^{n,+} + r(-J_{j-1/2}^n)^+, \quad \mathcal{T}_2 := (-q_{j-1/2}^n \rho_L + r \mathcal{B}_{j-1/2}^n)^+.$$

Utilizing $q_{j+1/2}^n = q_{j+1/2}^{n,+} + q_{j+1/2}^{n,-}$ and $\mathcal{B}_{j+1/2}^n = X_{j+1} q_{j+1/2}^{n,-} + X_j q_{j+1/2}^{n,+}$, we get

$$\begin{aligned} \mathcal{T}_1 + \mathcal{T}_2 &= (q_{j+1/2}^{n,+}(\rho_L - r X_j^n) + q_{j+1/2}^{n,-}(\rho_L - r X_{j+1}^n))^+ \\ &\quad + (-q_{j-1/2}^{n,+}(\rho_L - r X_{j-1}^n) - q_{j-1/2}^{n,-}(\rho_L - r X_j^n))^+ \\ &= (q_{j+1/2}^{n,+} L_j^n + q_{j+1/2}^{n,-} L_j^{n+1})^+ + (-q_{j-1/2}^{n,+} L_{j-1}^n - q_{j-1/2}^{n,-} L_j^n)^+ \\ &\leq (q_{j+1/2}^{n,+} - q_{j-1/2}^{n,-}) L_j^n \leq L_j^n \|q\|_\infty. \end{aligned}$$

For the rest of the terms, we have from Lemma 3.3.2 and (3.40):

$$\begin{aligned} r G_{j-1/2}^{n,+} &\leq r \|f_b\|_\infty = \frac{L_j^n}{\rho_L - r X_j^n} r \|f_b\|_\infty \leq \frac{L_j^n}{\rho_X - X_{\max}} \|f_b\|_\infty, \\ r(-J_{j+1/2}^{n,+})^+ + r J_{j-1/2}^{n,+} &\leq \frac{r 2D(X_j^n)}{\Delta z} \leq \frac{L_j^n}{\rho_X - X_{\max}} \frac{2D(X_{\max})}{\Delta z}. \end{aligned}$$

The reaction term of (3.41) is handled as

$$\Delta t \gamma_j \frac{\partial R_{L,j}^{(k),n}}{\partial P_{L,j}^{(k),n}} = \Delta t \gamma_j L_j^n \frac{\partial R_{L,j}^{(k),n}}{\partial S_j^{(k),n}} \geq -\Delta t L_j^n M_S^L.$$

The CFL condition implies

$$(\Psi_{L,j}^{(k),n})'(P_{L,j}^{(i),n}) \geq L_j^n \left(1 - \lambda \|q\|_\infty - \frac{\lambda \|f_b\|_\infty + 2\eta D(X_{\max})}{\rho_X - X_{\max}} - \Delta t M_S^L \right) \geq 0.$$

As in the proof of Lemma 3.3.4 we have $\Psi_{L,j}^{(k),n}(0) \geq 0$ by the assumption on $R_L^{(k)}$ corresponding to (3.6). Hence, $\Psi_{L,j}^{(k),n} = \Psi_{L,j}^{(k),n}(P_{L,j}^{(k),n}) \geq 0$ holds for all $k = 1, \dots, k_X$. Since (see (3.38))

$$\sum_{i=1}^{k_X} [\Delta(P_X^{(i),n} F_X^n)]_j = F_{X,j+1/2}^n - F_{X,j-1/2}^n = [\Delta F_X^n]_j,$$

we have, by (3.35c), (3.35d) and (3.19) with $\mathcal{R} = 0$,

$$\begin{aligned}
\sum_{k=1}^{k_L} \Psi_{X,j}^{(k),n} &= L_j^n + \lambda \left(-[\Delta F_L^n]_j + \delta_{j,j_f} L_f^n q_f^n \right) + \Delta t \gamma_j \tilde{R}_{L,j}^n \\
&= \rho_L - r X_j^n + \lambda \left(-\rho_L [\Delta q^n]_j + r [\Delta F_X^n]_j + \delta_{j,j_f} (\rho_L - r X_f^n) q_f^n \right) - r \Delta t \gamma_j \tilde{R}_{X,j}^n \\
&= \rho_L - r \left(X_j^n + \lambda \left(-[\Delta F_X^n]_j + \delta_{j,j_f} X_f^n q_f^n \right) + \Delta t \gamma_j \tilde{R}_{X,j}^n \right) - \lambda (\rho_L [\Delta q^n]_j - \delta_{j,j_f} \rho_L q_f^n) \\
&= \rho_L - r X_j^{n+1} - \lambda \rho_L ([\Delta q^n]_j - \delta_{j,j_f} q_f^n) = L_j^{n+1} - \lambda \rho_L ([\Delta q^n]_j - \delta_{j,j_f} q_f^n) \\
&= L_j^{n+1},
\end{aligned}$$

where we in the latter equality has used (3.31), which implies $[\Delta q^n]_j = 0$ for $j \neq j_f$ and $[\Delta q^n]_{j_f} = q_u^n - (q_u^n - q_f^n) = q_f$. It follows that $\Psi_{L,j}^{(k),n} \leq L_j^{n+1}$ and have proved that $0 \leq \mathbf{P}_{L,j}^{n+1} \leq 1$. \square

Theorem 3.3.1. *If (3.7) and (CFL) hold, then Ω is invariant under the scheme (3.35) with $q_{j+1/2}^{\text{reac},n} := 0$ for all j and n , i.e., $\mathbf{U}_j^n \in \Omega \Rightarrow \mathbf{U}_j^{n+1} \in \Omega$ for all j and n .*

Proof. The bounds on X_j^n , $\mathbf{P}_{X,j}^n$ and $\mathbf{P}_{L,j}^n$ for all j and n were proved in Lemmas 3.3.3–3.3.5. We get $\rho_L - r X_{\max} \leq L_j^{n+1} = \rho_L - r X_j^{n+1} \leq \rho_L$. Summing all equations in (3.35b) and using (3.35a), we get

$$\sum_{i=1}^{k_X} P_{X,j}^{(i),n+1} = 1.$$

By definition (3.35f) we have

$$\sum_{i=1}^{k_L} P_{L,j}^{(i),n+1} = 1.$$

\square

3.4 Numerical Examples

The biological reactions are those of a model of denitrification, which is conversion of bound nitrogen to free nitrogen (N_2) that occurs in SSTs in wastewater treatment [13]. The $k_X = 2$ particulate concentrations are X_{OHO} (ordinary heterotrophic organisms) and X_U (undegradable organics), and the $k_L - 1 = 3$ soluble concentrations S_{NO_3}

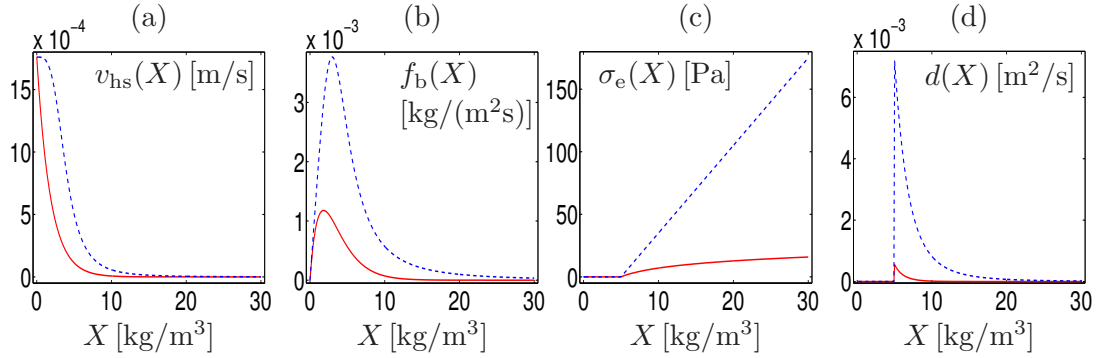


Figure 3.2: Graphs of the constitutive functions used in Examples 1 and 2 (dashed blue) and 3 (solid red): (a) hindered settling velocity, (b) batch settling flux, (c) effective solids stress, (d) compression. Properly elaboration, published in [23].

(nitrate), S_S (readily biodegradable substrate) and S_{N_2} (nitrogen), so that $\mathbf{p}_X X = \mathbf{C} = (X_{\text{OHO}}, X_U)^T$ and $\mathbf{S} = (S_{\text{NO}_3}, S_S, S_{N_2})^T$. The reaction terms are

$$\mathbf{R}_X = X_{\text{OHO}} \begin{pmatrix} \mu(\mathbf{S}) - b \\ f_P b \end{pmatrix} Z(X), \quad \mathbf{R}_L = X_{\text{OHO}} \begin{pmatrix} -\frac{1-Y}{2.86Y} \mu(\mathbf{S}) \\ -\frac{1}{Y} \mu(\mathbf{S}) + (1-f_P)b \\ \frac{1-Y}{2.86Y} \mu(\mathbf{S}) \\ 0 \end{pmatrix},$$

where $Y = 0.67$ is a yield factor, $b = 6.94 \times 10^{-6} \text{ s}^{-1}$ is the decay rate of heterotrophic organisms and $f_P = 0.2$ is the portion of these that decays to undegradable organics. The continuous function $Z(X)$ should be equal to one for low concentrations and decrease to zero at some large concentration so that the second technical assumption in (3.7) is satisfied. The function $Z(X)$ should not influence the condition (CFL). We have used $Z(X) \equiv 1$ for all simulations and still obtained bounded solutions. Hence, after some trial simulations, the maximum concentration X_{max} can be defined and used in (CFL). We have used $X_{\text{max}} = 30 \text{ kg/m}^3$. The specific growth rate function is

$$\mu(\mathbf{S}) := \mu_{\text{max}} \frac{S_{\text{NO}_3}}{K_{\text{NO}_3} + S_{\text{NO}_3}} \frac{S_S}{K_S + S_S},$$

where $\mu_{\text{max}} = 5.56 \times 10^{-5} \text{ s}^{-1}$, $K_{\text{NO}_3} = 5 \times 10^{-4} \text{ kg/m}^3$, $K_S = 0.02 \text{ kg/m}^3$. We get

$$\tilde{\mathbf{R}}_X = (\mu(\mathbf{S}) - (1-f_P)b) X_{\text{OHO}} Z(X), \quad \tilde{\mathbf{R}}_L = - \left(\frac{\mu(\mathbf{S})}{Y} - (1-f_P)b \right) X_{\text{OHO}}.$$

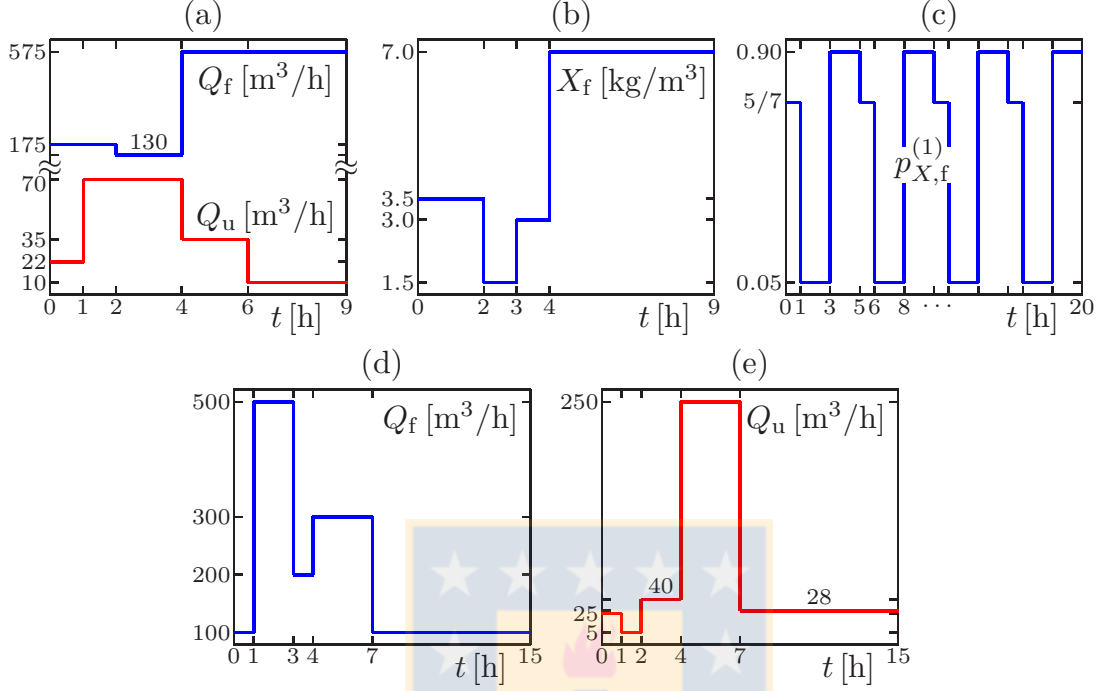


Figure 3.3: Graphs of control parameters for examples. In Examples 1 (a, b), 2 (c) and 3 (d, e): (a, d, e) volumetric flows, (b) solids feed concentration, (c) particulate feed percentages. The piecewise constant values and time points of changes are indicated. Properly elaboration, published in [23].

In light of (3.13), this implies

$$|\mathcal{R}(\mathbf{C}, \mathbf{S})| \leq \left(\mu_{\max} \left| \frac{1}{\rho_X} - \frac{1}{\rho_L Y} \right| + (1 - f_P) b \left| \frac{1}{\rho_X} - \frac{1}{\rho_L} \right| \right) X_{\max} = 7.0792 \times 10^{-7} \text{ m/s},$$

so that q^{reac} is negligibly small in comparison to the bulk velocities q_e and q_u in continuous sedimentation. It is also negligible in batch sedimentation (although $q_e = q_u = 0$), where the interval of settling velocities is $[0, v_0]$ with $v_0 = 1.76 \times 10^{-3} \text{ m/s}$. For Examples 8 and 9, we choose the constitutive functions for hindered settling and compression (where $Z(X) \equiv 1$ is used in the simulations)

$$v_{\text{hs}}(X) = \frac{v_0}{1 + (X/\bar{X})^{\bar{r}}} Z(X), \quad \sigma_e(X) = \begin{cases} 0 & \text{for } X < X_c, \\ \alpha(X - X_c) & \text{for } X > X_c, \end{cases}$$

where $v_0 = 1.76 \times 10^{-3} \text{ m/s}$, $\bar{X} = 3.87 \text{ kg/m}^3$, $\bar{r} = 3.58$, $\alpha = 0.2 \text{ m}^2/\text{s}^2$ and $X_c = 5 \text{ kg/m}^3$. Other constants used are $A = 400 \text{ m}^2$, $\rho_X = 1050 \text{ kg/m}^3$, $\rho_L = 998 \text{ kg/m}^3$

Table 3.1: Coefficients for the calculation of the CFL condition (CFL), where $\kappa := \|q\|_\infty/\Delta z$. Properly elaboration, published in [23].

N	Δz [m]	Examples 8 and 9					Example 3				
		κ [s ⁻¹]	β_X [s ⁻¹]	$\beta_{\mathbf{P}_X}$ [s ⁻¹]	$\beta_{\mathbf{P}_L}$ [s ⁻¹]	Δt [s]	κ [s ⁻¹]	β_X [s ⁻¹]	$\beta_{\mathbf{P}_X}$ [s ⁻¹]	$\beta_{\mathbf{P}_L}$ [s ⁻¹]	Δt [s]
10	0.400	0.001	3.178	0.007	0.166	0.311	0.001	3.182	0.011	0.166	0.311
30	0.133	0.003	3.207	0.037	0.166	0.308	0.003	3.247	0.076	0.167	0.304
90	0.044	0.009	3.420	0.249	0.167	0.288	0.008	3.776	0.606	0.167	0.261
270	0.015	0.027	5.175	2.004	0.171	0.190	0.023	8.384	5.213	0.173	0.117
405	0.010	0.040	7.591	4.420	0.176	0.129	0.035	14.81	11.64	0.181	0.066
810	0.005	0.081	20.49	17.32	0.205	0.048	0.070	49.37	46.20	0.223	0.020
2430	0.002	0.243	156.9	153.7	0.515	0.006	0.211	416.8	413.6	0.670	0.002

and $g = 9.81 \text{ m/s}^2$. For Example 3, we choose the constitutive functions

$$v_{\text{hs}}(X) = v_0 e^{-r_V X} Z(X), \quad \sigma_e(X) = \begin{cases} 0 & \text{for } X < X_c, \\ \tilde{\alpha} \log((X - X_c + \tilde{\beta})/\tilde{\beta}) & \text{for } X > X_c, \end{cases}$$

with $r_V = 0.55 \text{ m}^3/\text{kg}$, $\tilde{\alpha} = 7.0 \text{ Pa}$ and $\tilde{\beta} = 2.9 \text{ kg/m}^3$. Graphs of the constitutive functions are shown in Figure 3.2. All other parameters are as in Examples 1 and 2.

All simulations start from a steady state obtained by a long-time simulation. For Examples 1 and 2, $Q_f(0) = 175 \text{ m}^3/\text{h}$, $Q_u(0) = 22 \text{ m}^3/\text{h}$ and $X_f(0) = 3.5 \text{ kg/m}^3$, whereas Example 3 starts from $Q_f(0) = 100 \text{ m}^3/\text{h}$, $Q_u(0) = 25 \text{ m}^3/\text{h}$, and $X_f(0) = 3 \text{ kg/m}^3$. These feed inputs are kept constant for a while, but then varied with time according to Figure 3.3. The vector of particulate feed percentages is $\mathbf{p}_{X,f}(0) = (5/7, 2/7)^T$ in all examples, and this value is varied only in Example 2; see Figure 3.3 (c). The feed substrate concentrations have the following constant values during all simulations: $S_{S,f}(t) = 9.00 \times 10^{-4} \text{ kg/m}^3$, $S_{\text{NO}_3,f}(t) = 6.00 \times 10^{-3} \text{ kg/m}^3$, and $S_{\text{N}_2,f}(t) = 0 \text{ kg/m}^3$. Different simulation times are used and the values of Δt for different N determined from (CFL) are given in Table 3.1. For fine mesh resolutions, the large values of β_X and $\beta_{\mathbf{P}_X}$ establish the expected fact that the time step Δt is limited by the second-order derivative term modelling compression.

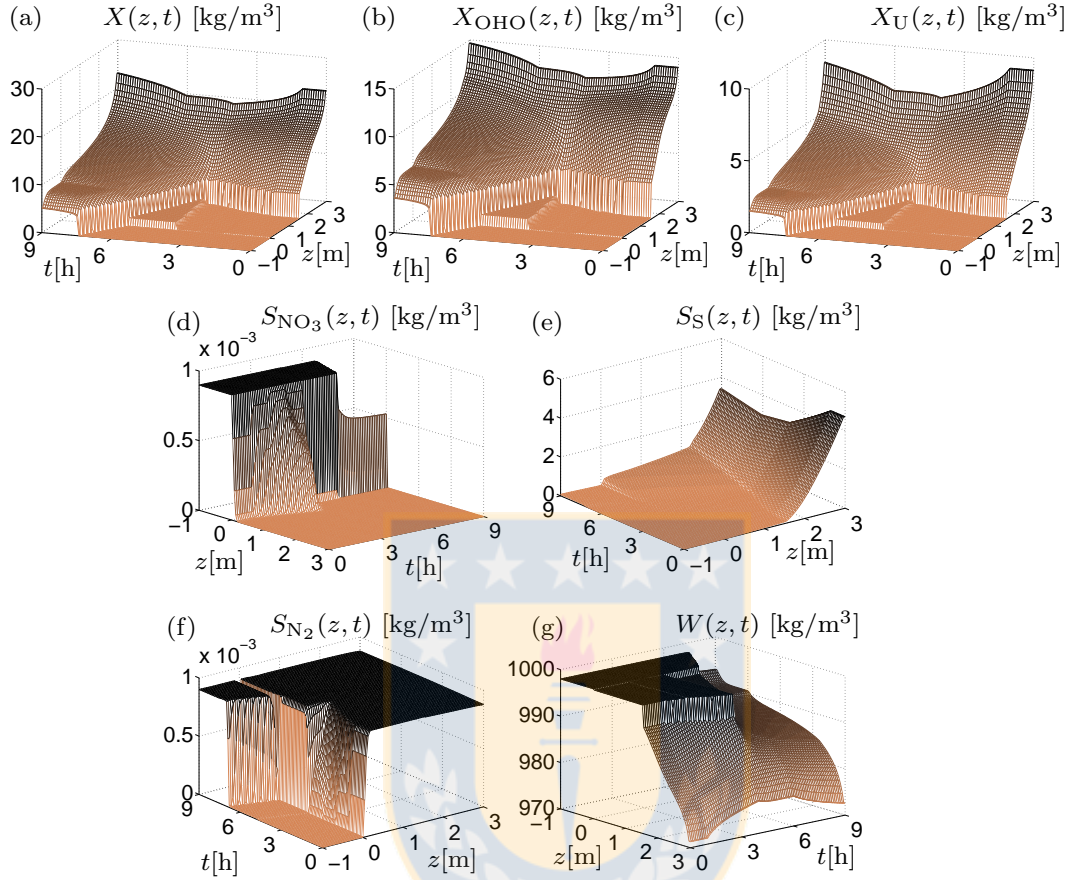


Figure 3.4: Example 1: Simulation of reactive settling in an SST starting from a stationary state followed by variations of the volumetric flows Q_u and Q_f and of the solids feed concentration X_f . Here and in Figures 3.6 and 3.8, the solution displayed is the reference solution obtained with $N = N_{\text{ref}} = 2430$ projected onto a coarser visual grid, and plots (d) and (g) have been rotated. Properly elaboration, published in [23].

3.4.1 Example 1: variations of feed flow and particle concentration

We choose the volume flows $Q_f(t)$, $Q_u(t)$ and the feed concentration $X_f(t)$ as piecewise constant functions of time specified in Figures 3.3 (a) and (b), respectively, and we let $\mathbf{p}_{X,f}$ and $\mathbf{p}_{L,f}$ be constant in time. We have chosen these extreme variations to test the scheme. The initial steady state is kept during the first hour of the simulation; see Figure 3.4. There is a sludge blanket, i.e., a discontinuity from a low concentration up to the critical concentration $X_c = 5 \text{ kg/m}^3$ separating the hyperbolic and parabolic

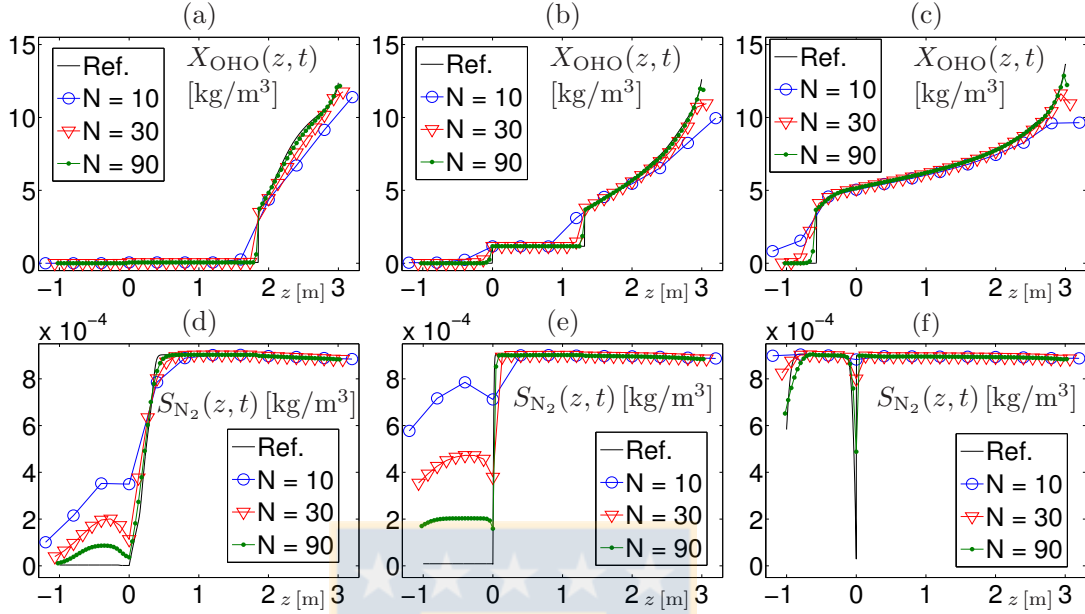


Figure 3.5: Example 1: Numerical solutions for coarse discretizations ($N = 10, 30, 90$) at (a, d) $t = 3$ h, (b, e) $t = 5$ h, (c, f) $t = 7$ h. The reference solution ($N = N_{\text{ref}} = 2430$) is included. Properly elaboration, published in [23].

regions; see also Figure 3.5 (a). The movement of this discontinuity is of particular interest to model in wastewater treatment. Below the discontinuity, the solution is continuous because of the compression effect. At $t = 4$ h, the step increase in $Q_f(t)$, decrease in $Q_e(t)$ and simultaneous increase in the fed bacteria X_{OHO} to the SST imply a rapidly rising sludge blanket that reaches the top of the SST around $t = 7$ h, which means that the SST becomes overloaded with solids leaving also through the effluent. The fast reactions imply that the soluble nitrate (NO_3) is quickly converted to N_2 in regions where the bacteria OHO are present, which is below the sludge blanket. At the end of the simulation, this phenomenon is clearly seen by the peak near $z = 0$ in Figure 3.4 (d) and the corresponding dip in Figure 3.4 (f) and Figure 3.5 (f).

3.4.2 Example 2: variations of the feed percentages

In this case Q_f, Q_u, X_f and $\mathbf{p}_{L,f}$ are kept the same constants as for the initial steady-state solution. Only $\mathbf{p}_{X,f}(t)$ is chosen as a periodically varying function of time as shown in Figure 3.3 (c). The resulting waves in the particle components through from the feed to the bottom are shown in Figure 3.6 (b) and (c). A part of the incoming nitrate (NO_3) is transported upwards to the effluent without undergoing any reaction

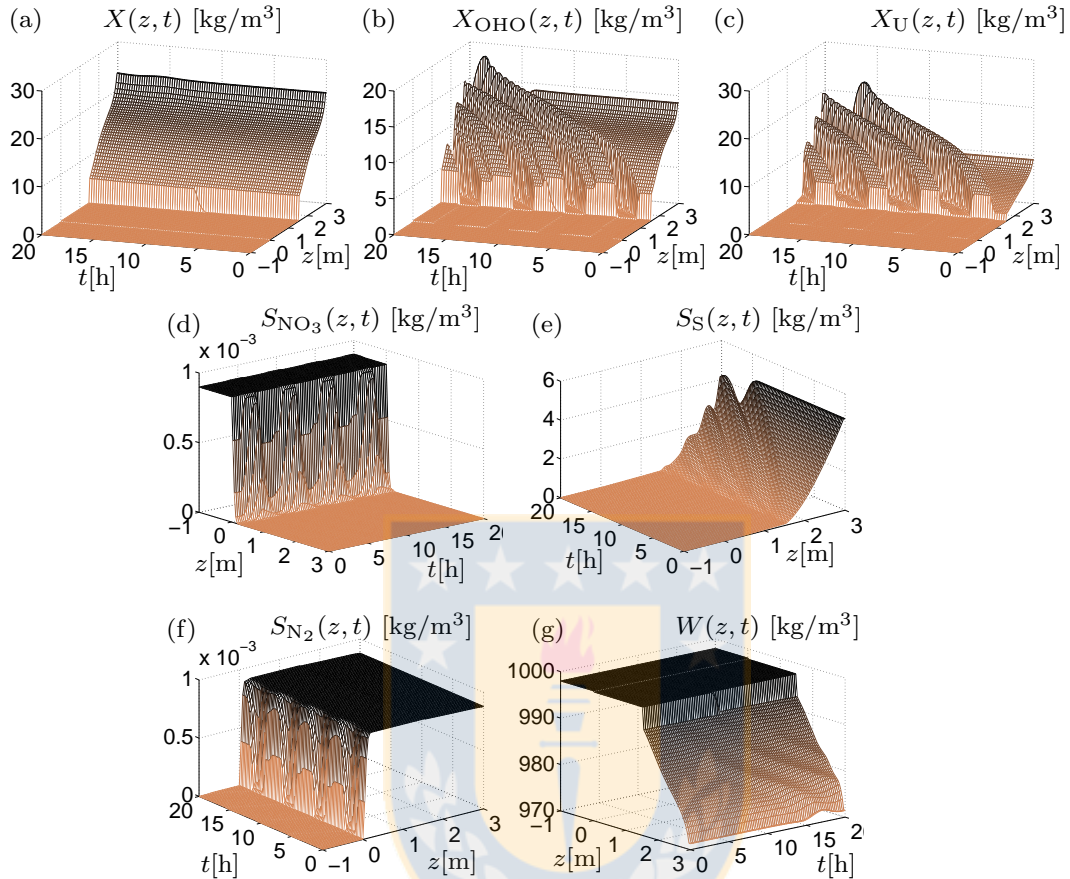


Figure 3.6: Example 2: Simulation of reactive settling in an SST starting from a stationary state followed by variations of the feed percentages of the substrates. Properly elaboration, published in [23].

since there is no solids in the clarification zone. The need for a high mesh resolution for such extremely varying particle concentrations can be seen in Figure 3.7 (a)–(c).

3.4.3 Example 3: transitions between steady states

In this simulation, shown in Figures 3.8 and 3.9, only the volumetric flows $Q_f(t)$ and $Q_u(t)$ are varied in a piecewise constant way according to Figure 3.3 (d) and (e). After 7 h the volumetric flows are set to constant values slightly different from the initial ones and a new steady state arises after a transient period with a sludge blanket rising into the clarification zone above the feed inlet. The rise of this discontinuity ends

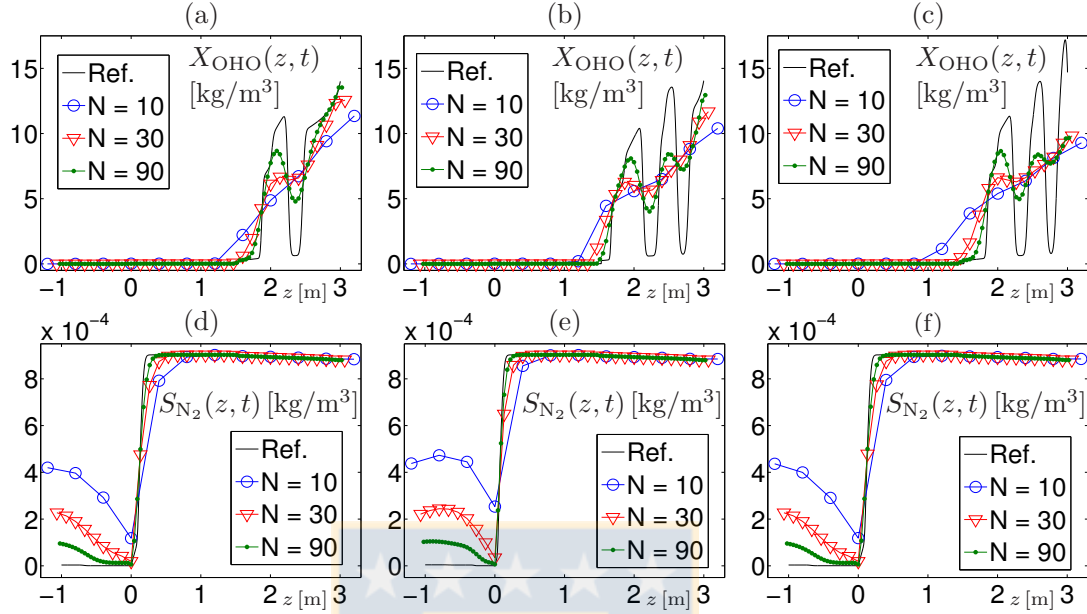


Figure 3.7: Example 2: Numerical solutions for coarse discretizations ($N = 10, 30, 90$) at (a, d) $t = 8$ h, (b, e) $t = 12$ h and (c, f) $t = 18$ h. The reference solution ($N = N_{\text{ref}} = 2430$) is included. Properly elaboration, published in [23].

at $t = 3$ h where $Q_f(t)$ is lowered substantially. After $t = 4$ h, the sludge blanket sinks because of the increased volumetric underflow $Q_u(t)$. The transport of N_2 in the thickening zone is in accordance with the changes of the bulk flows. The short appearance of particulate bacteria in the clarification zone implies that some of the otherwise non-reacted overflow of nitrate (NO_3) is converted to N_2 ; see Figures 3.8 (d) and (f).

3.4.4 Approximate errors

For a given spatial discretization $\Delta z = (B + H)/N$, we denote by $X_{\text{OHO},N}$ the piecewise constant function with $X_{\text{OHO},N}(z, t) = P_{X,j}^{(1),n} X_j^n$ if $z \in (z_{j-1/2}, z_{j+1/2}]$ and $t \in (t_{n-1}, t_n]$, and define the approximate relative L^1 error

$$e_{N, X_{\text{OHO}}}^{\text{rel}}(t) := \frac{\|(X_{\text{OHO},N} - X_{\text{OHO},N_{\text{ref}}})(\cdot, t)\|_{L^1(-H,B)}}{\|X_{\text{OHO},N_{\text{ref}}}(\cdot, t)\|_{L^1(-H,B)}},$$

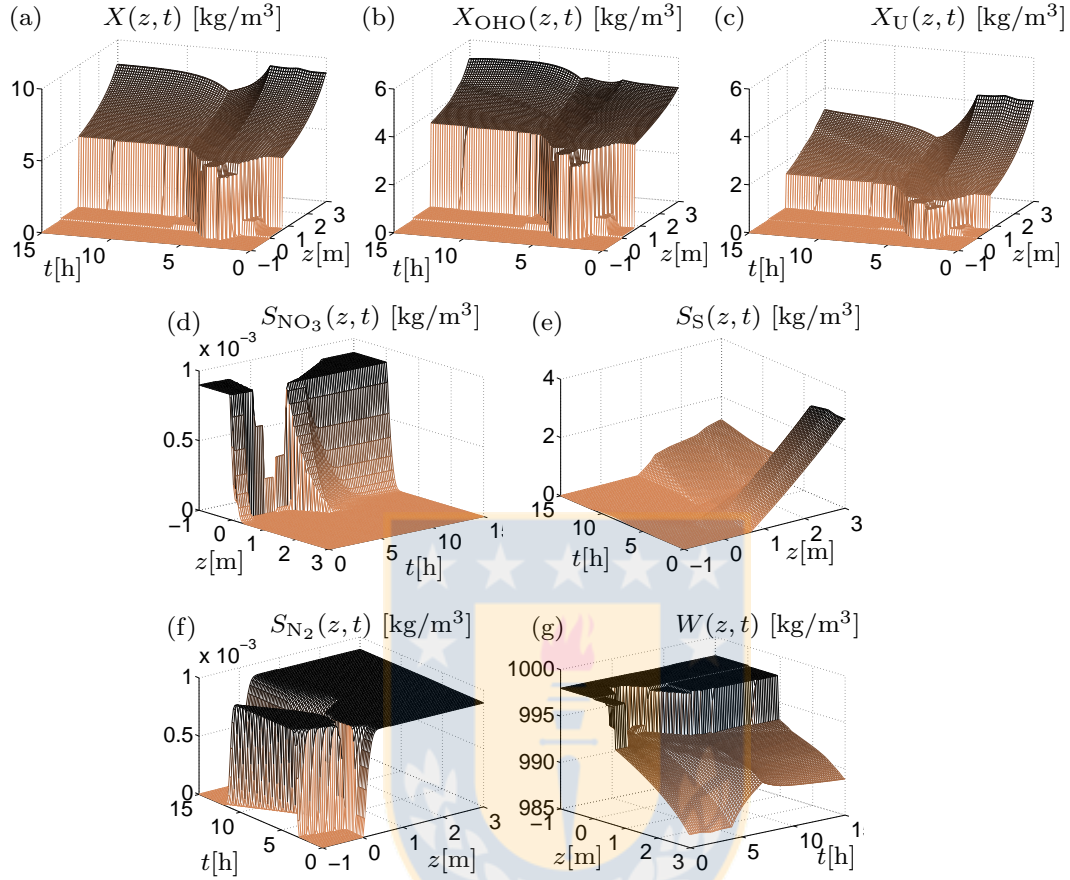


Figure 3.8: Example 3: Simulation reactive settling in an SST starting and ending in two different steady states. Properly elaboration, published in [23].

where $N_{\text{ref}} = 2430$. The corresponding quantities for X_U , S_{NO_3} , S_{N_2} and S_S are defined in the same way. We define the total approximate relative error

$$e_N^{\text{rel}}(t) := e_{N, X_{\text{OHO}}}^{\text{rel}}(t) + e_{N, X_U}^{\text{rel}}(t) + e_{N, S_{\text{NO}_3}}^{\text{rel}}(t) + e_{N, S_{\text{N}_2}}^{\text{rel}}(t) + e_{N, S_S}^{\text{rel}}(t)$$

and the observed convergence rate between two discretizations $N = N_1$ and $N = N_2$,

$$\theta(t) := -\frac{\log(e_{N_1}^{\text{rel}}(t)/e_{N_2}^{\text{rel}}(t))}{\log(N_1/N_2)}.$$

Table 3.2 shows values of $e_N^{\text{rel}}(t)$, $\theta(t)$ and corresponding CPU times, for selected examples and times of those used in Figures 3.5, 3.7 and 3.9. We observe that all approximate total relative errors tend to zero as N is increased. The rates θ assume values between

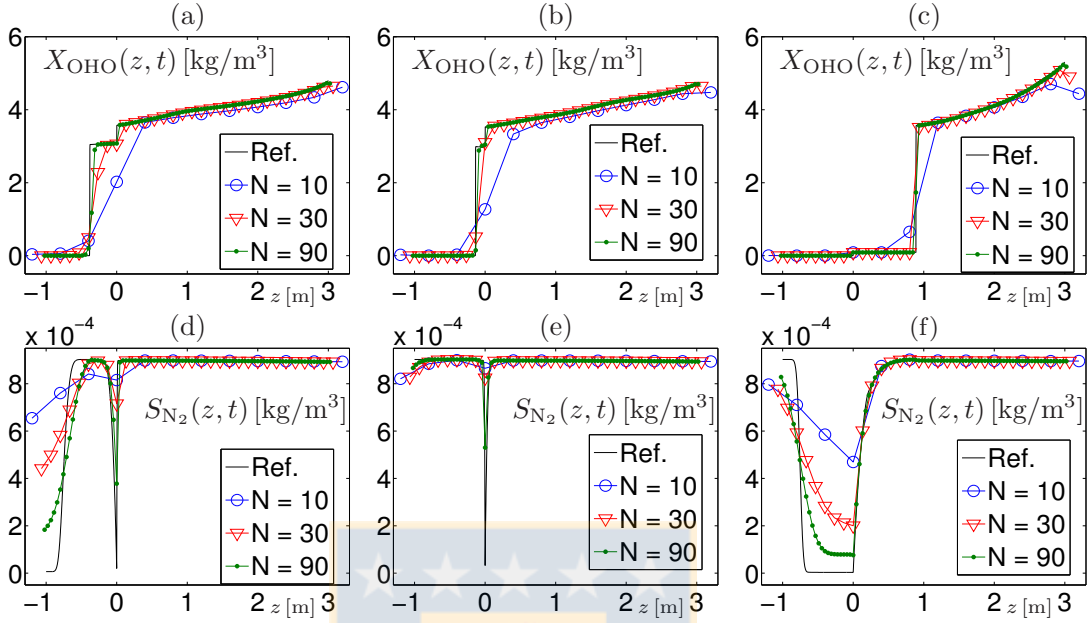


Figure 3.9: Example 3: Numerical solutions for coarse discretizations ($N = 10, 30, 90$) at (a, d) $t = 3$ h, (b, e) $t = 5$ h and (c, f) $t = 10$ h. The reference solution ($N = N_{\text{ref}} = 2430$) is included. Properly elaboration, published in [23].

zero and one for $N \leq 270$ (among the selected values of N), as should be expected for a first-order discretization in time and for the convective flux (see [25, 27] for comparable results). The values $\theta > 1$ observed for $N = 810$ do, however, alert to the limitations of error analysis via a reference solution with $N_{\text{ref}} = 2430$.

Table 3.2: Total approximate relative L^1 errors $e_N^{\text{rel}}(t)$, convergence rates $\theta(t)$ and CPU times for selected examples and indicated simulated times. Properly elaboration, published in [23].

N	Example 1, $t = 3$ h			Example 1, $t = 5$ h			Example 1, $t = 7$ h		
	$e_N^{\text{rel}}(t)$	$\theta(t)$	CPU [s]	$e_N^{\text{rel}}(t)$	$\theta(t)$	CPU [s]	$e_N^{\text{rel}}(t)$	$\theta(t)$	CPU [s]
10	0.570	—	0.08	0.639	—	0.13	0.257	—	0.17
30	0.233	0.812	0.19	0.324	0.618	0.31	0.133	0.598	0.43
90	0.085	0.924	0.56	0.136	0.791	0.92	0.056	0.789	1.26
270	0.029	0.973	2.41	0.047	0.971	4.03	0.024	0.772	5.44
405	0.018	1.190	5.28	0.031	1.045	8.66	0.018	0.732	11.97
810	0.007	1.264	28.18	0.012	1.306	47.35	0.007	1.276	65.06
	Example 2, $t = 8$ h			Example 2, $t = 12$ h			Example 2, $t = 18$ h		
10	0.679	—	0.24	0.646	—	0.30	0.722	—	0.55
30	0.497	0.284	0.48	0.711	-0.087	0.72	0.789	-0.080	1.04
90	0.317	0.410	1.40	0.537	0.255	2.08	0.632	0.201	3.10
270	0.156	0.643	6.05	0.293	0.553	9.07	0.373	0.480	13.42
405	0.113	0.797	13.61	0.212	0.801	20.26	0.276	0.744	30.25
810	0.056	1.003	75.02	0.105	1.006	110.58	0.138	1.004	167.98
	Example 3, $t = 3$ h			Example 3, $t = 5$ h			Example 3, $t = 10$ h		
10	0.302	—	0.05	0.381	—	0.08	0.332	—	0.15
30	0.102	0.990	0.12	0.226	0.477	0.19	0.183	0.540	0.35
90	0.053	0.599	0.32	0.120	0.572	0.50	0.072	0.855	0.92
270	0.020	0.878	0.94	0.054	0.722	1.50	0.029	0.817	2.78
405	0.012	1.299	1.53	0.039	0.809	2.41	0.022	0.735	4.37
810	0.005	1.220	3.96	0.018	1.107	6.28	0.009	1.207	11.64

Summary and concluding remarks

Conclusions Chapter 1

With the aim of finding an efficient time-integration method for the simulation of sedimentation with compression, we have in this work confined to two batch sedimentation tests for the comparison of some methods. The ideas of the new LI method and its implementation have been provided. When evaluated on the batch settling tests, we believe that is a good approach for make more research. In this area, convergence proof is under preparation. We show a benchmark of current methods in Table 3.3.

Conclusions Chapter 2

A reduced model of simultaneous biological reactions and sedimentation of flocculated particles in batch operation is written as a system of convection-diffusion-reaction PDEs, and a numerical scheme for its simulation is suggested. The idea of introducing a percentage vector for the composition of the flocculated particles [43] can be used in a natural way also when the effects of compression and reactions are included in the equations. In the present reduced model, with only two particulate components, this vector is simply $(p, 1 - p)^T$. The advantage of this approach is that since the vector appears linearly in each term of the equations for the particle concentrations, the sum of these equations yields an equation of the total suspended solids concentration X except for a reaction term. This equation is the Bürger-Diehl settler model equation with an additional reaction term. Consequently, we can utilize the ingredients by [18] for a correct spatial discretization into computational cells (layers). The time discretization

Explicit Euler method	
Pros:	Implementation easy. Convergence proof exists also for continuous sedimentation (numerical approximate solutions converge to the PDE solution as $\Delta z \rightarrow 0$) by Bürger et al. (2005). Robust method.
Cons:	Slow performance and not efficient
Semi-implicit method	
Pros:	Most efficient of the investigated methods. Under the assumption that the Newton-Raphson iterations find a solution each time step, convergence of the numerical method was proved for batch sedimentation by [16].
Cons:	Implementation more complex than Euler and LI. At each time step, a nonlinear system of algebraic equations is solved e.g. by Newton-Raphson iterations, which require tolerance parameter to be set. There is no guarantee that these iterations converge.
Linear-implicit method	
Pros:	Implementation easy. The ingredient in addition to the Euler method is basically that a linear system of equations is solved at each time step. Robust method.
Cons:	second most efficient for $N \approx 100$ for batch sedimentation. The efficiency can be adjusted to some extent by a parameter. Fastest method for a given $N \geq 30$, but least accurate.
Matlab ode15s	
Pros:	Ready-to-use standard time solver.
Cons:	Implementation most complex of the investigated methods. Well-established robust ODE solver for stiff problems, but not developed for solutions containing discontinuities. Least efficient of the investigated methods.

Table 3.3: Benchmark of different numerical schemes for compute a batch sedimentation

utilizes that X can be updated first, so that the numerical fluxes between the layers are known, which is then utilized in the updates of the percentage vectors.

Numerical examples for the modelling of the last stage of an SBR process, where denitrification occurs, indicate that the suggested numerical scheme works well and the expected denitrification process is simulated correctly. Furthermore, numerical tests with other initial data, resulting in non-monotone concentration profiles and movement of particles upwards, indicate that the numerical method could be extended to the case of continuous sedimentation in secondary settlers of WWTPs. The latter is an obvious continuation of this initial work on reactive settling for batch sedimentation. Other potential improvements are: a more accurate modelling of the liquid, in which the substrates are dissolved; the extension to include a full activated sludge model for the biokinetic reactions; an analysis of the convergence properties of the numerical scheme; the development of more efficient time discretizations; and the extension of the model to polydisperse particles and several space dimensions.

Concerning the latter two points, we finally mention that more rigorous mathematical and numerical treatments are available in the non-reactive case [7, 19, 28] that in particular deal with the necessity to solve additional equations for the motion of the mixture in several space dimensions. On the other hand, the non-spatial ASM1 model [69] is more involved than the reactive model incorporated into our model. However, here does not present a simpler version of any more rigorous published model since the *combined* description of the mechanical sedimentation-compression process with biological reactions is new.

Conclusions Chapter 3

The one-dimensional model equations (3.1) for continuous sedimentation of multi-component solid particles in a liquid, containing several soluble components, with possible biochemical reactions have been derived. Previous model ingredients such as hindered settling and compression at high concentrations have been complemented with the transport and reactions of components. Focus has been laid on the application to wastewater treatment, for which special simplifying model assumptions have been made. One assumption is that the solid and liquid phases have constant densities. This is not restrictive in wastewater treatment, where the concentrations of the soluble substrates are negligible in the water component.

Although there are only two densities, their difference and the reactions cause a volume change of the suspension; see the bulk velocity component due to reactions q^{reac} of the

total bulk velocity q in (3.20). In wastewater treatment, q^{reac} seems to be negligible. Hence, our numerical scheme will produce very similar solutions when setting $q^{\text{reac}} = 0$. The latter was, however, done to obtain a three-point explicit scheme with the monotonicity properties that lead to the invariant-region property; see Theorem 3.3.1. For other applications with larger q^{reac} , our scheme can still be used.

We are focussed on the model formulation, the development of a numerical scheme and its applications, the well-posedness analysis is still open. The basic difficulties associated with the model (3.1) are discussed in Section 3.1.1. The numerical results confirm that solutions are discontinuous due to changes in the definitions of fluxes across the inlet $z = 0$ and outlets $z = -H, B$ (visible, for instance, in Figure 3.4 (a) at $z = 0$), the nonlinearity of the flux as a function of X , and the strongly degenerating behaviour of D . The combined effect of both becomes visible, for instance, in the sharpness of the solution at the typical sludge blanket in Figure 3.4 (a), which moves up into the clarification zone and eventually overloads the SST. Moreover, the invariant-region principle (Theorem 3.3.1) is not only an asset in itself for practical purposes (concentrations are nonnegative and percentages satisfy their natural requirements, properties that are not automatically built into finite volume schemes [74]), but along with the underlying monotonicity could also form an important step towards proving existence of a weak solution of the problem via convergence of a scheme, as was done in [25, 27, 81] and many other works for related problems.

Our numerical scheme entails the well-known drastic growth of CPU time concomitant with mesh refinement for explicit discretizations of convection-diffusion-reaction problems. It is therefore highly desirable to develop more efficient solvers for the model, for example, a semi-implicit variant of the scheme that would limit this growth [16]. Such a scheme would be based on an implicit discretization of the diffusive terms arising in the fully discrete formulation (3.35), with the consequence that the corresponding CFL condition imposes a limitation on $\Delta t/\Delta z$ instead of $\Delta t/\Delta z^2$ as in the present treatment (cf. (CFL), (3.36)). While parts of the analysis related to the invariant-region principle can easily be adapted to such an implicit treatment (for instance, Lemma 3.3.3 can be adapted to a semi-implicit scheme by following [16, Lemma 3.2]), it is not obvious how to define (in the semi-implicit case) several quantities, for instance the analogue of $F_{X,j+1/2}^n$, that arise in the update formulas for the percentage vectors, (3.35b) and (3.35e). We therefore leave the definition of efficient semi-implicit or implicit-explicit (IMEX) schemes as an open research problem.

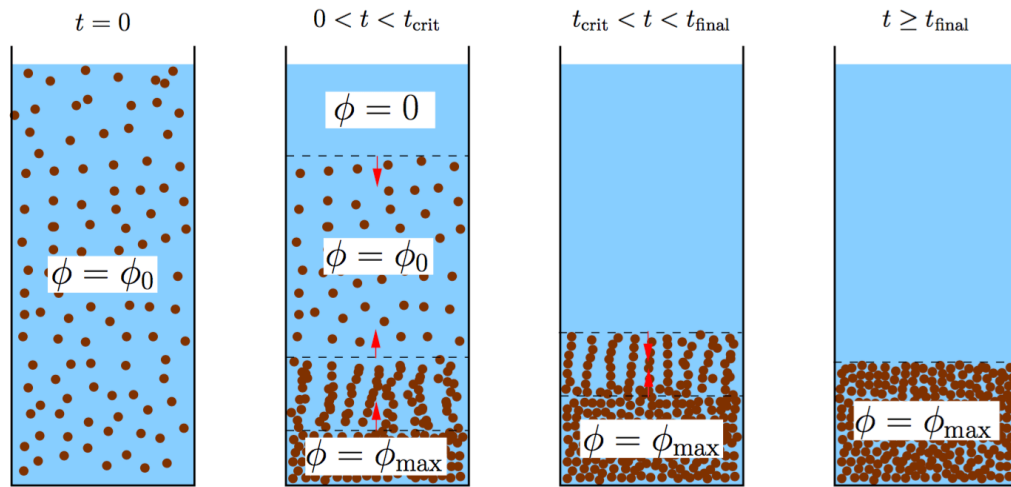


Figure 3.10: Batch sedimentation scheme. Solids particles turn down to the bottom under a external force, the gravity. Raimund Bürger, private communication.

Outlook

A different point of view

At the end of 2017 in together with another colleague and a friend, Diego Maldonado, with focus in discrete mathematics and theoretical informatics we decided that is necessary for academy and our country make a technological transfer to industry and society. Become hybrids from research and practical solutions and we created a company namely *Hibring Ingeniería* (translated is a acronym from hybrid and engineering). Our mission is contribute to industry knowledge given solutions to engineering problems using new developments and technological transfer and we try to be the main connection (or bridge) academy-industry in Chile, improving the productive sector using scientific innovation following the idea: *knowledge as way to development*. This chapter is a summary of the main research that we are developed.

This work isn't possible without CORFO funding and Everis support (an NTT data Company [99]) for offices and workspaces and of course all the people that as part of Hibring, they are (Daniel Fernández (Informatics eng.), Edison San Martín (Electronic eng. and 3D designer), Emilio Cifuentes (student eng.), Elias Godoy (student eng.), Manuel Silva (Metallurgical eng.), Greco Mora (aerospace eng.)).

Thickening is a very important process in industry, e.g. copper mine or wastewater treatment, because is dedicated to water recovery as was well explained in Introduction.

Greater effort was made for understand physical process and develop reliable mathematical models that can simulate and predict real data operation. Most of them find concentration $\phi(x, t)$ in each time and space steps.

One of the first contribution was Coe and Clevenger [35] tracking the sedimentation curve $h(t)$ in a small vessel (assuming scalability in height) and get estimate unit area for build thickener units. Coe and Clevenger made a biig improvement at early years of past century and even now is widely used, but this technique has limitations and arise new models.

Roughly speak, for modelling a thickener process must have the material properties, namely constitutive functions as $f_b = f_b(\phi)$ (batch flux function) and σ_e and are calculated from laboratory experiments and batch sedimentation. The most widely method used for compute f_b consist in a parametric reconstruction, where given a few batch sedimentation and clear water - sediment profile $h(t)$, is compute parameters for fitting a curve for f_b , as Richardson and Zaki method [109] or Vesilind method [129]. For σ_e is calculated using samples from lateral pipes in a continuous experiment under laboratory conditions. This method is really invasive and can't use in excess because the assumption of constant volume (or constant height) is altered.

In this chapter we show real data experiment that suggest consider particle size, namely γ for find and compute batch flux function, that is, we propose $f_b = f_b(\phi, \gamma)$.

Light as way for calculate batch flux function

We develope a new mechanism following the next principle: In a homogeneous liquid-solid mixture at a transparent vessel, the light that pass from one point to the other in a constant cross section area is inversely proportional to the concentration of solids. This means that in a mixture with a few solids particles, a beam light cross freely without interferences, but in a high number of solids particles (or greater solids concentration), jus a little quantity of light cross the vessel from one to the other side of the vessel as show Figure 3.11.

Using a right calibration, we postulate that just we need light concentration measure in both sides of the vessel for compute the solids concentration at the cross sectional area. So we developed a preliminar instrument as show Figure 3.12 in which we explain the rough idea for send data and take measurements. The prototype has the following essential parts:

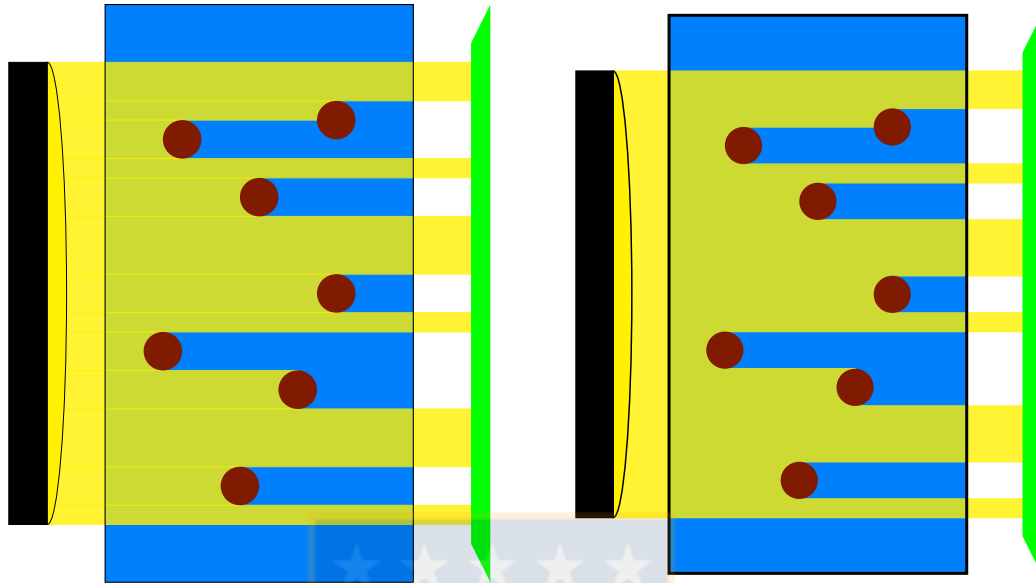


Figure 3.11: Schematic view of the light influence across a transparent vessel. (left) A sedimentation with a few particles (low concentration). (Right) A sedimentation with more particles. Properly elaboration.

- Laser array: They are adapter as a light source and send a constant beam. Each laser has different height and is adapted such that his light across the vessel just for his diameter avoid refraction issues.
- Vessel: Is a transparent tube with constant circular cross section along the height.
- Photoresistor: They are sensible with light. So every laser beam will be measure with a Photoresistor at the same height but to the other side of the vessel if the laser beam cross the vessel.

Application from scientific computation to online platform with many users

In order to find the way for many people are interacting with new mathematical developments is we build a robust architecture for support that. In Figure 3.13 we show a different way for compute a numerical result. Previously in [94] we explain with a diagram how compute a thickener simulation from different operational parameters and constitutive functions, now we coupled to those result a informatic backend using python language and Django framework [50]. This alternative has many advantages, for example you can couple other results in different languages as modules, that is the

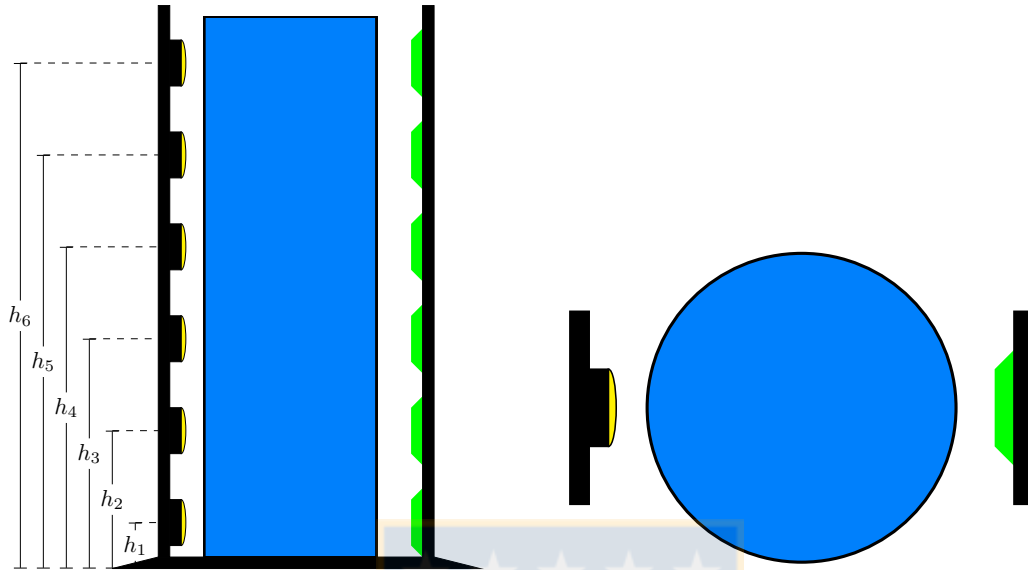


Figure 3.12: Diagram of a prototype that measure the light quantity and transform to a concentration value. (left) Array of different light source and light sensors along the vessel. (Right) A scheme for one sensor and light source. Properly elaboration.

case of *electronic backend*: is a mini-system that compile real data using a wide kind of sensors and this results are used as input for mathematical models. Here we use Flask framework [56] for make inner connection. All the results are showed for users using a continuously updating backup in a database. This is a key point, the user never see scientific computation and his electronic device never compute that, just is a visualisation from a database using ajax. After that, the front end is a couple of widgets that make more comfortable the visualisation in different size screen (responsive), with colourful and less buttons (minimalistic). In general, we use Bootstrap [9] framework programming in HTML [73] with Javascript [75] application. Is important for dashboard use a Sufee framework [113] and some graphic motor tools as Highcharts [71], D3 [38] or D3plus [39].

Previous system description makes it possible to compute a scientific result, add experimental results and couple with operational control parameters for make possible to build an automatic system of prevent alerts. We apply the system to thickener and clarifier process, but the architecture is adaptable for many other industries using essentially same modules.

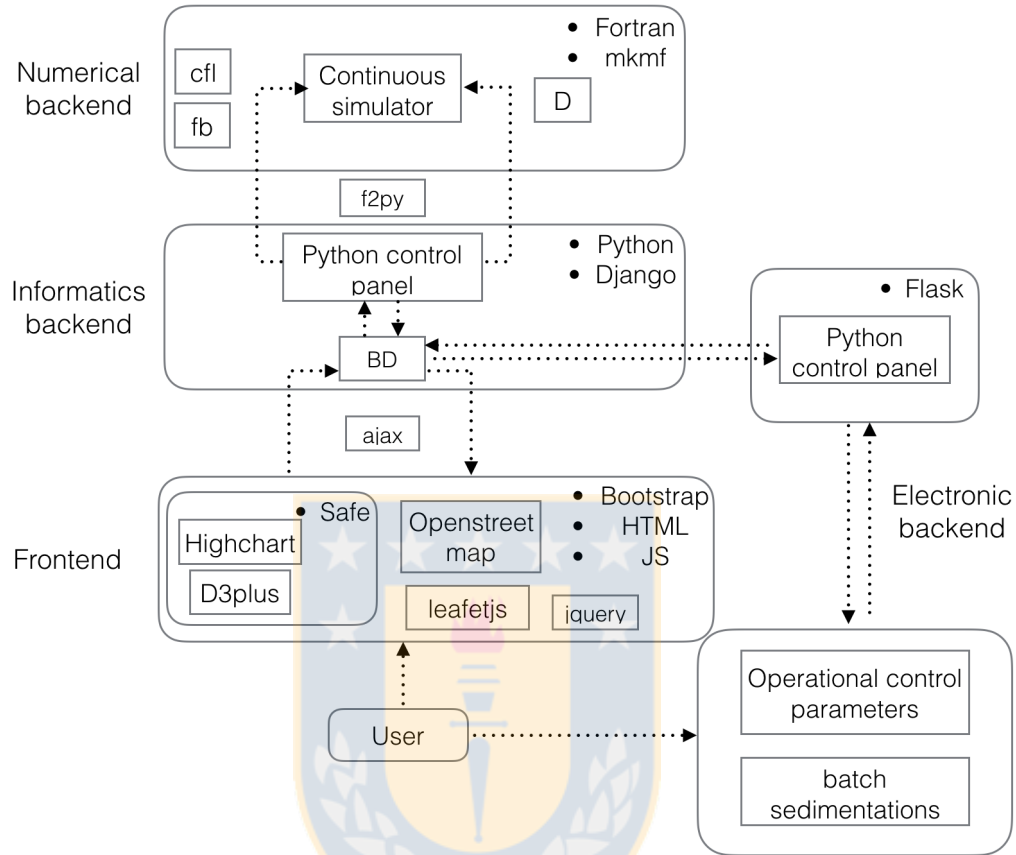


Figure 3.13: Flow diagram of *RelaveSeco* platform. At the first part is as [94] and after is coupled with a FullStack development (informatic backend and frontend) and a Electronic background for manage remotely operation control parameters. Properly elaboration.

Future work

Along my PhD research we found and develop initially many ideas for aboard. One of them was the Biofilm area. We put here an introduction to the problema and related word for be used in a future work. Actually is under construction.

Biofilms

Since 2017 we work developing a mathematical model and reliable numerical scheme, that consider the biofilm behaviour in two different spatial scales, *biofilm scale* and

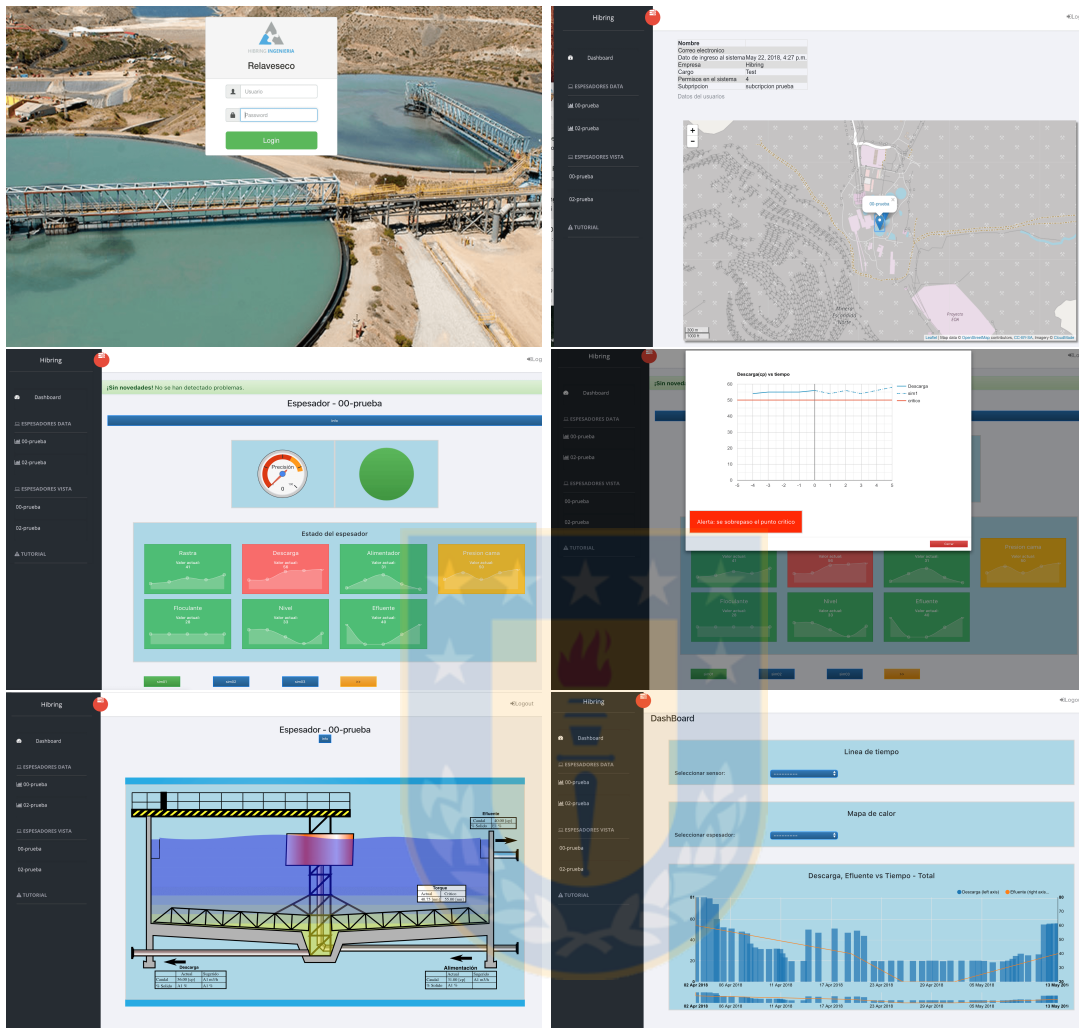


Figure 3.14: Screenshot of RelaveSeco plataform. A couple of thickener in operation in Chile and Australia. In order from left to right and upper to down: (a) Escondida mine, Chile (b) Collahuasi mine, Chile (c) Candelaria mine, Chile (d) CODELCO Chuquicamata mine, Chile, (e) CODELCO DMH mine, Chile (f) APEX Wiluna Gold Mine, Australia. Adapted from Imagery ©2018 Google Maps, by Elias Godoy and Camilo Mejías, Retrieved October 01, 2018, from <http://www.maps.google.com/>. adapted with permission.

reactor scale and are separate by a boundary layer as a stagnant liquid layer, using approximate Fick's Law when the phases between the granule and water are changed. In the Figure 3.15 we can see a conceptual idea of the model with the different stages define by a radial axis. We assume radial symmetry so we work in just one dimension.

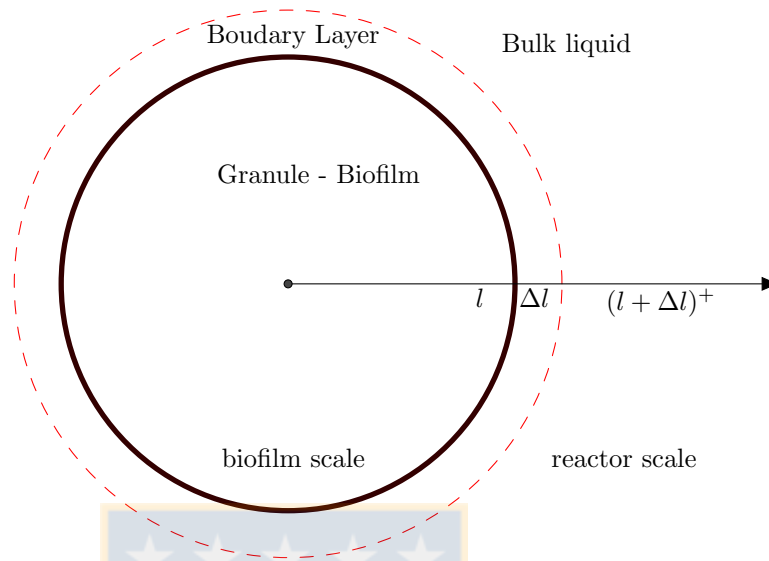


Figure 3.15: Schematic view of a granule. A 1D scheme of the granule and the boundary layer that is a quiet liquid and is the transition between the granule to the bulk reactor. Fick's Law is available here. Properly elaboration.

The granules are a special kind of biofilm that not obey the assumption "grouting of cell attached over a solid surface". In this case (granules) the bacterias be attach over itself. The standard assumption for create granules is work over a SBR (sequencing batch reactors) with lows settling residencial time. If his sedimentation time is low, then when you wash the small particles that not reach to settled, with this manner you chose just bacteria that settled and attached itself. Summarising the formation stages are:

- Starting of attachment (young bacterias)
- Grouting of granules by grouting of cell mass and adhesion of suspended and flocculent biomass
- Re-granulation from detachment of old granules.

The isolating of anammox in the center of the granule occur by natural selection and you can build your anammox granules this in a anoxic SBR and then add nitrificant biomass and transform the system to a CANON system with change of substrate and add aeration.

Biofilm related work

In the last years mathematical models have been developed to understand the partial nitrification processes and the biofilm and granule knowledge. One of that work was [87] who used a dynamic model to compare competition between autotrophic and heterotrophic biomass in a developing biofilm. In these work they never considerate detachment. This variable was first added in [133] as result of a mass balance and some upgrades in [134] with changes of the biofilm porosity and simultaneous detachment and attachment processes. This model is widely used and is called *Wanner and Gujer model*. Many researchers work in the detachment process, for example in [95] they concluded that mathematical models assuming constant biofilm thickness produce wrong results in performance of systems. Some upgrades you can find in [139]. On the other hand [90] work in experimental models to detachment velocity and [121, 123] introduced a free surface model with varying the large L as a function between growth and detachment velocity, they said *“The biofilm structure is determinated by the ratio between detachment forces and biomass production rate in biofilm”*. Another point of view was given by [102, 103] that build a model applied to simulate growth of biofilm attached on solid flat surfaces and write the boundary conditions for PDE system solved with cellular automata. In the same time [108, 135] work in a complete model for capture all small process inside the granule like a particulate materia suspended in the liquid and introduce a *porosity* concept for the granule. With this basis papers Reichert built the AQUASIM software [106, 107] that 20 year over is widely used yet.

Wanner et. al. in [132] gave a review of all works in the area and summarise some things under the same notation. Moreover introduce a new mass balance. The granule size and its importance to the whole processes was studied by [55, 90, 97, 128, 130, 131] and biofilm shape is also an important parameter for the stability of the reactor showed by [58].

Recently [126] using a systematic modelling framework in [68] and some ideas about reaction vector as ASM1 in [70] suggest a new free surface coupled with nonlinear flux model for explain the liquid diffusion and particulate advection with reactions inside the granule. This model result a simplification of Wanner and Reichert model [108, 135] but applied for granules itself and not over a solid surface. They validate this model in a steady state and fix L in [127] while in [96] work in stoichiometric reaction for nitrogen consume. All was summarized in [125] using a realistic test given by [77]. Some approaches for a numerical consumption scheme were showed in [124] but is an incomplete discretization.

Other ways for model granules are Wood in [137] that introduced a method like volume averaging for the models and [51] gave a first model that consider the biomass as a viscous fluid. This is called *Dockery model* and is very used too.

First approach in build a reliable framework with mathematical emphases, analysis error are studied by Eberl in [54].

Some reviews in Biofilm modelling you can find in [72, 104, 111, 132].

So our future work can be summarised in:

- Proof the numerical scheme convergence for linearly implicit method in Chapter 1. Here we made some approaches, but still we have issues in a certain parameters independence.
- Apply mathematical model proves in Chapter3 for other industrial process, such that leaching.
- Finish the Biofilm model with applications to CANON and SNAD processes.
- Investigate more about the influence of granule size to the sedimentation velocities and how this granulometry affects to the determination of $f_b(\phi)$, where ϕ is the volume concentration.
- Make a better architecture for provide a online simulator for strongly degenerate parabolic partial differential equations.

Bibliography

- [1] R. Adimurthi, G.D. Dutta, G. Veerappa, and J. Jaffré. Monotone (a,b) entropy stable numerical scheme for scalar conservation laws with discontinuous flux. *ESAIM: Mathematical Modelling and Numerical Analysis*, 48(6):1725 – 1755, 2014.
- [2] G. Agrícola. *De re metallica; translated from the first Latin edition of 1556*. Dover Publications, 1950.
- [3] J. Alex, S.G.E. Rönnner-Holm, M. Hunze, and N.C. Holm. A combined hydraulic and biological SBR model. *Water Science and Technology*, 64:1025 – 1031, 2011.
- [4] T. Arbogast, C.-S. Huang, and T.F. Russell. A locally conservative Eulerian–Lagrangian method for a model two-phase flow problem in a one-dimensional porous medium. *SIAM Journal on Scientific Computing*, 34(4):A1950 – A1974, 2012.
- [5] J. Balbás and G. Hernández-Dueñas. A positivity preserving central scheme for shallow water flows in channels with wet-dry states. *ESAIM: Mathematical Modelling and Numerical Analysis*, 48(3):665 – 696, 2014.
- [6] A.E. Berger, H. Brezis, and J.W. Rogers. A numerical method for solving the problem $u_t - \delta f(u) = 0$. *RAIRO Analyse numérique*, 13:297 – 312, 1979.
- [7] S. Berres, R. Bürger, K.H. Karlsen, and E.M. Tory. Strongly degenerate parabolic-hyperbolic systems modeling polydisperse sedimentation with compression. *SIAM Journal on Applied Mathematics*, 64:41 – 80, 2003.
- [8] F. Betancourt, R. Bürger, S. Diehl, and C. Mejías. Advanced methods of flux identification for clarifier-thickener simulation models. *Minerals Engineering*, 63:2 – 15, 2014.
- [9] Bootstrap. <https://getbootstrap.com/>. Retrieved October 20, 2018.

- [10] S. Borazjani, A.J. Roberts, and P. Bedrikovetsky. Splitting in systems of PDEs for two-phase multicomponent flow in porous media. *Applied Mathematics Letters*, 53:25 – 32, 2016.
- [11] O. Bernard A.-C. Boulanger M.-O Bristeau and J. Sainte-Marie. A 2d model for hydrodynamics and biology coupling applied to algae growth simulations. *ESAIM: Mathematical Modelling and Numerical Analysis*, 47(5):1387 – 1412, 2013.
- [12] R. Bürger, M.C. Bustos, and F. Concha. Settling velocities of particulate systems: 9. Phenomenological theory of sedimentation processes: Numerical simulation of the transient behaviour of flocculated suspensions in an ideal batch or continuous thickener. *International Journal of Mineral Processing*, (55):267 – 282, 1999.
- [13] R. Bürger, J. Careaga, S. Diehl, C. Mejías, I. Nopens, P.A. Vanrolleghem, and E. Torfs. Simulations of reactive settling of activated sludge with a reduced biokinetic model. *Computers and Chemical Engineering*, 92:216 – 229, 2016.
- [14] R. Bürger and F. Concha. Mathematical model and numerical simulation of the settling of flocculated suspensions. *International Journal of Multiphase Flow*, 24:1005 – 1023, 1998.
- [15] R. Bürger, A. Coronel, and M. Sepúlveda. On an upwind difference scheme for strongly degenerate parabolic equations modelling the settling of suspensions in centrifuges and non-cylindrical vessels. *Applied Numerical Mathematics*, 56:1397 – 1417, 2006.
- [16] R. Bürger, A. Coronel, and M. Sepúlveda. A semi-implicit monotone difference scheme for an initial- boundary value problem of a strongly degenerate parabolic equation modelling sedimentation-consolidation processes. *Mathematics of Computation*, 75:91 – 112, 2006.
- [17] R. Bürger, J.J.R. Damasceno, and K.H. Karlsen. A mathematical model for batch and continuous thickening in vessels with varying cross section. *International Journal of Mineral Processing*, 73(2):183 – 208, 2004.
- [18] R. Bürger and S. Diehl. Convexity-preserving flux identification for scalar conservation laws modelling sedimentation. *Inverse Problems*, 29(4):045008, 2013.
- [19] R. Bürger, S. Diehl, S. Farås, and I. Nopens. On reliable and unreliable numerical methods for the simulation of secondary settling tanks in wastewater treatment. *Computers and Chemical Engineering*, 41:93 – 105, 2012.

- [20] R. Bürger, S. Diehl, S. Farås, I. Nopens, and E. Torfs. A consistent modelling methodology for secondary settling tanks: a reliable numerical method. *Water Science and Technology*, 68:102 – 208, 2013.
- [21] R. Bürger, S. Diehl, and C. Mejías. On time discretizations for the simulation of the batch settling-compression process in one dimension. *Water Science and Technology*, 73(5):1010 – 1017, 2016.
- [22] R. Bürger, S. Diehl, and C. Mejías. A model for continuous sedimentation with reactions for wastewater treatment. In G. Mannia, editor, *Frontiers in Wastewater Treatment and Modelling (FICWTM 2017), Lecture Notes in Civil Engineering*, volume 4, pages 596 – 601, Cham, Switzerland, 2017. Springer International Publishing.
- [23] R. Bürger, S. Diehl, and C. Mejías. A difference scheme for a degenerating convection-diffusion-reaction system modelling continuous sedimentation. *ESAIM: Mathematical Modelling and Numerical Analysis*, 52(2):365 – 392, 2018.
- [24] R. Bürger, S. Diehl, and I. Nopens. A consistent modelling methodology for secondary settling tanks in wastewater treatment. *Water Research*, 45:2247 – 2260, 2011.
- [25] R. Bürger, K.H. Karlsen, N.H. Risebro, and J.D. Towers. Well-posedness in BV_t and convergence of a difference scheme for continuous sedimentation in ideal clarifier-thickener units. *Numerische Mathematik*, 97:25 – 65, 2004.
- [26] R. Bürger, K.H. Karlsen, H. Torres, and J.D. Towers. Second-order schemes for conservation laws with discontinuous flux modelling clarifier-thickener units. *Numerische Mathematik*, 116(4):579 – 617, 2010.
- [27] R. Bürger, K.H. Karlsen, and J.D. Towers. A model of continuous sedimentation of flocculated suspensions in clarifier-thickener units. *SIAM Journal on Applied Mathematics*, 65:882 – 940, 2005.
- [28] R. Bürger, S. Kumar, and R. Ruiz-Baier. Discontinuous finite volume element discretization for coupled flow-transport problems arising in models of sedimentation. *Journal of Computational Physics*, 299:446 – 471, 2015.
- [29] R. Bürger, P. Mulet, and L.M. Villada. Regularized nonlinear solvers for imex methods applied to diuvisely corrected multi-species kinematic flow models. *SIAM Journal on Scientific Computing*, 35:B751 – B777, 2013.

- [30] R. Bürger, R. Ruiz, K. Schneider, and M. Sepúlveda. Fully adaptive multiresolution schemes for strongly degenerate parabolic equations in one space dimension. *ESAIM: Mathematical Modelling and Numerical Analysis*, 42(4):535 – 563, 2008.
- [31] R. Bürger, W.L. Wedland, and F. Concha. Model equations for gravitational sedimentation-consolidation processes. *ZAMM - Journal of Applied Mathematics and Mechanics*, 80:79 – 92, 2000.
- [32] M.C. Bustos, F. Concha, R. Bürger, and E.M. Tory. *Sedimentation and Thickening: Phenomenological Foundation and Mathematical Theory*. Kluwer Academic Publishers, Dordrecht, The Netherlands, 1999.
- [33] T.-C. Chao and D.B. Das. Numerical simulation of coupled cell motion and nutrient transport in NASA’s rotating bioreactor. *Chemical Engineering Journal*, 259:961 – 971, 2015.
- [34] J. De Clercq, I. Nopens, J. Defrancq, and P.A. Vanrolleghem. Extending and calibrating a mechanistic hindered and compression settling model for activated sludge using indepth batch experiments. *Water Research*, 42:781 – 791, 2008.
- [35] H.S. Coe and G.H. Clevenger. Methods for determining the capacities of slime settling tanks. *Transactions of the American Institute of Mining Engineers*, 55:356 – 385, 1916.
- [36] F. Concha. *Solid-Liquid Separation in the Mining Industry. Fluid Mechanics and Its Application Series*. Springer, Cham, 2014.
- [37] F. Concha and R. Bürger. Thickening in the 20th century: a historical perspective. *Minerals and Metallurgical Processing*, 20:57 – 67, 2003.
- [38] Data-Driven Documents. <https://d3js.org/>. Retrieved October 20, 2018.
- [39] Data visualization made easy. <https://d3plus.org/>. Retrieved October 20, 2018.
- [40] S. Diehl. On scalar conservation laws with point source and discontinuous flux function. *SIAM Journal on Mathematical Analysis*, 26(6):1425 – 1451, 1995.
- [41] S. Diehl. A conservation law with point source and discontinuous flux function modelling continuous sedimentation. *SIAM Journal on Applied Mathematics*, 56(2):388 – 419, 1996.
- [42] S. Diehl. Continuous sedimentation of multi-component particles. *Mathematical Methods in the Applied Sciences*, 20:1345 – 1364, 1997.

- [43] S. Diehl. Dynamic and steady-state behavior of continuous sedimentation. *SIAM Journal on Applied Mathematics*, 57:991 – 1018, 1997.
- [44] S. Diehl. On boundary conditions and solutions for ideal clarifier-thickener units. *Chemical Engineering Journal*, 80:119 – 133, 2000.
- [45] S. Diehl. Estimation of the batch-settling flux function for an ideal suspension from only two experiments. *Chemical Engineering Science*, 62:4589 – 4601, 2007.
- [46] S. Diehl. A uniqueness condition for nonlinear convection-diffusion equations with discontinuous coefficients. *Journal of Hyperbolic Differential Equations*, 6:127 – 159, 2009.
- [47] S. Diehl. Numerical identification of constitutive functions in scalar nonlinear convection-diffusion equations with application to batch sedimentation. *Applied Numerical Mathematics*, (154 – 172), 95.
- [48] S. Diehl and S. Farås. A reduced-order ode-pde model for the activated sludge process in wastewater treatment: classification and stability of steady states. *Mathematical Methods in the Applied Sciences*, 23:369 – 405, 2013.
- [49] S. Diehl, S. Farås, and G. Mauritsson. Fast reliable simulations of secondary settling tanks in wastewater treatment with semi-implicit time discretization. *Computers and Mathematics with Applications*, 70:459 – 477, 2015.
- [50] Django. <https://www.djangoproject.com/>. Retrieved October 20, 2018.
- [51] J. Dockery and I. Klapper. Finger formation in biofilm layers. *SIAM Journal on Applied Mathematics (SIAP)*, 62(3):853 – 869, 2001.
- [52] J. V. N. Dorr. The use of hydrometallurgical apparatus in chemical engineering. *Journal of Industrial and Engineering Chemistry*, 7:119 – 130, 1915.
- [53] D.A. Drew and S.L. Passman. *Theory of Multicomponent Fluids*. Springer-Verlag, New York, 1999.
- [54] H.J. Eberl, D. Parker, and M.C.M van Loosdrecht. A new deterministic spatio-temporal continuum model for biofilm development. *Journal of Theoretical Medicine*, 3(3):161 – 175, 2001.
- [55] M. Figueroa, J.R. Vázquez-Padín, A. Mosquera-Corral, and R. Méndez. Is the canon reactor an alternative for nitrogen removal from pre-treated swine slurry? *Biochemical Engineering Journal*, 65:23 – 29, 2012.
- [56] Flask. <http://flask.pocoo.org/>. Retrieved October 20, 2018.

- [57] X. Flores-Alsina, K.V. Gernaey, and U. Jeppsson. Benchmarking biological nutrient removal in wastewater treatment plants: influence of mathematical model assumptions. *Water Science and Technology*, 65:1496 – 1505, 2012.
- [58] J.M. Garrido, W.A.J. van Benthum, M.C.M van Loosdrecht, and J.J. Heijnen. Influence of dissolved oxygen concentration on nitrite accumulation in a biofilm airlift suspension reactor. *Biotechnology and Bioengineering*, 53:168 – 178, 1997.
- [59] R. Georges. E. Ardaillon, les mines du laurion dans l'antiquité. *Revue des Études Anciennes*, 1(1):83 – 88, 1989.
- [60] K.V. Gernaey, U. Jeppsson, D.J. Batstone, and O. Ingildsen. Impact of reactive settler models on simulated wwtp performance. *Water Science and Technology*, 53(1):159 – 167, 2006.
- [61] K.V. Gernaey, U. Jeppsson, P.A. Vanrolleghem, and J.B. Copp. *Benchmarking of Control Strategies for Wastewater Treatment Plants. IWA Scientific and Technical Report No. 23*. IWA Publishing, London, UK, 2014.
- [62] T. Gimse and N.H. Risebro. Solution of the Cauchy problem for a conservation law with a discontinuous flux function. *SIAM Journal on Mathematical Analysis*, 23(3), 635 – 648 1992.
- [63] Global Citizen. <https://www.globalcitizen.org/en/issue/water-sanitation/>. Asked October 20, 2018.
- [64] J.M.N.T. Gray and C. Ancey. Multi-component particle-size segregation in shallow granular avalanches. *Journal of Fluid Mechanics*, 678:535 – 588, 2011.
- [65] J. Guerrero, X. Flores-Alsina, A. Guisasola, J.A. Baeza, and K.V. Gernaey. Effect of nitrite, limited reactive settler and plant design configuration on the predicted performance of simultaneous c/n/p removal wwtps. *Bioresource Technology*, 136:680 – 688, 2013.
- [66] E. Guyonvarch, E. Ramin, M. Kulahci, and B.G. Plósz. icfd: Interpreted computational fluid dynamics - degeneration of cfd to one-dimensional advection-dispersion models using statistical experimental design - the secondary clarifier. *Water Research*, 65:396 – 411, 2015.
- [67] J. Hamilton, R. Jain, P. Antoniou, S.A. Svoronos, B. Koopman, and G. Lyberatos. Modeling and pilot-scale experimental verification for predenitrification process. *Journal of Environmental Engineering*, 118:38 – 55, 1992.

- [68] M. Heitzig, G. Sin, P. Glarborg, and R. Gani. A computer-aided framework for regression and multi-scale modelling needs in innovative product-process engineering. *20th European Symposium on Computer Aided Process engineering*, 28:379 – 384, 2010.
- [69] M. Henze, C.P.L Grady, W. Gujer, G.V.R. Marais, and T. Matsuo. *Activated Sludge Model no. 1*. Scientific and Technical Report No. 1, IAWQ, London, UK, 1987.
- [70] M. Henze, W. Gujer, T. Mino, and M.C.M van Loosdrecht. *Activated Sludge Models ASM1, ASM2, ASM2D and ASM3*. IWA Scientific and Technical Report no. 9, IWA Publishing, 2000.
- [71] Highcharts. <https://www.highcharts.com/>. Retrieved October 20, 2018.
- [72] H. Horn and S. Lackner. Modeling of biofilm systems: A review. *Advances in Biochemical Engineering/Biotechnology*, 146:53 – 76, 2014.
- [73] HTML. <https://www.w3.org/html/>. Retrieved October 20, 2018.
- [74] S. Jaouen and F. Lagoutière. Numerical transport of an arbitrary number of components. *Computer Methods in Applied Mechanics and Engineering*, 196(33–34):3127 – 3140, 2007.
- [75] JavaScript. <https://developer.mozilla.org/bm/docs/web/javascript>. Retrieved October 20, 2018.
- [76] U. Jeppsson and S. Diehl. An evaluation of a dynamic model of the secondary clarifier. *Water Science and Technology*, 34(5–6):19 – 26, 1996.
- [77] U. Jeppsson, M.-N. Pons, I. Nopens, J. Alex, J.B. Copp, K.V. Gernaey, C. Rosen, J.-P. Steyer, and P.A. Vanrolleghem. Benchmark simulation model no 2: General protocol and exploratory case studies. *Water Science & Technology*, 56(8):67 – 78, 2007.
- [78] J. Jonhson and A. Accioly. Feedwell is the heart of a thickener. In A. Wu and R. Jewell, editors, *Proceedings of the 20th International Seminar on Paste and Thickened Tailings*, pages 23 – 28, Beijing, 2017. University of Science and Technology Beijing.
- [79] K.H. Karlsen and N.H. Risebro. On the uniqueness and stability of entropy solutions of nonlinear degenerate parabolic equations with rough coefficients. *Discrete Continuous Dynamical Systems*, 9(5):1081 – 1104, 2003.

- [80] K.H. Karlsen, N.H. Risebro, and E.B. Storrøsten. On the convergence rate of finite difference methods for degenerate convection-diffusion equations in several space dimensions. *ESAIM: Mathematical Modelling and Numerical Analysis*, 50(2):499 – 539, 2016.
- [81] K.H. Karlsen, N.H. Risebro, and J.D. Towers. Upwind difference approximations for degenerate parabolic convection-diffusion equations with a discontinuous coefficient. *IMA Journal of Numerical Analysis*, 22(4):623 – 664, 2002.
- [82] K.H. Karlsen, N.H. Risebro, and J.D. Towers. L^1 stability for entropy solutions of nonlinear degenerate parabolic convection-diffusion equations with discontinuous coefficients. *Preprint series. Pure mathematics* <https://www.duo.uio.no/handle/10852/10639>, pages 1 – 49, 2003.
- [83] A.A. Kazmi, M. Fujita, and H. Furumai. Modeling effect of remaining nitrate on phosphorus removal in sbr. *Water Science and Technology*, 43(3):175 – 182, 2001.
- [84] A.A. Kazmi and H. Furumai. Field investigations on reactive settling in an intermittent aeration sequencing batch reactor activated sludge process. *Water Science and Technology*, 41(1):127 – 135, 2000.
- [85] A.A. Kazmi and H. Furumai. A simple settling model for batch activated sludge process. *Water Science and Technology*, 42(3–4):9 – 16, 2000.
- [86] J. Keller and Z. Yuan. Combined hydraulic and biological modelling and full-scale validation of SBR process. *Water Science and Technology*, 45(6):219 – 228, 2002.
- [87] J.C. Kissel, L. Perry, L. McCarty, and R.L. Street. Numerical simulation of mixed-culture biofilm. *Journal of Environmental Engineering*, 110(2):393 – 411, 1984.
- [88] G. Koch, R. Pianta, P. Krebs, and H. Siegrist. Potential of denitrification and solids removal in the rectangular clarifier. *Water Research*, 33:309 – 318, 1999.
- [89] G.J. Kynch. A theory of sedimentation. *Transactions of the Faraday Society*, 48:166 – 176, 1952.
- [90] S. Lackner, A. Terada, and B.F. Smets. Heterotrophic activity compromises autotrophic nitrogen removal in membrane-aerated biofilms: Results of a modeling study. *Water Research*, 42(4-5):1102 – 1112, 2008.

- [91] B. Li and M.K. Stenstrom. Research advances and challenges in one-dimensional modeling of secondary settling tanks - a critical review. *Water Research*, 65:40 – 63, 2014.
- [92] B. Li and M.K. Stenstrom. Practical identifiability and uncertainty analysis of the one-dimensional hindered-compression continuous settling model. *Water Research*, 90:235 – 246, 2016.
- [93] Z. Li, R. Qi, B. Wang, Z. Zou, G. Wei, and M. Yang. Cost-performance analysis of nutrient removal in a full-scale oxidation ditch process based on kinetic modeling. *Journal of Environmental Sciences*, 25(1):26 – 32, 2013.
- [94] C. Mejías. *Identificación de la Función Densidad de Flujo Mediante Medición de Curvas de Asentamiento de Suspensiones y Simulación Numérica de Sedimentación Continua*. Habilitación Profesional para obtener el Título de Ingeniero Civil Matemático, Universidad de Concepción, Chile, 2015.
- [95] E. Morgenroth and P.A. Wilderer. Influence of detachment mechanisms and competition in biofilms. *Water Research*, 34(2):417 – 426, 2000.
- [96] A.G. Mutlu, A.K. Vangsgaard, G. Sin, and B.F. Smets. An operational protocol for facilitating start-up of single-stage autotrophic nitrogen-removing reactors based on process stoichiometry. *Water Science & Technology*, 68(3):514 – 521, 2013.
- [97] B.-J. Ni, Y.-P. Chen, S.-Y. Liu, F. Fang, W.-M. Xie, and H.-Q. Yu. Modeling a granule-based anaerobic ammonium oxidizing (anammox) process. *Biotechnology and Bioengineering*, 103(3):490 – 499, 2009.
- [98] I. Nopens. *Modelling the activated sludge flocculation process: a population balance approach*. PhD thesis, Faculty of Bioscience Engineering. Ghent University, 2005.
- [99] NTT data. <https://www.nttdata.com/global/en/>. Retrieved October 20, 2018.
- [100] G.S. Ostace, V.M. Cristea, and P.S. Agachi. Evaluation of different control strategies of the waste water treatment plant based on a modified activated sludge model no. 3. *Environmental Engineering and Management Journal*, 11:147 – 164, 2012.
- [101] B. Parent. Positivity-preserving high-resolution schemes for systems of conservation laws. *Journal of Computational Physics*, 231(1):173 – 189, 2012.

- [102] C. Picioreanu, M.C.M van Loosdrecht, and J.J. Heijnen. Mathematical modeling of biofilm structure with a hybrid differential-discrete cellular automaton approach. *Biotechnology and Bioengineering*, 58(1):101 – 116, 1998.
- [103] C. Picioreanu, M.C.M van Loosdrecht, and J.J. Heijnen. A new combined differential-discrete cellular automaton approach for biofilm modeling: Application for growth in gel beads. *Biotechnology and Bioengineering*, 57(6):718 – 731, 1998.
- [104] C. Picioreanu, J.B. Xavier, and M.C.M van Loosdrecht. Advances in mathematical modeling of biofilm structure. *Biofilms*, 1(4):337 – 349, 2004.
- [105] E. Ramin, D.S. Wágner, L. Yde, P.J. Binning, M.R. Rasmussen, P.S. Mikkelsen, and B.G. Plósz. A new settling velocity model to describe secondary sedimentation. *Water Research*, 66:447 – 458, 2014.
- [106] P. Reichert. Aquasim - a tool for simulation and data analysis of aquatic systems. *Water Science and Technology*, 30(2):21 – 30, 1994.
- [107] P. Reichert. Design techniques of a computer program for the identification of processes and the simulation of water quality in aquatic systems. *Environmental Software*, 10(3):199 – 210, 1995.
- [108] P. Reichert and O. Wanner. Movement of solids in biofilms: Significance of liquid phase transport. *Water Science & Technology*, 36(1):321 – 328, 1997.
- [109] J.F. Richardson and W.N. Zaki. Sedimentation and fluidization: part i. *Transactions of the Institution of Chemical Engineers (London)*, 32:35 – 53, 1954.
- [110] V.V. Shelukhin. Quasistationary sedimentation with adsorption. *Journal of Applied Mechanics and Technical Physics*, 46(4):213 – 522, 2005.
- [111] L. Shen, Y. Lu, and Y. Liu. Mathematical modeling of biofilm-covered granular activated carbon: a review. *Journal of Chemical Technology and Biotechnology*, 87(11):1513 – 1520, 2012.
- [112] H. Siegrist, P. Krebs, R. Bühler, I. Purtschert, C. Röck, and R. Rufer. Denitrification in secondary clarifiers. *Water Science and Technology*, 31(2):205 – 214, 1995.
- [113] Sufee framework. <https://colorlib.com/polygon/sufee/>. Retrieved October 20, 2018.

- [114] Sustainable Development Goal No. 6. <https://www.globalgiving.org/sdg/clean-water-and-sanitation/>. *Asked October 20*, 2018.
- [115] Sustainable Development Goals. <https://www.globalgiving.org/sdg/>. *Asked October 20*, 2018.
- [116] L. Svarovsky. *Solid-Liquid Separation*, chapter Chapter 15: Countercurrent washing of solids, pages 442 – 475. Butterworth-Heinemann, Oxford, fourth edition edition, 2001.
- [117] I. Takács, G.G. Patry, and D. Nolasco. A dynamic model of the clarification-thickening process. *Water Research*, 25:1263 – 1271, 1991.
- [118] G. Tchobanoglous, F. Burton, and H. Stensel. *Wastewater Engineering: Treatment and reuse*. Metcalf and Eddy. McGraw - Hill, New York, USA, 4th edition, 2003.
- [119] E. Torfs, S. Balemans, F. Locatelli, J. Laurent, P. François, R. Bürger, S. Diehl, and I. Nopens. On constitutive functions for hindered settling velocity in 1-d settler models: Selection of appropriate model structure. *Water Research*, 110:38 – 47, 2016.
- [120] E. Torfs, T. Maere, R. Bürger, S. Diehl, and I. Nopens. Impact on sludge inventory and control strategies using the benchmark simulation model no. 1 with the bürger-diehl settler model. *Water Science and Technology*, 71:1524 – 1535, 2015.
- [121] M.C.M van Loosdrecht, D. Eikelboom, A. Gjaltema, A. Mulder, L. Tjihuis, and J.J. Heijnen. Biofilm structures. *Water Science & Technology*, 32(8):35 – 43, 1995.
- [122] M.C.M van Loosdrecht, C.M. Lopez-Vazquez, S.C.F. Meijer, C.M. Hooijmans, and D. Brdjanovic. Twenty-five years of asm1: past, present and future of wastewater treatment modelling. *Journal of Hydroinformatics*, 17:697 – 718, 2015.
- [123] M.C.M van Loosdrecht, C. Picioreanu, and J.J. Heijnen. A more unifying hypothesis for biofilm structures. *FEMS Microbiology Ecology*, 24(2):181 – 183, 1997.
- [124] A.K. Vangsgaard. *Modeling, Experimentation, and Control of Autotrophic Nitrogen Removal in Granular Sludge Systems*. PhD thesis, Technical University of Denmark, 2013.

- [125] A.K. Vangsgaard, M. Mauricio-Iglesias, K.V. Gernaey, and G. Sin. Development of novel control strategies for single-stage autotrophic nitrogen removal: A process oriented approach. *Computers & Chemical Engineering*, 66:71 – 81, 2014.
- [126] A.K. Vangsgaard, M. Mauricio-Iglesias, K.V. Gernaey, B.F. Smets, and G. Sin. Sensitivity analysis of autotrophic n removal by a granule based bioreactor: Influence of mass transfer versus microbial kinetics. *Bioresource Technology*, 123:230 – 241, 2012.
- [127] A.K. Vangsgaard, A.G. Mutlu, K.V. Gernaey, B.F. Smets, and G. Sin. Calibration and validation of a model describing complete autotrophic nitrogen removal in a granular sbr system. *J Chem Technol Biotechnol*, 88:2007 – 2015, 2013.
- [128] J.R. Vázquez-Padín, I. Fernández, M. Figueroa, A. Mosquera-Corral, and J.L. Campos. Applications of anammox based processes to treat anaerobic digester supernatant at room temperature. *Bioresource Technology*, 100(12):2988 – 2994, 2009.
- [129] P.A. Vesilind. Design of prototype thickeners from batch settling tests. *Water Sewage Works*, 115:302 – 307, 1968.
- [130] S.E. Vlaeminck, A. Terada, B.F. Smets, H. De Clippeleir, T. Schaubroeck, S. Bolea, L. Demeestere, J. Mast, N. Boon, M. Carballa, and W. Vestraete. Aggregate size and architecture determine microbial activity balance for one-stage partial nitrification and anammox. *Applied and Environmental Microbiology*, 76(3):900 – 909, 2010.
- [131] E.I.P. Volcke, C. Picioreanu, B. De Baets, and M.C.M van Loosdrecht. Effect of granule size on autotrophic nitrogen removal in a granular sludge reactor. *Environmental Technology*, 31(11):1271 – 1280, 2010.
- [132] O. Wanner, H.J. Eberl, E. Morgenroth, D.R. Noguera, C. Picioreanu, B.E. Rittmann, and M.C.M van Loosdrecht. *Mathematical Modeling of Biofilms*. IWA Scientific and Technical Report No.18, IWA Publishing, 2006.
- [133] O. Wanner and W. Gujer. Competition in biofilms. *Water Science & Technology*, 17:27 – 44, 1984.
- [134] O. Wanner and W. Gujer. A multispecies biofilm model. *Biotechnology and Bioengineering*, 28:314 – 328, 1986.
- [135] O. Wanner and P. Reichert. Mathematical modeling of mixed-culture biofilms. *Biotechnology and Bioengineering*, 49:172 – 184, 1996.

- [136] Water.org ONG. <http://water.org>. Retrieved October 20, 2018.
- [137] B.D. Wood and S. Whitaker. Cellular growth in biofilms. *Biotechnology and Bioengineering*, 64(6):656 – 670, 1999.
- [138] World Health Organization. <http://www.who.int/news-room/detail/12-07-2017-2-1-billion-people-lack-safe-drinking-water-at-home-more-than-twice-as-many-lack-safe-sanitation>. Retrieved October 20, 2018.
- [139] J.B. Xavier, C. Picioreanu, and M.C.M van Loosdrecht. A general description of detachment for multidimensional modelling of biofilms. *Biotechnology and Bioengineering*, 91(6):651 – 669, 2005.

